DRAFT VERSION APRIL 20, 2016
Preprint typeset using LaTeX style emulateapj v. 12/16/11

THE INFRARED SPECTRAL PROPERTIES OF MAGELLANIC CARBON STARS

G. C. SLOAN[1,2], K. E. KRAEMER[3], I. MCDONALD[4], M. A. T. GROENEWEGEN[5], P. R. WOOD[6], A. A. ZIJLSTRA[4], E. LAGADEC[7], M. L. BOYER[8,9], F. KEMPER[10], M. MATSUURA[11], R. SAHAI[12], B. A. SARGENT[13], S. SRINIVASAN[10], J. TH. VAN LOON[14], & K. VOLK[15]

Draft version April 20, 2016

ABSTRACT

The Infrared Spectrograph on the *Spitzer Space Telescope* observed 184 carbon stars in the Magellanic Clouds. This sample reveals that the dust-production rate (DPR) from carbon stars generally increases with the pulsation period of the star. The composition of the dust grains follows two condensation sequences, with more SiC condensing before amorphous carbon in metal-rich stars, and the order reversed in metal-poor stars. MgS dust condenses in optically thicker dust shells, and its condensation is delayed in more metal-poor stars. Metal-poor carbon stars also tend to have stronger absorption from C_2H_2 at 7.5 μm. The relation between DPR and pulsation period shows significant apparent scatter, which results from the initial mass of the star, with more massive stars occupying a sequence parallel to lower-mass stars, but shifted to longer periods. Accounting for differences in the mass distribution between the carbon stars observed in the Small and Large Magellanic Clouds reveals a hint of a subtle decrease in the DPR at lower metallicities, but it is not statistically significant. The most deeply embedded carbon stars have lower variability amplitudes and show SiC in absorption. In some cases they have bluer colors at shorter wavelengths, suggesting that the central star is becoming visible. These deeply embedded stars may be evolving off of the AGB and/or they may have non-spherical dust geometries.

Subject headings: circumstellar matter — infrared: stars — stars: carbon — stars: AGB and post-AGB

1. INTRODUCTION

Intermediate-mass stars contribute to the chemical evolution of galaxies when they shed their envelopes and seed their environments with freshly condensed dust and the products of nuclear fusion from their cores. The sensitivity of the Infrared Spectrograph (IRS; Houck et al. 2004) on the *Spitzer Space Telescope* (Werner et al. 2004) made it possible to observe many mass-losing stars in nearby galaxies like the Large and Small Magellanic Clouds (LMC and SMC). These stars are at known distances, and they probe different metallicities. While the metallicity distribution functions are broad enough to overlap and depend on age, for statistical treatment of large samples it is safe to claim that the LMC is more metal-poor than the Galaxy, and the SMC is more metal-poor still. As an example, Piatti (2013) find that in the LMC, [Fe/H] increased from ~-0.7 to ~-0.3 from 5 to 1 Gyr ago, compared to ~-1.2 to ~-0.6 over the same time interval in the SMC (Piatti 2012).

Carbon stars dominated the spectral samples of evolved stars observed early in the *Spitzer* mission. Sloan et al. (2006) examined carbon stars in the SMC while Zijlstra et al. (2006) considered the LMC. Matsuura et al. (2006) studied the molecular absorption in these samples, and other studies followed (Buchanan et al. 2006; Lagadec et al. 2007; Leisenring et al. 2008; Sloan et al. 2008). Further observing programs added considerably to the spectral sample of carbon stars in both galaxies, including two programs which added fainter carbon stars to the samples in the LMC (Kemper et al. 2010) and SMC (Program 50240).

These earlier efforts led to the finding that the amount of dust observed around carbon stars does not show a strong dependence on metallicity (Sloan et al. 2008). Carbon stars result from the dredge-up of freshly fused carbon from the cores of stars as they burn He in thermal pulses while on the asymptotic giant branch (AGB). The formation of CO leaves only carbon or oxygen available to form other molecules and condense into dust so that when the C/O ratio exceeds unity, the gas and dust shift from an O-rich to a C-rich chemistry. Matsuura et al. (2005) noted that because dredged-up material on the AGB is dominated by carbon in most stars, the amount of free carbon left after the formation of CO should actually *increase* in more metal-poor stars. Sloan et al. (2012) accounted for the changing oxygen abundances at lower metallicity and reached a similar conclusion. Thus, the question is not one of

[1] Cornell Center for Astrophysics & Planetary Science, Cornell Univ., Ithaca, NY 14853-6801, USA, sloan@isc.astro.cornell.edu
[2] Department of Physics and Astronomy, University of North Carolina, Chapel Hill, NC 27599-3255, USA
[3] Institute for Scientific Research, Boston College, 140 Commonwealth Avenue, Chestnut Hill, MA 02467, USA
[4] Jodrell Bank Centre for Astrophysics, Univ. of Manchester, Manchester M13 9PL, UK
[5] Koninklijke Sterrenwacht van België, Ringlaan 3, B–1180 Brussels, Belgium
[6] Research School of Astronomy and Astrophysics, Australian National University, Canberra, ACT 2611, Australia
[7] Observatoire de la Côte d'Azur, 06300, Nice, France
[8] CRESST and Observational Cosmology Lab, Code 665, NASA Goddard Space Flight Center, Greenbelt, MD, 20771, USA
[9] Department of Astronomy, University of Maryland, College Park, MD 20742, USA
[10] Academia Sinica, Institute of Astronomy and Astrophysics, 11F Astronomy-Mathematics Building, NTU/AS, No. 1, Sec. 4, Roosevelt Rd., Taipei 10617, Taiwan, R.O.C.
[11] School of Physics and Astronomy, Cardiff University, Queen's Buildings, The Parade, Cardiff, CF24 3AA, UK
[12] Jet Propulsion Laboratory, California Institute of Technology, MS 183-900, Pasadena, CA 91109, USA
[13] Center for Imaging Science and Laboratory for Multiwavelength Astrophysics, Rochester Institute of Technology, 54 Lomb Memorial Drive, Rochester, NY 14623, USA
[14] Lennard Jones Laboratories, Keele University, Staffordshire ST5 5BG, UK
[15] Space Telescope Science Institute, 3700 San Martin Dr., Baltimore, MD 21218, USA

why the amount of carbon-rich dust is not *declining* as metallicity drops, but why is it not *increasing*.

The infrared spectrographic studies of Magellanic carbon stars have revealed several dependencies on metallicity. In more metal-poor samples, the SiC dust emission feature at $\sim$11.3 μm weakens, the molecular absorption bands from C_2H_2 at 7.5 and 13.7 μm grow stronger, and the appearance of MgS dust is more delayed.

This work builds on the earlier works by adding the rest of the IRS observations and comparing the samples as a whole. Section 2 describes the samples of carbon stars in the Magellanic Clouds and the Galaxy and the spectroscopic and photometric data. Section 3 describes the data analysis, and Section 4 presents the results. In Section 5, we discuss the issues raised, and in Section 6, summarize our findings. Appendix A presents useful relations between infrared filter sets and colors for carbon stars. Appendices B and C present new periods for several sources based on the analysis of multi-epoch photometry in the near-IR and mid-IR, respectively.

2. OBSERVATIONS

2.1. *Samples and targets*

Table 1 lists the 144 objects in the LMC and 40 in the SMC observed with the IRS and identified as carbon stars. Our objective was to build a sample including all of the carbon-rich AGB stars observed by the IRS while excluding post-AGB objects. Our selection criteria are based on the infrared (IR) spectral classification of Kraemer et al. (2002, see Section 2.5 below). Generally, spectra are considered carbon-rich if they show SiC dust emission at $\sim$11.3 μm or the acetylene absorption bands at 7.5 and/or 13.7 μm. The 26–30 μm feature attributed to MgS dust appears in many of the spectra and helps to confirm their carbon-rich nature.

Goebel & Moseley (1985) identified MgS dust as the carrier of the 26–30 μm feature, but some doubt has been cast on that identification due to abundance constraints (e.g. Zhang et al. 2009). Sloan et al. (2014) examined these and other concerns about MgS and concluded that it remains a strong candidate for the carrier of the feature. Section 5.4 investigates this issue, but in the meantime, we will refer to this feature as the MgS feature for convenience.

We excluded objects if their spectra peak at wavelengths above $\sim$20 μm (in F_ν units), because for carbon-rich sources, that indicates that they have evolved past the AGB. These excluded objects are part of the carbon-rich post-AGB sample studied by Sloan et al. (2014).

Two other classes of post-AGB objects have warmer spectral energy distributions (SEDs) peaking shortward of $\sim$20 μm and are also excluded. R CrB stars have smooth spectra showing only emission from amorphous carbon dust and no other significant spectral features. Kraemer et al. (2005) examined two in the SMC, but the IRS sample contains additional R CrB stars (Clayton et al., in preparation). The other class of warm post-AGB objects includes two sources showing absorption bands from aliphatic hydrocarbons[16]: SMP LMC 011 (Bernard-Salas et al. 2006), and MSX SMC 029 (Kraemer et al. 2006).

A variety of *Spitzer* observing programs contributed to the present sample of carbon stars (see Table 2). Each program comes with its own selection criteria and biases, which means that the present sample is neither uniform nor complete. However, thanks to the efforts of the designers of all the previous programs, the present sample probes carbon stars spanning a wide range of luminosities, colors, and evolutionary stages.

The first two programs listed in Table 2 were developed prior to launch as part of the guaranteed-time observations (GTOs). Both sampled a variety of evolved stars, with Program 200 focused on supergiants and AGB stars identified as variable stars in the optical and near-IR in both the SMC and LMC. Program 1094 covered a range of post-main-sequence evolutionary stages in the LMC (and the Galaxy).

The next four programs were Guest Observer (GO) programs in Cycle 2 of the mission. Program 3277 started with the mid-IR sources in the SMC identified by the *Mid-course Space Experiment* (*MSX*; Price et al. 2001) to generate a sample spanning color-color space in the near- and mid-IR. Program 3426 sampled a randomly chosen subset of the brightest 150 sources in the LMC. Program 3505 identified AGB stars in several previous infrared surveys with the help of near-IR color-magnitude diagrams (CMDs). It covered both the LMC and SMC. Program 3591 extended Program 1094 to a larger sample in the LMC.

More programs followed later in the *Spitzer* mission. Program 37088 concentrated on heavily embedded and thus more evolved stars in the LMC. Program 40650 targeted about 300 candidate young stellar objects (YSOs) in the LMC, as well as several sources described as extremely red objects (EROs) and subsequently identified as deeply embedded carbon stars (Gruendl et al. 2008). The latter group is included in our sample. Program 40519 expanded on all previous programs studying the LMC by observing about 200 targets covering undersampled regions of color-color and color-magnitude space. It included evolved stars and YSOs, relied on the mid-IR photometry from the SAGE survey of the LMC (Surveying the Agents of Galactic Evolution; Meixner et al. 2006), and is known as SAGE-Spec. This program added a number of faint carbon-rich targets to the sample. Program 50240 expanded the targets observed in the SMC in a similar manner. Finally, Program 50338 concentrated on post-AGB candidates in the LMC.

2.2. *Adopted distances*

The known distances to the LMC and SMC enable us to study the total luminosities of the stars in our sample. We adopt distance moduli for the LMC and SMC of 18.5 and 18.9, respectively. Measurements of the distance modulus to the LMC cluster around our adopted value. The review by Feast (2013) leads to 18.50; another good example of a recent result is 18.49 $\pm$ 0.05 (Pietrzyński et al. 2013). Similarly, our adopted distance modulus to the SMC is close to the mean value reported by Rubele et al. (2015), 18.91 $\pm$ 0.02. The distances to these galaxies are only important to our determinations of absolute bolometric magnitudes, and because these have uncertainties larger than 0.1 magnitudes, we are not concerned with precision in the distance modulus to further significant figures.

The SMC has a complicated structure, with considerable depth along the line of sight (Gardiner & Hawkins 1991). Most of the stars reside in the Bar region, where the mean distance modulus to different regions can vary from $\sim$18.85 to 19.02 (Rubele et al. 2015). Typical depths in this region are only 2–3 kpc ($\Delta(m-M)\lesssim 0.1$), but in the extended Wing region to the east, Nidever et al. (2013) report depths up to $\sim$20 kpc ($\Delta(m-M)\lesssim 0.8$). Rubele et al. (2015) find mean dis-

[16] I.e. non-aromatic species such as C_2H_6, longer chains, and other similar molecules.

TABLE 1
THE *Spitzer* SAMPLE OF MAGELLANIC CARBON STARS

Target	Alias	RA (J2000)	Decl. (J2000)	Position reference	Period (days)	Period reference[a]	Program identifier[b]
GM 780		8.905255	−73.165604	2MASS	611	OGLE	3505
MSX SMC 091		9.236293	−72.421547	2MASS	···	···	3277
MSX SMC 062		10.670455	−72.951599	2MASS	550	OGLE	3277
MSX SMC 054		10.774604	−73.361282	2MASS	396	OGLE	3277
2MASS J004326		10.860405	−73.445366	2MASS	330	R05	50240
MSX SMC 044		10.914901	−73.249336	2MASS	440	OGLE	3277
MSX SMC 105		11.258941	−72.873428	2MASS	668	OGLE	3277
MSX SMC 036		11.474785	−73.394775	2MASS	553	OGLE	3277
GB S06	MSX SMC 060	11.668442	−73.279793	2MASS	435	OGLE	3277
MSX SMC 200		11.711623	−71.794250	2MASS	426	OGLE	3277

NOTE. — Table 1 is published in its entirety in the electronic edition of the Astrophysical Journal. A portion is shown here for guidance regarding its form and content.

[a] OGLE = Soszyński et al. (2009, 2011, Optical Gravitational Lensing Experiment); GO7 = Groenewegen et al. (2007); G09 = Groenewegen et al. (2009); K10 = Kamath et al. (2010); N00 = Nishida et al. (2000); R05 = Raimondo et al. (2005); S06 = Sloan et al. (2006); W89 = Whitelock et al. (1989); W03 = Whitelock et al. (2003); Z06 = Zijlstra et al. (2006); App. B and C = the appendices in this paper.

[b] See Table 2.

TABLE 2
SPECTROSCOPIC *Spitzer* PROGRAMS THAT OBSERVED MAGELLANIC CARBON STARS

Program ID	Project leaders	Description
200	J. R. Houck & G. C. Sloan	Evolved stars in the LMC and SMC
1094	F. Kemper	AGB evolution in the LMC (and Galaxy)
3277	M. P. Egan & G. C. Sloan	*MSX*-based sample in the SMC
3426	J. H. Kastner & C. L. Buchanan	Bright infrared sources in the LMC
3505	P. R. Wood & A. A. Zijlstra	AGB stars in the LMC and SMC
3591	F. Kemper	AGB evolution in the LMC
37088	R. Sahai	Embedded carbon stars in the LMC
40650	L. W. Looney & R. A. Gruendl	YSOs and red sources in the LMC
40519	A. G. G. M. Tielens & F. Kemper	Extended the IRS sample in the LMC
50240	G. C. Sloan & K. E. Kraemer	Extended the IRS sample in the SMC
50338	M. Matsuura	Carbon-rich post-AGB candidates in the LMC

tance moduli in the eastern regions between ∼18.65 and 18.8. Most of the targets are in the Bar, and we will assume they are at our canonical distance modulus (18.9).

We have several targets in the cluster NGC 419, which is in the direction of the SMC. Glatt et al. (2008) give a distance modulus of 18.50, the same as for the LMC and about 10 kpc in front of the SMC. They describe how the model which best fits the optical CMD gives $(m-M)_o = 18.75$, while other models give values of 18.60 and 18.94. It is unclear what justifies the reported value of 18.50, and as discussed below, a value of 18.90 is more consistent with the IR data (see Section 4.3).

2.3. *IRS observations*

The IRS observed the majority of the sources in the standard low-resolution nod sequence, most of them with both the Short-Low (SL) and Long-Low (LL) modules. SL and LL provide spectral coverage from 5–14 μm and 14–37 μm, respectively, with a resolution ($\lambda/\Delta\lambda$) of ∼80–120. Some of the fainter sources were observed only in SL. Generally, sources were observed in each of the two SL apertures, providing first- and second-order spectra, then the two LL apertures. Each source was observed in two nod positions in each aperture. Thus a full low-resolution spectrum requires eight pointings.

The carbon-rich EROs observed by Gruendl et al. (2008) used the SL module, along with Short-High (SH) and Long-High (LH), which cover 10–19 and 19–36 μm, respectively, at a resolution of ∼300.

The reduction and calibration of the low-resolution spectra followed the standard Cornell algorithm (see Sloan et al. 2015a, for a more detailed description). The Cornell processing begins with the flatfielded images provided by version S18.18 of the pipeline at the *Spitzer* Science Center (SSC). Bad pixels in each image are identified and replaced with values based on their neighbors. All images for a given nod position are averaged, then a suitable background image is subtracted from the target image. In SL, the default is an aperture differerence, where the background for a given target is the image with the target in the other aperture, while in LL, the default is a nod difference, with the target in the same aperture, but the other nod. In some cases, the design of the observation or structure or other sources in the background forced a change from the default.

We deviated from the reduction sequence described by Sloan et al. (2015a) by using an optimal-extraction algorithm to extract spectra from the images (Lebouteiller et al. 2010). This method fits a supersampled point-spread function (PSF) to the spatial profile in each row of the spectral image and can improve the SNR up to 80%. It proved essential to generating usable spectra for the faintest sources in our sample. However, the method only works for point sources. For extended or mispointed objects, we used the default extraction algorithm which simply sums data in each wavelength element with no weighting.

Our pipeline continues with the standard step of combining spectra from the two nods and comparing the data to identify and reject spikes or divots which had survived the cleaning process. Spectral segments are then stitched together, shifting spectra upwards multiplicatively to the presumably best-centered segment. Finally, extraneous data are removed from the ends of each segment.

Several previous papers on Magellanic carbon stars used the above algorithm, but without the optimal-extraction method which came later (Sloan et al. 2006; Zijlstra et al. 2006; Lagadec et al. 2007; Leisenring et al. 2008; Sloan et al. 2008; Kemper et al. 2010). The optimal extraction has generally improved the quality of the spectra.

2.4. *Photometric data*

For all of our targets, we have constructed SEDs based on multi-epoch photometry in the optical, near-IR, and mid-IR.

The mid-IR data come from the SAGE survey of the LMC (Meixner et al. 2006) and the SAGE-SMC survey for the SMC (Gordon et al. 2011), which incorporates the S^{3}MC survey (*Spitzer* Survey of the SMC; Bolatto et al. 2007). The SAGE surveys give two epochs, spaced approximately three months apart, for the Infrared Array Camera (IRAC) and the Multi-Imaging Photometer for *Spitzer* (MIPS). The S^{3}MC survey provides one additional epoch in the core of the SMC. We use all four IRAC filters at 3.6, 4.5, 5.8, and 8.0 μm and the MIPS 24 μm filter. The SAGE-VAR survey adds four epochs from the Warm *Spitzer* Mission at 3.6 and 4.5 μm for portions of the LMC and SMC (Riebel et al. 2015). We found matches with the SAGE-VAR survey for 61 of our carbon stars in the LMC and 26 in the SMC.

We also used additional epochs at 3.4 and 4.6 μm from the *Wide-field Infrared Survey Experiment* (*WISE*; Wright et al. 2010) and the *NEOWISE* reactivation mission (Mainzer et al. 2014).[17] For all *WISE* data, we utilized the multi-epoch data tables and collapsed them to one epoch approximately every six months. The publicly available data typically give us four epochs, two in 2010 and two in 2014.

Applying the color corrections derived for carbon stars in Appendix A allows us to convert W1 (3.4 μm) to [3.6] and W2 (4.6 μm) to [4.5]. The combination of the SAGE surveys, including SAGE-VAR, and the *WISE* data can give us 10 or more epochs at 3.6 and 4.5 μm for some of the stars in our sample.

The *WISE* survey is less sensitive and has lower angular resolution than the SAGE data, forcing us to reject some questionable data. We rejected both W1 and W2 for NGC 419 LE 35 and MIR 1 due to crowding. For IRAS 05026 and IRAS 05042, the multi-epoch data indicated a detection at W1, but the *WISE* images of the field showed nothing, even though the sources could be seen in W2. The W1−W2 colors were inconsistent with the SAGE data, so we rejected the W1 data but kept W2.

Near-IR photometry comes from the 2MASS survey, and the deeper 2MASS-6X survey provides a second epoch at J, H, and K_s (Skrutskie et al. 2006; Cutri et al. 2006). Additional epochs come from the Deep Near-IR Survey of the Southern Sky (DENIS) at J and K_s (Cioni et al. 2000) and the IR Survey Facility (IRSF) at J, H, and K_s (Kato et al. 2007).

In the optical, we relied on the Magellanic Clouds Photometric Survey (MCPS) at U, B, V, and I (Zaritsky et al. 2002, 2004). DENIS adds data at I. Additional mean magnitudes at V and I in the LMC come from the OGLE-III Shallow Survey (Ulaczyk et al. 2013). Where possible, we replaced the V and I data with mean magnitudes from the OGLE-III surveys of the Magellanic Clouds, which also give pulsation periods and amplitudes (Soszyński et al. 2009, 2011).

We searched for matches to the IRS sources first with the SAGE surveys, using positions estimated from the pointing of the IRS. The optimal extraction algorithm estimates the position of a source along a given slit (i.e., in the cross-dispersion direction). For most observations, the nearly perpendicular orientation of the SL and LL slits helps to constrain the position of the source, despite the widths of the slits ($\sim$3.″6 and 10.″6, respectively). Where possible, we used matches to IRAC to update the initial IRS-based coordinates, then searched for 2MASS counterparts, again updating positions where possible, and then searched the other catalogs. The positions in Table 1 are the result.

The median offset from the estimated IRS position to IRAC is 0.″37, consistent with a typical IRS pointing error of 0.″4. The median offset between the IRAC and 2MASS positions is 0.″20. Comparing positions in the IRAC and MIPS catalogs, we find a median offset of 0.″20.

For the most embedded sources, the expected photometry in the near-IR and at 3.6 μm is near or below the detection limit, making it possible to mismatch the photometry to blue sources close to the expected positions of our carbon stars. We examined the environments of the most embedded sources, searching for targets within 1′ to estimate the source density. For IRAC, the source densities are 1.1–4.8$\times10^{-3}$, and for 2MASS-6X, they are higher, 7.0–8.2 $\times10^{-3}$. Our maximum search radius in the LMC was 1.″25, which gives a search field of 4.9 square arcsec and makes the odds of a mismatch for a given source 0.5–2.4%. For 2MASS-6X, the odds of a mismtach are 3.4–4.0% for a given source. Thus, mismatches are unlikely.

However, the above calculations were for field stars. For stars in clusters, we compared our near-IR results to the photometry reported by van Loon et al. (2005), and we used these data to replace the J magnitude of one source, NGC 1978 MIR 1.

Tables 3 and 4 present the resulting photometry. For each photometric filter, the magnitude is a mean magnitude, and the uncertainty is the standard deviation of the data. When only one epoch of data in a given filter was available, we left the reported uncertainty undefined. While we can have over ten epochs at 3.6 and 4.5 μm, at longer wavelengths we are limited to three epochs in the heart of the SMC and two epochs in the LMC and the outskirts of the SMC.

2.5. *Galactic comparison spectra*

We also consider a Galactic control sample using spectra from the Short-Wavelength Spectrometer (SWS; de Graauw et al. 1996) on the *Infrared Space Observatory* (*ISO*; Kessler et al. 1996). Leisenring et al. (2008) presented the original list of 34 carbon stars used in earlier comparisons to Magellanic samples. The present sample includes eight additional objects, for a total of 42.

The comparison SWS sample was chosen from spectra classified as carbon stars by Kraemer et al. (2002). Their classification scheme assigns spectra to groups based on the overall shape of the spectrum, with naked stars in Group 1, stellar spectra showing some dust emission in Group 2, spectra dominated by warm dust in Group 3, and spectra dominated by

[17] We used the AllWISE Multiepoch Photometry Table and the NEOWISE-R Single Exposure Source Table available online at the Infrared Science Archive (IRSA).

TABLE 3
OPTICAL AND NEAR-INFRARED PHOTOMETRY

Target	U (mag.)	B (mag.)	V (mag.)	I (mag.)	J (mag.)	H (mag.)	K (mag.)
GM 780	···	···	16.760 ± ···	14.235 ± 0.040	12.098 ± 0.740	10.658 ± 0.564	9.934 ± 0.402
MSX SMC 091	···	···	···	15.781 ± 0.060	13.764 ± 0.374	12.259 ± 0.284	10.829 ± 0.191
MSX SMC 062	···	···	···	16.985 ± ···	13.261 ± 1.398	11.418 ± 0.159	10.281 ± 0.769
MSX SMC 054	···	···	21.430 ± ···	20.383 ± ···	16.536 ± 0.854	14.449 ± 0.182	12.281 ± 0.369
2MASS J004326	···	···	18.658 ± ···	15.170 ± 0.040	13.041 ± 0.117	11.857 ± 0.108	10.970 ± 0.151
MSX SMC 044	19.762 ± 0.135	19.230 ± 0.039	19.920 ± 0.045	16.406 ± 1.882	13.154 ± 1.336	12.178 ± 1.822	10.492 ± 0.943
MSX SMC 105	···	22.447 ± 0.391	21.099 ± 0.303	18.370 ± 0.081	15.151 ± 0.446	13.082 ± 0.382	11.245 ± 0.290
MSX SMC 036	···	···	···	19.462 ± 0.090	15.170 ± 1.013	13.553 ± 0.898	11.743 ± 0.632
GB S06	···	···	20.137 ± ···	18.114 ± ···	15.348 ± 0.364	13.146 ± 0.283	11.211 ± 0.242
MSX SMC 200	···	···	21.203 ± ···	17.557 ± 0.200	14.612 ± 0.899	12.724 ± 0.804	11.371 ± 0.413

NOTE. — Table 3 is published in its entirety in the electronic edition of the Astrophysical Journal. A portion is shown here for guidance regarding its form and content.

TABLE 4
MID-INFRARED PHOTOMETRY AND BOLOMETRIC MAGNITUDES

Target	[3.6] (mag.)	[4.5] (mag.)	[5.8] (mag.)	[8.0] (mag.)	[24] (mag.)	M_{bol} (mag.)
GM 780	8.738 ± 0.454	8.288 ± 0.413	8.283 ± 0.064	7.916 ± 0.066	6.771 ± 0.368	−5.90
MSX SMC 091	9.602 ± 0.366	8.976 ± 0.322	8.260 ± 0.008	7.864 ± 0.029	7.328 ± 0.060	−4.88
MSX SMC 062	8.941 ± 0.266	8.375 ± 0.304	7.639 ± 0.026	7.092 ± 0.023	6.272 ± 0.178	−5.50
MSX SMC 054	9.940 ± 0.327	9.037 ± 0.313	8.408 ± 0.201	7.771 ± 0.142	6.595 ± 0.142	−4.58
2MASS J004326	10.495 ± 0.400	10.476 ± 0.257	10.196 ± 0.095	9.615 ± 0.061	9.316 ± 0.056	−4.56
MSX SMC 044	9.300 ± 0.256	8.661 ± 0.230	8.189 ± 0.191	7.713 ± 0.155	7.216 ± 0.077	−5.29
MSX SMC 105	9.312 ± 0.129	8.544 ± 0.151	8.007 ± 0.079	7.370 ± 0.078	5.928 ± 0.220	−5.04
MSX SMC 036	9.698 ± 0.314	8.790 ± 0.274	8.051 ± 0.199	7.515 ± 0.160	6.529 ± 0.131	−4.62
GB S06	8.666 ± 0.259	7.927 ± 0.373	6.922 ± 0.157	6.241 ± 0.182	4.874 ± 0.098	−5.62
MSX SMC 200	9.298 ± 0.180	8.806 ± 0.198	8.362 ± 0.062	7.894 ± 0.030	7.276 ± 0.206	−4.81

NOTE. — Table 4 is published in its entirety in the electronic edition of the Astrophysical Journal. A portion is shown here for guidance regarding its form and content.

cold dust (so that the spectrum peaks past ∼20 μm) in Groups 4 and 5. Spectra are assigned to subgroups based on the dominant features in the spectra. The carbon stars are those with the following classifications: 1.NC (naked star with carbon-rich molecular absorption bands), 2.CE and 3.CE (optically thin carbon-rich dust emission), and 3.CR (reddened spectra from optically thick carbon-rich dust emission). The original sample of 34 described by Leisenring et al. (2008) did not include any naked carbon stars; we have added three 1.NC sources. Nor did it consider the 23 slower SWS scans, which adds three more sources. The additional two sources were simply overlooked before.

3. ANALYSIS

3.1. *The Manchester method*

Sloan et al. (2006) and Zijlstra et al. (2006) introduced the Manchester method to extract and compare information uniformly from large samples of infrared spectra from carbon stars. The key metric is the [6.4]−[9.3] color, which samples the spectrum at two wavelengths that are relatively free of molecular absorption bands and solid-state emission features. This color reddens as the amount of amorphous carbon grows above the stellar photosphere. Groenewegen et al. (2007) found that the [6.4]−[9.3] color increased linearly with the log of the dust-production rate (DPR). The current sample includes bluer sources which deviate from a linear relationship, and it requires a more complex formulation (e.g. Matsuura et al. 2009; Gullieuszik et al. 2012; Riebel et al. 2012). All of these formulations are based on a tight relationship between color and DPR and reinforce our assumption that the [6.4]−[9.3] color is a good proxy for DPR.

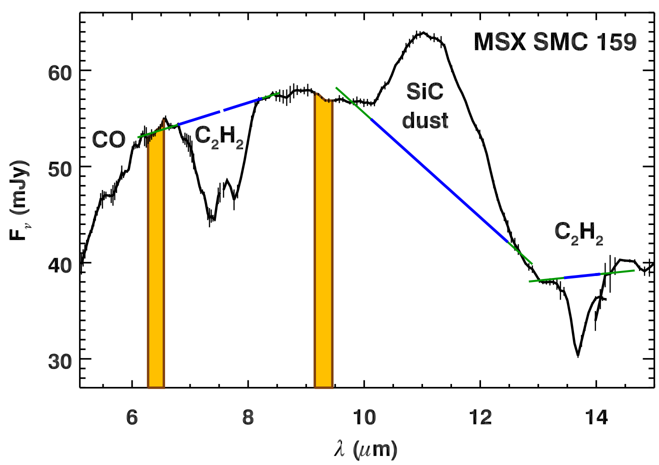

FIG. 1.— The Manchester method applied to the 5–15 μm spectrum of MSX SMC 159. The [6.4]−[9.3] color provides an estimate of the relative contributions of stellar photosphere and amorphous carbon dust in two spectral regions relatively free of absorption or emission features. Line segments are used to estimate the continuum under or over the C_2H_2 absorption band at 7.5 μm, the Q branch of the C_2H_2 band at 13.7 μm, and the SiC dust emission feature at ∼11.3 μm.

The Manchester method measures the equivalent width of the acetylene absorption bands at 7.5 and 13.7 μm by fitting line segments to the continua to either side. The 13.7 μm band is actually just the Q branch of a broader feature, and we will focus on the stronger 7.5 μm band. The strength of the SiC

TABLE 5
SPECTROSCOPIC DATA — IRS SAMPLE

Target	Eq. width of C_2H_2 at 7.5 um	F_{SiC} / continuum	[6.4]−[9.3] (mag.)	[16.5]−[21.5] (mag.)	F_{MgS} / continuum	IR spectral classification
GM 780	0.162 ± 0.010	0.316 ± 0.006	0.403 ± 0.008	0.165 ± 0.024	···	CE2
MSX SMC 091	0.146 ± 0.015	0.147 ± 0.007	0.528 ± 0.007	0.073 ± 0.025	···	CE2
MSX SMC 062	0.117 ± 0.006	0.062 ± 0.003	0.675 ± 0.008	0.174 ± 0.024	···	CE3
MSX SMC 054	0.177 ± 0.006	0.179 ± 0.003	0.756 ± 0.004	0.101 ± 0.016	0.191 ± 0.021	CE3
2MASS J004326	0.196 ± 0.007	0.080 ± 0.006	0.234 ± 0.019	···	···	CE1
MSX SMC 044	0.050 ± 0.005	0.024 ± 0.004	0.517 ± 0.006	−0.101 ± 0.046	···	CE2
MSX SMC 105	0.184 ± 0.008	0.157 ± 0.005	0.866 ± 0.003	0.226 ± 0.022	0.254 ± 0.029	CE3
MSX SMC 036	0.234 ± 0.006	0.088 ± 0.004	0.774 ± 0.005	0.286 ± 0.017	0.279 ± 0.021	CE3
GB S06	0.113 ± 0.005	0.058 ± 0.002	0.969 ± 0.003	0.284 ± 0.020	0.358 ± 0.025	CE4
MSX SMC 200	0.032 ± 0.007	0.010 ± 0.003	0.443 ± 0.008	0.067 ± 0.029	···	CE2

NOTE. — Table 5 is published in its entirety in the electronic edition of the Astrophysical Journal. A portion is shown here for guidance regarding its form and content.

TABLE 6
SPECTROSCOPIC DATA — SWS SAMPLE

Target	Alias	Eq. width of C_2H_2 at 7.5 um	F_{SiC} / continuum	[6.4]−[9.3] (mag.)	[16.5]−[21.5] (mag.)	F_{MgS} / continuum	IR spectral classification
WZ Cas	···	0.347 ± 0.007	−0.022 ± 0.002	0.029 ± 0.002	0.438 ± 0.004	···	CE0
VX And	···	0.238 ± 0.001	0.182 ± 0.001	0.123 ± 0.003	0.067 ± 0.010	···	CE1
HV Cas	···	0.090 ± 0.001	0.226 ± 0.001	0.353 ± 0.002	−0.139 ± 0.004	···	CE2
R Scl	···	0.290 ± 0.002	0.205 ± 0.001	0.273 ± 0.002	0.266 ± 0.002	0.292 ± 0.004	CE1
R For	···	0.125 ± 0.001	0.279 ± 0.001	0.361 ± 0.001	0.131 ± 0.003	···	CE2
AFGL 341	V596 Per	0.063 ± 0.001	0.073 ± 0.001	1.665 ± 0.005	0.407 ± 0.008	0.411 ± 0.010	CE5
CIT 5	V384 Per	0.065 ± 0.001	0.305 ± 0.002	0.682 ± 0.001	0.323 ± 0.002	0.186 ± 0.002	CE3
U Cam	···	0.078 ± 0.001	0.327 ± 0.001	0.107 ± 0.002	0.157 ± 0.004	···	CE1
W Ori	···	0.064 ± 0.001	0.229 ± 0.001	0.055 ± 0.001	−0.054 ± 0.004	0.137 ± 0.002	CE1
IRC −10095	V1187 Ori	0.277 ± 0.002	0.192 ± 0.001	0.163 ± 0.003	0.196 ± 0.008	0.784 ± 0.012	CE1

NOTE. — Table 6 is published in its entirety in the electronic edition of the Astrophysical Journal. A portion is shown here for guidance regarding its form and content.

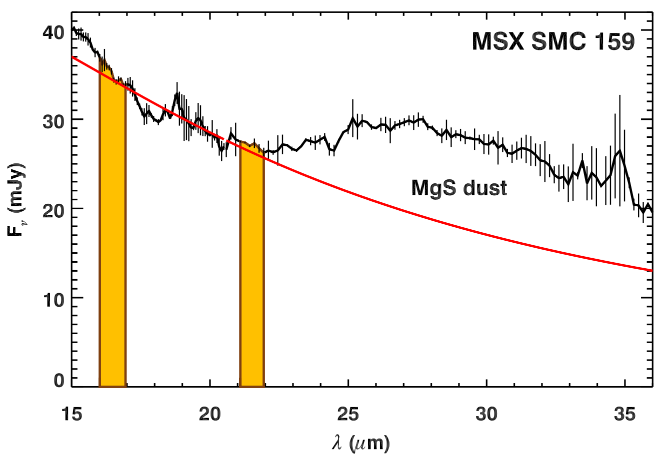

FIG. 2.— The Manchester method applied to the 15–37 μm spectrum of MSX SMC 159. The [16.5]−[21.5] color estimates the continuum temperature at longer wavelengths in order to estimate the continuum under the MgS dust emission feature at longer wavelengths.

dust emission feature at ∼11.5 μm is measured similarly and is reported as a ratio of integrated flux in the feature to the integrated flux in the underlying continuum.

We also measure the strength of the 26–30 μm feature attributed to MgS, but because the IRS spectral coverage cuts off the long-wavelength side of the feature, we use a two-step process. First we estimate a continuum based on the apparent color of the spectrum at 16.5 and 21.5 μm. Then we integrate the spectrum above this estimated continuum. If the spectra do not appear to be turning down at the long-wavelength cutoff, we assume that the 26–30 μm feature is not present or is contaminated in some way and do not report a value. As with the SiC feature, we report the integrated flux in the feature, divided by the integrated continuum.

Figures 1 and 2 illustrate the application of the Manchester method to the spectrum of one Magellanic carbon star, MSX SMC 159. Sloan et al. (2006) presented similar figures for the same star (see their Figures 4 and 5). The difference is that we used optimal extraction for the spectrum here, with a noticeable improvement in SNR.

Table 5 presents the results for the IRS sample of carbon stars in the Magellanic Clouds. Table 6 presents the 42 Galactic carbon stars observed with the SWS. The results in Table 6 differ from those presented by Leisenring et al. (2008) because of differences in how the continuum was estimated. As explained in Appendix A, the [6.4]−[9.3] colors of two sources, IRAS 04589 and IRAS 05306, were artificially reddened because the spectra were badly mispointed. For these, we replaced the [6.4]−[9.3] colors with values estimated from their photometric [5.8]−[8] color.

3.2. *Spectral classification*

Table 5 also includes infrared spectral classifications, which are based on modifications to the two-level scheme applied by Kraemer et al. (2002) to the SWS data (see Section 2.5). The original scheme envisioned a third level of classification for some of the more populated subgroups, but this level was

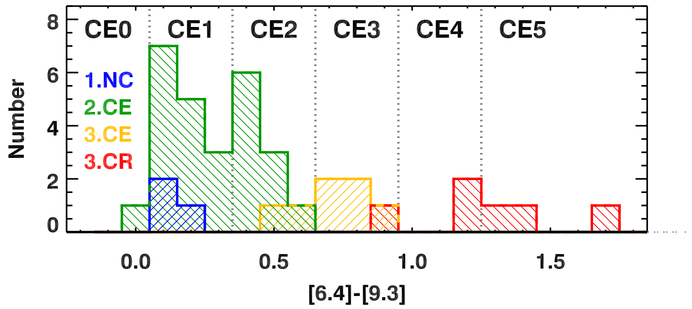

FIG. 3.— The distribution of the Galactic carbon stars in our control sample with [6.4]−[9.3] color, segregated by their infrared spectral classifications from Kraemer et al. (2002). The [6.4]−[9.3] color increases nearly monotonically along the sequence 1.NC–2.CE–3.CE–3.CR.

adopted only for the silicate emission (SE) sources by using the SE indices defined by Sloan & Price (1995).

The scheme as modified here changes how carbon stars are classified. Previously, they fell into four groups in the sequence 1.NC–2.CE–3.CE–3.CR as the carbon-rich dust shell grew progressively thicker and redder. The new scheme replaces this sequence with CE0–CE5, depending solely on the [6.4]−[9.3] color, with the breaks at a color of 0.05 and at intervals of 0.30 from there to 1.25.

Figure 3 uses the classifications of Galactic carbon stars by Kraemer et al. (2002) to show that the old classifications closely follow the [6.4]−[9.3] color. The new sequence shifts the boundaries between the subclasses, but presents them in a more easily recognizable sequence.

Some of the redder CE5 sources show negative values for the SiC-to-continuum ratio, because the SiC feature is in absorption instead of emission. For those sources with a 3σ detection or better, we have designated them as "CA" instead of "CE", for absorption instead of emission. This classification is analogous to "SA" versus "SE" introduced for silicates by Sloan & Price (1995).

4. RESULTS

The present sample has added over 70 sources to the previously published samples of Magellanic carbon stars. The first question to address is whether or not the larger sample contradicts any earlier conclusions. We therefore base our analysis, as before, on comparisons using the [6.4]−[9.3] color as a proxy for DPR. This approach compares the properties of the stars and their spectra from populations with different metallicities but similar DPRs.

4.1. *The [6.4]−[9.3] color*

Figure 4 shows how the [6.4]−[9.3] color of the carbon stars depends on pulsation period. The larger sample considered here reinforces the previous conclusions. First, the dust-production rate, as measured by the [6.4]−[9.3] color, generally increases with longer pulsation periods, once the period exceeds $\sim$250 d. Second, the scatter is significant, with a range of DPRs possible at a given pulsation period. Third, the three galaxies considered show no obvious differences, indicating that metallicity does not have a noticeable effect.

4.2. *Infrared spectral features*

4.2.1. *Silicon carbide dust*

Figure 5 shows that the dependence of the strength of the SiC feature on the [6.4]−[9.3] color changes with host galaxy. For the Galactic sources, the SiC dust emission increases

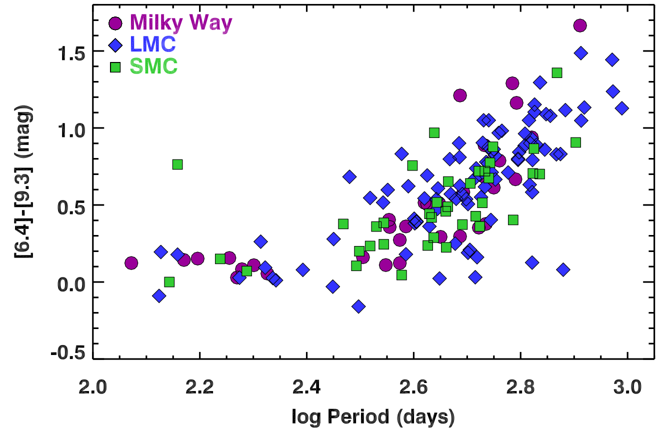

FIG. 4.— The [6.4]−[9.3] color of the carbon stars in the Galaxy, LMC, and SMC as a function of pulsation period. For periods $\gtrsim$250 days, the colors generally grow redder with longer periods, but with considerable scatter. No dependency on metallicity is apparent.

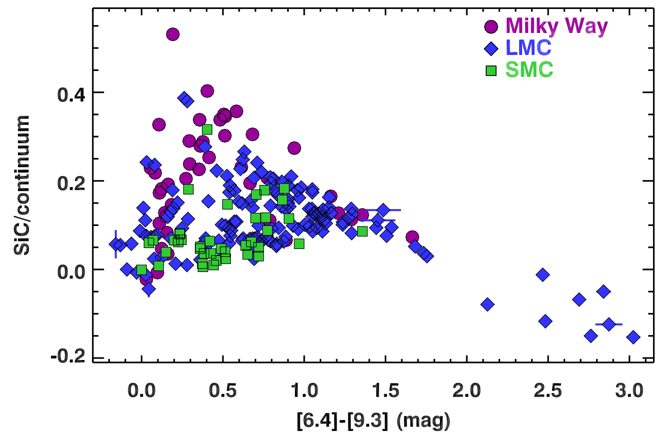

FIG. 5.— The strength of SiC dust emission as a function of [6.4]−[9.3] color. As the [6.4]−[9.3] color increases, stars follow one of two tracks. The SiC strength increases quickly in more metal-rich stars, then turns over and decreases. In metal-poor stars, the SiC strength increases more gradually. Most of the stars with [6.4]−[9.3] $\gtrsim$ 1.5 have negative SiC strengths, indicating absorption.

quickly from [6.4]−[9.3] = 0 to $\sim$0.4, then drops steadily to a color of $\sim$1.7, which is the maximum in the Galactic sample. Most of the carbon stars in the SMC sample behave differently, with SiC strength rising more gradually with color to [6.4]−[9.3] $\sim$ 1.4 for the reddest carbon star observed with the IRS in the SMC. The LMC sample is more evenly split between the upper and lower sequences.

Sloan et al. (2006) first noticed this metallicity-dependent difference when they compared samples from the Galaxy and the SMC. As more carbon stars were added from the SMC (Lagadec et al. 2007) and LMC (Zijlstra et al. 2006; Leisenring et al. 2008), the two tracks in Figure 5 remained separate. Zijlstra et al. (2006) pointed out that metallicity will determine the availability of silicon, so that metal-rich stars generally populate the sequence with stronger SiC emission while metal-poor stars show weaker SiC features.

All eight of the stars with [6.4]−[9.3] $\gtrsim$ 2.0 have negative SiC/continuum ratios, which indicate SiC absorption in optically thick dust shells. The seven carbon-rich EROs observed by Gruendl et al. (2008) all show SiC absorption; two of these were re-observed as potential post-AGB objects by Matsuura et al. (2014). The eighth source was part of the SAGE-Spec

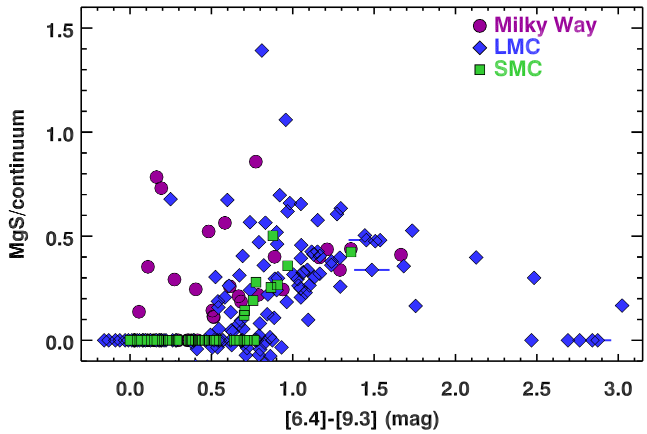

FIG. 6.— The strength of MgS dust emission as a function of [6.4]−[9.3] color. More metal-poor stars have to have redder [6.4]−[9.3] colors before MgS becomes visible.

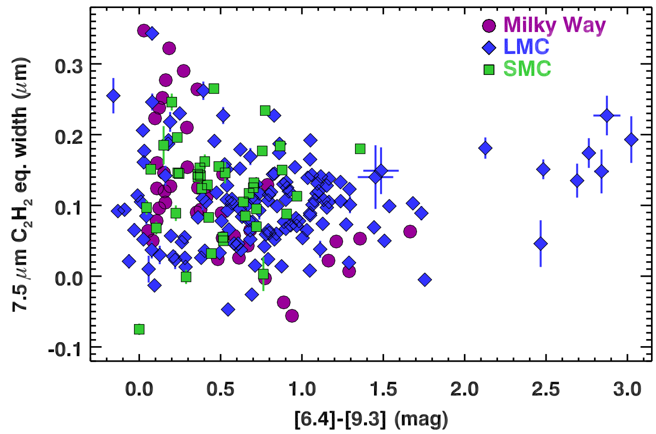

FIG. 8.— The strength of the 7.5 μm C_2H_2 absorption band versus [6.4]−[9.3] color.

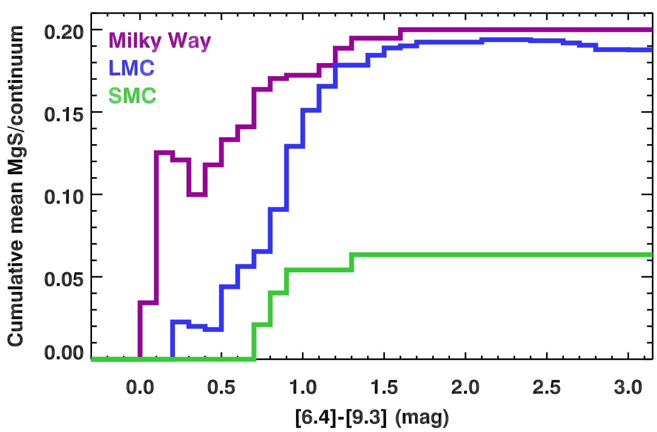

FIG. 7.— The cumulative mean MgS emission. At each color, the mean MgS/continuum strength for all sources with bluer colors is plotted.

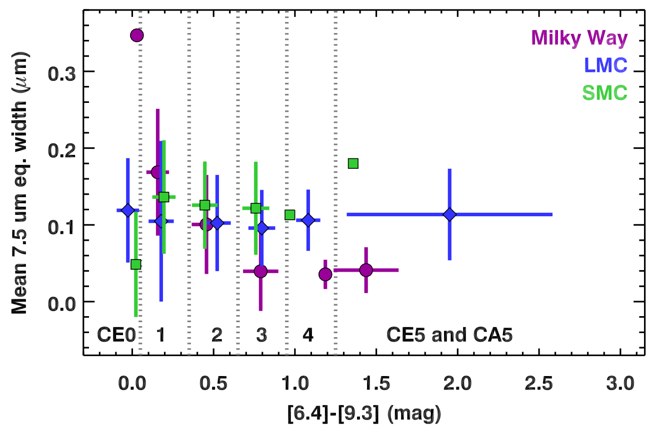

FIG. 9.— The strength of the 7.5 μm C_2H_2 absorption band versus [6.4]−[9.3] color, binned by CE class to illustrate the general trends in the data. When determining means, negative equivalent widths have been treated as zero, because acetylene emission is unlikely.

program (Kemper et al. 2010). All have spectroscopic properties consistent with deeply embedded objects near the end of their AGB lifetimes.

4.2.2. *Magnesium sulfide dust*

Figure 6 shows how the MgS emission increases with [6.4]−[9.3] in the different populations. MgS is apparent in the Galactic sample at all [6.4]−[9.3] colors, while in the LMC, the first MgS feature is at [6.4]−[9.3] $\sim$ 0.25. No other LMC source shows MgS until [6.4]−[9.3] reaches a value $\sim$0.5. In the SMC, MgS does not appear until [6.4]−[9.3] $\sim$ 0.7.

Figure 7 illustrates the behavior of the MgS emission differently, by plotting the mean MgS/continuum strength for all data up to a given [6.4]−[9.3] color. It shows more clearly how the LMC lags the Milky Way, with the SMC even further behind, as the [6.4]−[9.3] color increases. The traces for the Milky Way and SMC are unchanged past colors of $\sim$1.6 and 1.4, respectively, due to a lack of redder sources. The lower abundances of Mg and S in more metal-poor stars appear to be delaying the condensation of MgS until the dust-production rate is higher and the dust is cooler.

4.2.3. *Acetylene gas at 7.5 μm*

Figure 8 compares the behavior of the 7.5 μm absorption band from C_2H_2 for the different samples. For the less dusty stars ([6.4]−[9.3] $\lesssim$ 0.35), all three galaxies show a range of band strengths, but to the red, the upper bound diminishes. Figure 9 clarifies the behavior of each galaxy by plotting the mean equivalent width and color for each CE class. For CE2 and redder sources, the mean equivalent width of the 7.5 μm acetylene band is consistently strongest in the SMC and weakest in the Galaxy.

As shown below (Section 4.5), all of the CE0 and most of the CE1 sources are associated with relatively dust-free carbon stars which can have strong molecular absorption bands due to the lack of veiling from the dust surrounding the redder sources. Sloan et al. (2015b) found that in the SMC, the dusty stars with veiled molecular bands usually are pulsating in the fundamental mode with strong amplitudes as Mira variables, while the other group are detected as semi-regulars or irregulars. To focus on the dust-production process, we should focus on the stars classified as CE2 or later.

To make a quantitative comparison of the 7.5 μm acetylene band, we examine the CE2–3 sources, because the CE4 and CE5 classes have only one SMC source each. We set negative equivalent widths to zero, because 7.5 μm emission is unlikely. For the chosen color range, the mean equivalent width of the 7.5 μm band decreases from 0.12$\pm$0.01 μm in the SMC to 0.10$\pm$0.01 μm in the LMC and to 0.08$\pm$0.02 μm in the Galaxy (the quoted errors are the uncertainty in the

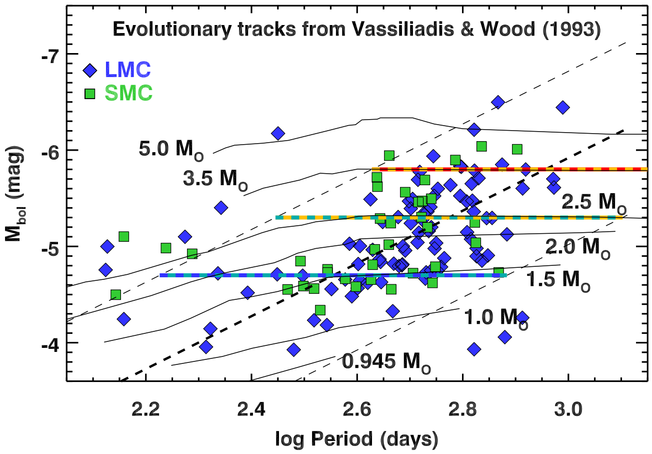

FIG. 10.— A period-luminosity plot showing how we binned the Magellanic carbon stars into four initial-mass groups based on their bolometric luminosities. The thick dashed line is the period-luminosity relation fitted to the fundamental-mode pulsators, and the thin dashed lines to either side enclose the range we will consider to be on the fundamental-mode sequence. Within this range, evolutionary tracks on the AGB are generally close to horizontal, as demonstrated by the tracks from Vassiliadis & Wood (1993). The multi-colored horizontal lines show the boundaries between the mass bins.

mean). While the spread in each sample is substantial, the steady drop in mean band strength is still apparent. Thus the expanded IRS sample has not changed the conclusions drawn before about the 7.5 μm acetylene band.

While the behaviors of the C_2H_2 absorption at 7.5 μm and the SiC emission at 11.5 μm differ quantitatively, their rough similarity raises a possible concern, which we have examined and ruled out. Acetylene also shows a strong absorption band centered at 13.7 μm, but the sharp absorption band apparent at 13.7 μm is just from the Q branch ($\Delta J = 0$), with the P and R branches extending the feature over a micron in either direction. The possible SiC emission could be affected by strong C_2H_2 absorption to the red, which could push the continuum fit down and artifically add to the measured emission. We investigated by shifting the wavelengths used to fit the continuum on the red side of the SiC feature. Figure 1 shows an inflection on the SiC feature at $\sim$12.0 μm. We shifted the red continuum wavelengths to this inflection and recalculated the intregated SiC flux for our samples, and found that, while the total SiC emission certainly grew smaller, the samples behaved the same qualitatively, and the differences in how the three galaxies behaved were unchanged.

4.3. *Bolometric magnitudes*

For each star in the Magellanic sample, we can estimate its bolometric magnitude ($M_{\rm bol}$) by integrating its spectral energy distribution, which is determined from the IRS spectra and the mean magnitudes from the multi-epoch photometry described in Section 2.4. We integrated through the photometry below 5 μm using linear interpolation, then integrated the IRS spectrum. To the blue of the optical photometry, we assumed a Wien distribution. To the red of the IRS data, we assumed a Rayleigh-Jeans tail. If the IRS spectrum only included data from SL (i.e. stopped at 14 μm), we also utilized the MIPS data at 24 μm. The resulting estimates for $M_{\rm bol}$ appear in the last column of Table 4.

Our IRS sample includes six carbon stars in NGC 419. At an assumed distance modulus of 18.90, the median absolute magnitude for these stars = -4.79 ± 0.23, with $M_{\rm bol} = -5.24$ for NGC 419 IR 1 and -4.73 for NGC 419 MIR 1. These values are consistent with an estimated zero-age main-sequence mass of 1.9 M$_\odot$ (Kamath et al. 2010) and an age of 1.35 Gyr (Girardi et al. 2009), based on models of the AGB and red clump, respectively. The bolometric magnitudes of NGC 419 compare well with the rest of the SMC, which has $<M_{\rm bol}> = -5.03 \pm 0.49$. If NGC 419 were in front of the SMC at a distance modulus of 18.50 (Glatt et al. 2008), then its median $M_{\rm bol}$ would lie outside the 1σ range for the SMC, making it older than most of the carbon stars observed by the IRS in the SMC.

TABLE 7
PERIOD-CORRECTED DIFFERENCES IN [6.4]−[9.3] COLOR

Approximate initial mass (M$_\odot$)	Δ(LMC) − Δ(SMC) (mag.)[a] Using one fitted line	Fitting to each mass bin
$\sim$4	0.083 ± 0.098	−0.001 ± 0.077
$\sim$3	0.147 ± 0.100	0.054 ± 0.103
$\sim$2	0.112 ± 0.048	0.032 ± 0.043
$\sim$1	0.157 ± 0.093	0.131 ± 0.100

[a] Δ = median { $([6.4]-[9.3])_{obs} - ([6.4]-[9.3])_{line}$ }.

Figure 10 includes evolutionary tracks from Vassiliadis & Wood (1993) on the period-luminosity plane and also shows the location of the P-L relation for fundamental-mode pulsators. For stars with higher initial mass and for lower-mass stars with longer periods, the evolutionary tracks are nearly horizontal, so that $M_{\rm bol}$ can be used as a proxy for initial mass. We have therefore divided the fundamental-mode pulsators into four mass bins with the horizontal lines defined in Figure 10 as boundaries. While the evolutionary tracks do deviate from horizontal for shorter pulsation periods, the figure shows that this has little impact on the stars in our sample, provided we only consider stars with periods $\gtrsim$ 250 days (log $P \sim 2.4$).

It should be emphasized that the estimates for initial mass are rough and are not to be taken too literally or quantitatively. The key is the steady bolometric magnitude on the late stages of the evolutionary tracks. These make it possible to use $M_{\rm bol}$ to segregate the data by initial mass for statistical purposes.

The thick black dashed line in Figure 10 is a period-luminosity relation, first fitted to all of the Magellanic stars in our sample with periods > 250 days, then fitted iteratively to only those within an envelope of $\pm$ 0.9 magnitudes to avoid stars not on the fundamental-mode sequence. The linear solution converges quickly:

$$M_{\rm bol} = 2.30 - 2.74 \log P \text{ (days)}. \qquad (1)$$

This line is steeper than the P-L relation by Whitelock et al. (2006). They found a slope of -2.54 using bolometric corrections to estimate $M_{\rm bol}$, while our estimates are based on integrations through the IRS data and the available photometry at shorter wavelengths. Sloan et al. (2015b) noted that the estimated bolometric magnitudes of the dustiest sources, which tend to have the longest periods, depend on the precise method used. Here, we have spectral data covering the peak of the spectral energy distribution for those sources, which should improve on the cases where only photometry is available.

4.4. *The period-color relation and initial mass*

Figure 11 reprises Figure 4, except that the sources are color-coded by our rough estimates of their initial mass. Figure 11 explains the width of the relationship of [6.4]−[9.3]

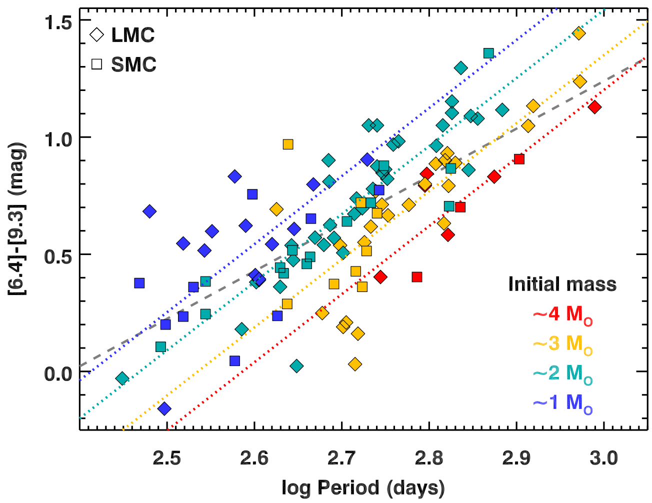

FIG. 11.— The [6.4]−[9.3] color as a function of pulsation period with the Magellanic sample, color-coded by their initial mass as estimated from their bolometric magnitude. Sources not assigned to a mass bin are not included. The width of the relation between [6.4]−[9.3] color and period clearly arises from the mass distribution of the samples. The gray dashed line is a line fitted to all of the data, while the colored dotted lines are fitted to each mass bin separately (see Section 4.3).

versus period. The Magellanic samples include a range of masses, each of which follows its own narrow relation. When stars switch from overtone pulsations to the fundamental mode, they begin to produce dust at significant rates for the first time, and this rate increases as their pulsation period increases. The slope to the period-luminosity relation means that this mode switch occurs at longer pulsation periods for more luminous (and thus more massive) stars, which explains why segregating by mass reveals the parallel tracks in Figure 11. The finite width of the period-luminosity relation suggests that this scenario of increasing pulsation period and increasing DPR and mass-loss rate can be sustained for a limited time.

Sloan et al. (2008) concluded that for Magellanic carbon stars, metallicity did not play a detectable role in dust production, because the Galaxy, LMC, and SMC showed indistinguishable relations between [6.4]−[9.3] color and pulsation period. However, more metal-poor carbon stars in other nearby Local Group dwarf galaxies ([Fe/H] $\lesssim -1$) do show less dust than might be expected for their pulsation period (Sloan et al. 2012).

The data in Figure 11 point to the need to account for the different mass distributions of the carbon stars observed by the IRS in the LMC and SMC in order to re-assess if the role of metallicity can be detected for [Fe/H] $\gtrsim -1$. A line fitted to all of the data gives

$$[6.4]-[9.3] = -4.52 + 1.91 \log P \text{ (days)}. \quad (2)$$

For each star, we used this line to predict the expected [6.4]−[9.3] color based on the pulsation period and compared it to the observed [6.4]−[9.3] color. For each mass bin and for each galaxy, we computed the median of these offsets. Table 7 gives the difference in these median offsets, along with the propagated uncertainty in the mean (in the column labeled "Using one fitted line"). Averaging the differences between LMC and SMC across the mass bins reveals a redder [6.4]−[9.3] color in the LMC of 0.125 ± 0.042 magnitudes, which is a 2.9 σ result.

The data in each mass bin in Figure 11 follow a steeper

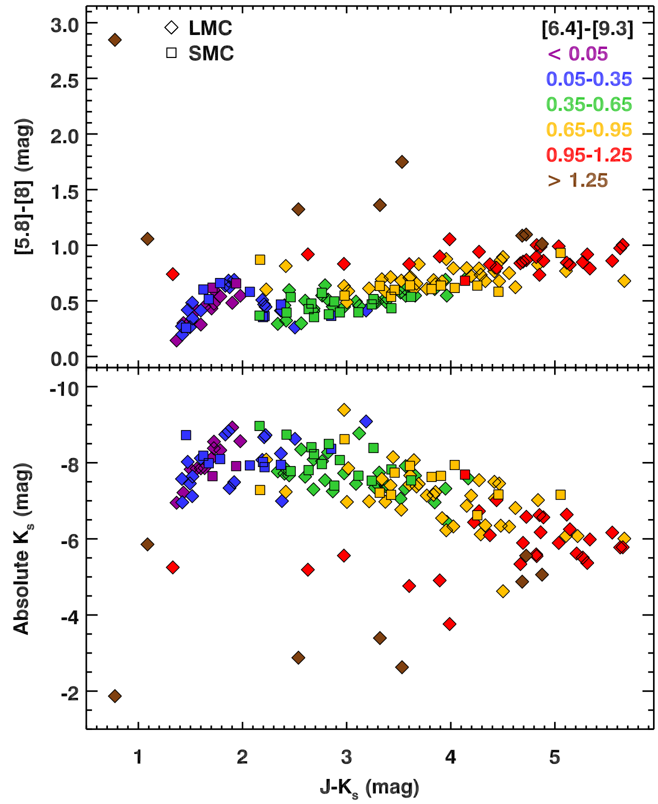

FIG. 12.— Color-color and color-magnitude diagrams featuring the $J-K_s$ colors on the horizontal axis. Symbols are coded for galaxy with shape and for [6.4]−[9.3] color with color. The [6.4]−[9.3] intervals correspond to the CE0–5 classifications. None of the CE5s and only about half of the CE4s follow the sequences. (CE4: $0.95 < [6.4]-[9.3] < 1.25$; CE5: $[6.4]-[9.3] > 1.25$.)

slope than the total data set, and the carbon stars in the LMC and SMC do not have the same period distributions. To further correct for this difference in the sample, we have fitted lines independently to the four mass bins. Because these lines are driven somewhat by the noise in our data, we found the weighted mean of the slopes (2.91 mags/dex) and used this slope for each mass bin. The colored dotted lines in the figure illustrate the results. Table 7 gives the resulting median difference in [6.4]−[9.3] between the LMC and SMC. The average from the four mass bins is 0.054 ± 0.040, which is only a 1.3 σ result.

We conclude that the full sample of Magellanic carbon stars observed by the IRS shows hints of a subtle dependence of dust-production rate with metallicity, but once we account for different distributions by initial mass and metallicity, our sample does not reveal a statistically significant result. The effects of pulsation period and initial mass on dust production are much stronger.

4.5. *Color-color and color-magnitude space*

Carbon stars fall along a well-defined sequence in most infrared color-color diagrams, with each color increasing steadily and monotonically as the DPR increases. The [5.8]−[8] color is an exception, because it is sensitive to both dust content and the strength of molecular absorption in the 5.8 μm filter (Srinivasan et al. 2011). Figure 12 plots the [5.8]−[8] color versus $J-K$ in the top panel. From $J-K \sim$ 1.3 to 2, increasing molecular absorption reddens [5.8]−[8], but for $J-K \gtrsim 2$, increasing dust opacity is the culprit. Sloan

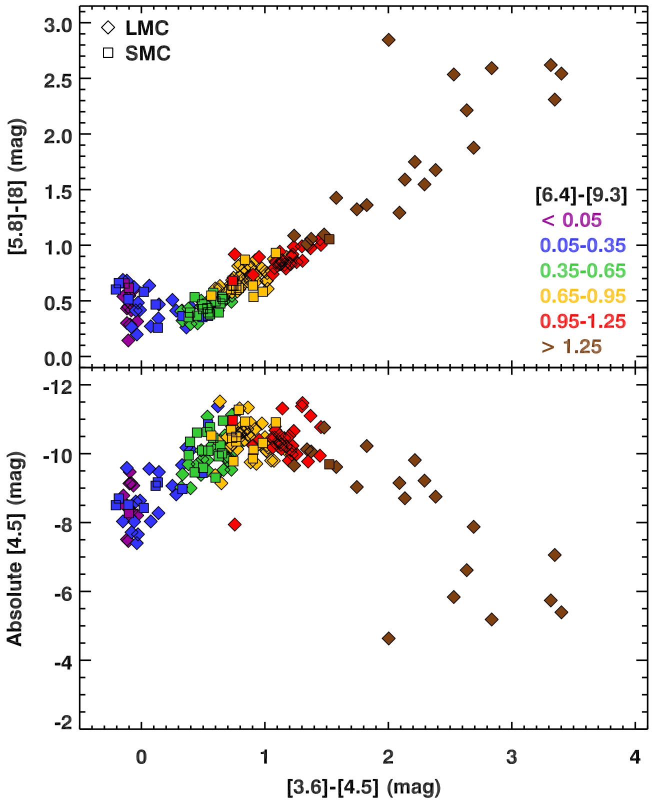

FIG. 13.— Color-color and color-magnitude diagrams featuring the [3.6] − [4.5] colors on the horizontal axis. Symbols are coded for galaxy with shape and for [6.4]−[9.3] color with color. The [6.4]−[9.3] intervals correspond to the CE0–5 classifications. Only a handful of the reddest sources in [5.8]−[8] are off the sequence, along with one CE4.

et al. (2015b) called these two sequences "molecular" and "dusty" to identify the agent responsible for the reddening. They found that semi-regular variables dominate the molecular sequence ($J-K \lesssim 2$), while Mira variables dominate the dusty sequence. This difference is not between overtone and fundamental-mode pulsators, as half of the semi-regulars are pulsating in the fundamental mode. Rather, it is a difference between stars pulsating with small and large amplitudes. Generally, it is the latter that are associated with dust production.

The bottom panel of Figure 12 presents the sample in a more familiar near-IR CMD. Blum et al. (2006) labeled the sequence extending to the red of $J-K_s \sim 2$ as the "extreme" AGB stars,[18] but this terminology is something of a misnomer, as the objects are only extreme in the sense that they are producing carbon-rich dust, something that all carbon stars must do before they end their lives on the AGB. Superlatives like "extreme" are more appropriate for the extremely red objects discovered in the LMC by Gruendl et al. (2008). These are the deeply embedded carbon stars analogous to targets in the Galaxy like AFGL 3068 (e.g., Lebofsky & Rieke 1977; Jones et al. 1977). We will follow the practice of Sloan et al. (2015b) and refer to objects with $J-K_s \gtrsim 2$ as "dusty" carbon stars, by which we mean carbon stars associated with significant and readily measurable quantities of dust.

Figure 13 replaces the J and K_s filters in Figure 12 with [3.6] and [4.5]. In all four panels of the two plots, the [6.4]−[9.3] color generally increases along the sequence from blue to red, but with some scatter. This scatter appears in any

[18] Formally, their criterion was $J-[3.6] > 3.1$.

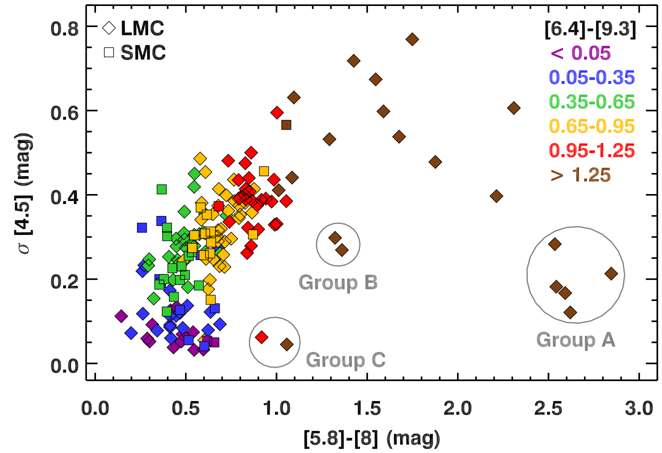

FIG. 14.— The amplitude of the variability at 4.5 μm (as measured by the standard deviation of the IRAC and *WISE* data) as a function of [5.8]−[8] color. The amplitude increases steadily from the naked carbon stars to the CE4 sources, then drops for those with the reddest [5.8]−[8] and [6.4]−[9.3] colors. The circled groups are discussed in Section 4.6.

color chosen, and it is consistent with what one would expect from variations in DPR as a function of time, with bluer colors sensitive to warmer and more recently formed dust.

The CE1 sources ($0.05 < [6.4]-[9.3] < 0.35$) straddle the boundary between the molecular and dusty sequences in both figures. On the molecular sequence, the overlap between CE0 and CE1 is complete, despite the presence of more dust in the CE1 sources, and it shows that the dust is not determining position on this sequence. The vertical spread of the molecular sequence in the bottom panel of Figure 13 shows that the [3.6]−[4.5] color is less sensitive to molecular bands than $J-K_s$.

In Figure 12, none of the CE5 stars ($[6.4]-[9.3] > 1.25$) follow the relationship between [5.8]−[8] and $J-K_s$ established by the sources with less dust. If they did, they would be off the right-hand edge of the plot, provided we could detect them at J and K_s. Because these sources are so embedded, if they followed the dusty sequence, they would actually be below the detection limit of the near-IR surveys we examined. Of the 21 CE5 sources, we have valid $J-K_s$ colors for only nine, and all appear with bluer $J-K_s$ colors than the dusty sequence would lead us to expect. In the bottom panel, all of the CE5 sources plotted are also off the sequence. Their behavior is fully consistent with a shift to bluer $J-K_s$ colors. Several of the CE4 and even some CE3 sources can also be seen to have shifted. In Figure 13, no sources are missing, and the number of off-sequence sources is greatly reduced, with only a few CE5 sources not on the dusty sequence in either panel.

As noted in Section 2.4, it is only for the deeply embedded sources that a photometric mismatch is a danger, and even then the odds of a mismatch are slight for a given source. We conclude that most or all of our off-sequence sources have colors indicative of the source itself and not a chance superposition of two sources in the search beam.

4.6. *Variability*

If the off-sequence sources in Figure 13 have really moved off the AGB, then the amplitude of their variability should have dropped. Figure 14 plots the variability amplitude of all of our carbon stars as a function of [5.8]−[8] color. The values plotted are the standard deviations (σ) of the mean magnitudes in Tables 3 and 4. For a pulsation cycle which follows a sine function, the peak-to-peak amplitude = $2\sqrt{2}\sigma$.

As the stars shift from CE0 (nearly naked) to CE5 (very dusty), the amplitude of their variability increases as they grow redder, but once [5.8]−[8] reaches a value of ∼1.5, the amplitude begins to decline. The three sources furthest from the carbon sequence in the top panel of Figure 13 are all in Group A in the bottom right-hand corner of Figure 14. These are both the reddest and the least variable sources in the sample. More recent photometry of the reddest carbon stars in the LMC at 3.6 and 4.5 μm extends the temporal baseline and confirms the trend of decreasing variability with increasing [5.8]−[8] color (Sargent et al., in preparation).

Had we chosen to use the variability amplitude at 3.6 μm instead of 4.5 μm, the results would have been the same qualitatively. Dropping the color corrections derived in Appendix A also does not change the result qualitatively. It does change the apparent variabilities quantitatively, increasing the apparent amplitudes for the stars which are most variable because it increases the apparent scatter in the data, but for the relatively non-variable sources, this effect is much smaller. By using the 4.5 μm data, we have reduced possible errors from the corrections even more, since the *WISE*-to-IRAC corrections are much smaller at 4.5 μm than at 3.6 μm.

Four more sources appear to be relatively non-variable for their [5.8]−[8] color, and are labelled as Groups B and C in Figure 14. Group C includes one CE4 source (red diamond), SAGE J054546, which is also off-sequence in the bottom panel of Figure 13. The remaining three are all CE5, and except for unusually low-variability amplitude, none stands out in any other significant way.

5. DISCUSSION

5.1. *Evolution off the AGB*

The three sources most clearly off the carbon sequence in the color-color diagram in Figure 13 have [5.8]−[8] > 2.5 and [3.6]−[4.5] < 3. They are IRAS 05133, IRAS 05191, and IRAS 05260, in order of increasing [3.6]−[4.5] color. The other two sources with [5.8]−[8] > 2.5 are IRAS 05026 and IRAS 05042. Group A in Figure 14 consists of these five stars. They are much less variable than the rest of the sources with [5.8]−[8] $\gtrsim$ 1.5. And all five are also SiC absorption (CA) sources.

In the top panel of Figure 12, the only CA source with a $J-K_s$ color is IRAS 05133, and it is bluer than any other carbon star in our sample! Whatever has led to its unusually blue [3.6]−[4.5] color has allowed us to detect an even bluer source at J and K_s. With K_s = 16.6 and J = 17.4, it is just at the detection limit. The other four sources are redder at [3.6]−[4.5], have more extinction in the near-IR, and consequently are undetected at J and K_s.

Thus the five most embedded carbon stars in our sample (as measured with [5.8]−[8]) have properties consistent with evolution off the AGB. Their variability is lower than the less embedded sources, they show SiC absorption, indicating high column densities of dust, and three appear to be developing double-peaked SEDs as the central star becomes visible.

However, other stars are relatively non-variable, and others also show SiC absorption. Of the other non-variable sources, all but SAGE J054546 (CE4) are either CE5 or CA5 (i.e. [6.4]−[9.3] > 1.25). These sources may be approaching the end of their AGB evolution.

The steady decline in variability past [5.8]−[8] ∼ 1.5 (Figure 14) suggests that more than just the handful of sources most obviously off of the sequences in Figure 13 are approaching the end of their AGB lifetimes.

5.2. *Non-spherical dust shells*

For the off-sequence sources, the excess blue flux indicates that we are able to peer into the dust and glimpse the central star, either directly or through scattered light. The dust envelope may be growing patchy or it may be distributed asymmetrically, perhaps in a torus or possibly even a disk.

Figure 12 reveals other sources which do not follow the carbon-star sequence at J and K_s, even though they are on the sequence in the longer-wavelength filters in Figure 13. In particular, a number of CE4 sources (in red) are off-sequence in both panels of Figure 12, with much bluer $J-K_s$ colors than expected for either their [5.8]−[8] colors or K_s magnitudes. More of the CE5 sources also behave similarly.

The opacity of amorphous carbon dust drops as $\sim\lambda^{-2}$, making it difficult to explain how we could directly observe the central source at J and K but not at 3.6 and 4.5 μm. If we are detecting the central source via light scattered above and below a disk or in the polar regions of an asymmetric dust shell, then we would expect to see a bluer color at $J-K_s$ than at [3.6]−[4.5], because the scattering efficiency drops as λ^{-4}. Bernard-Salas et al. (2006) proposed scattering in a system with a disk viewed close to edge-on to explain the unusual object SMP LMC 011, which presents an optically thick carbon-rich dust spectrum with molecular absorption bands in the infrared but shows Hα in emission in the optical. Sloan & Egan (1995) suggested scattering from the poles of an asymmetric dust distribution in the embedded Galactic carbon star IRC +10216 to explain emission from relatively warm dust above and below the central source. This hypothesis could be tested for the embedded Magellanic carbon stars by measuring their polarization as a function of wavelength in the near-IR.

The nature of the dust geometry has significant consequences. Sloan & Egan (1995) noted that the deviation from spherical symmetry they argued for in IRC +10216 was subtle and did not prevent spherically symmetric radiative transfer models from working. Disks are a different story. Their non-isotropic emission would lead to significant uncertainties in bolometric luminosities and thus our basic knowledge about the sources. Boyer et al. (2012) noted that the ten dustiest AGB stars detected in the SAGE surveys of the SMC accounted for 17% of the total dust input to the galaxy when assuming spherical symmetry. If the dust in embedded carbon stars were in disks and not outflowing shells, the amount of dust produced by AGB stars would have to be revised downward, because the dust-production rate scales with outflow velocity, which in disks would be zero.

Disks imply binarity, which leads to more consequences. Equatorial disks can result from binaries interacting during the AGB phase (e.g., Soker & Livio 1989). If the sources we have identified as off-sequence are interacting binaries, then they may have have never been on sequence and are instead following a different evolutionary path in color-color space. High-resolution imaging of Galactic sources show that binary interactions are not rare at all. The Mira variable R Scl is embedded in a spiral structure indicative of interactions of the outflows from the carbon star with a companion (Maercker, et al. 2012). L_2 Pup, the nearest AGB star in the sky, has a dusty disk, evidence of a companion, and the beginnings of bipolar nebulosity (Kervella et al. 2014, 2015). These observations add to the evidence that binaries and their interactions on the AGB strongly influence the structure of post-AGB objects and planetary nebulae (e.g., Lagadec & Chesneau 2014; Jones 2015).

As already stated, near-IR polarimetry of the most embedded carbon stars in the present sample would help diagnose the geometry of these systems. Radiative transfer modeling would also help by translating the constraints imposed by the SEDs to constraints on the dust morphology.

5.3. *SiC and luminosity*

Carbon stars in the SMC generally show very little SiC emission compared to their counterparts in the LMC and the Galaxy, but there are exceptions. Sloan et al. (2006) found five stars in the SMC that had significantly more SiC for their [6.4]−[9.3] color, and the present sample adds two more SiC-rich sources, both with bluer [6.4]−[9.3] colors than the other five (see Figure 5). Sloan et al. (2006) examined a number of properties for the five SiC-rich stars in their sample and could not find anything that distinguished them besides their SiC emission strength.

To compare the SiC-rich and SiC-poor sources in the current sample, we concentrate on [6.4]−[9.3] colors between 0.35 and 0.95 (CE2–3), where the two tracks are most distinct, and consider the sources above and below SiC/continuum = 0.125 separately. In the SMC, the mean bolometric magnitude for the SiC-rich group is -5.05 ± 0.41, compared to -5.08 ± 0.50 for the SiC-weak group. The uncertainties in the mean are 0.17 and 0.11, respectively. The two groups are indistinguishable in luminosity, which implies that they have similar mass, age, and metallicity distributions.

In the LMC, the SiC-rich group has $M_{\rm bol} = -4.91 \pm 0.45$, versus -5.20 ± 0.53 for the SiC-poor group. The uncertainties in the mean are 0.08 and 0.09, respectively. While the separation is larger and more statistically significant, it is in the opposite sense to what we might expect, with the more luminous stars, which presumably would be more massive and more metal-rich, associated with the weaker SiC features.

Thus, while the relative numbers of stars showing strong and weak SiC emission in the Galaxy, LMC, and SMC support the hypothesis that the strength of the SiC feature is tracing metallicity, we find no support for the hypothesis *within* a given galaxy. Sloan et al. (2006) were unable to explain why some sources in the SMC showed strong SiC emission while most did not, and we are unable to improve on that situation.

5.4. *Layered grains*

Lagadec et al. (2007) suggested that the condensation sequence of SiC and amorphous carbon differed in metal-rich and metal-poor stars, with SiC forming first in the Galaxy and later in the SMC. Leisenring et al. (2008) followed with a proposal for multiple evolutionary tracks for dust grains, with the extremes determined by whether SiC or amorphous carbon formed first. Figure 15 simplifies the proposal of Leisenring et al. (2008) and presents two tracks consistent with the infrared properties of Galactic and Magellanic carbon stars. The key is that the dust grains must be layered, which may wreak havoc with attempts to use the grain properties to estimate the masses of the refractory elements in dust grains.

MgS is a case in point. MgS grains do not form until the dust shells pass an optical thickness limit which depends on the metallicity of the sample, as Figures 6 and 7 show. The MgS could condense as grains independently, but then, in order to explain the strength of the MgS feature in post-AGB

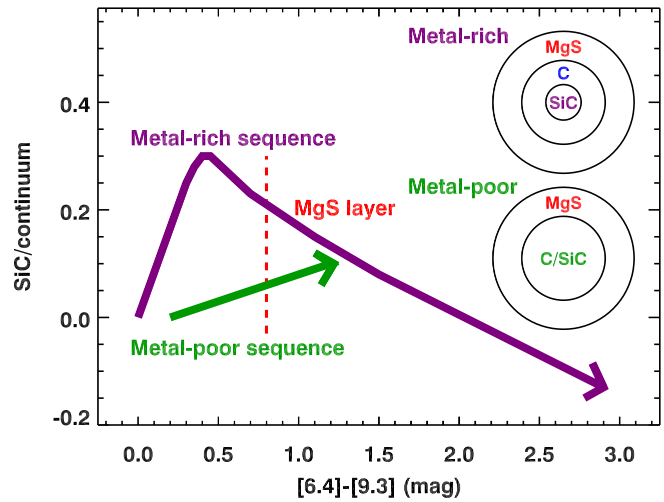

FIG. 15.— A possible scenario for the evolution of dust grains, modeled on a figure by Leisenring et al. (2008). The dust around more metal-rich stars tends to follow the upper track, with a rapid growth in SiC emission with increasing [6.4]−[9.3] color, then a steady decline until the feature finally goes into self-absorption in the most optically thick shells. Around more metal-poor stars, the SiC emission grows much more gradually as the dust shells redden. MgS emission begins at different [6.4]−[9.3] colors, depending on the metallicity of the star.

objects and young planetary nebulae (PNe), more S would be required than can exist around these stars. On these grounds, Zhang et al. (2009) argued that MgS could not be the carrier of the 26–30 μm feature.

Zijlstra et al. (2006) proposed that MgS formed as a layer on pre-existing seeds of SiC and amorphous carbon. Lombaert et al. (2012) argued that the optical properties of a grain coated with MgS would mimic those of a solid MgS grain, which would account for the strength of the MgS feature in PNe without violating abundance constraints. Sloan et al. (2014) explained why other concerns raised about MgS as the carrier of the 26–30 μm feature can be discarded. All of the evidence is consistent with MgS forming a layer on carbonaceous grains, with the condensation trigger depending on metallicity.

However, it is unlikely that any of the layers are pure. The metal-rich track suggests that metal-rich carbonaceous grains should consist of SiC cores surrounded by amorphous carbon mantles. In the most optically thick dust shells, these would be mostly coated by MgS, and yet the spectra from these sources show *absorption* from SiC. Thus some SiC must be present within one optical depth of the surface of the grains, which means that not all grains are coated with MgS, or the coatings are incomplete. Furthermore, if the grains consist of a SiC core and an amorphous carbon mantle, that mantle cannot be pure and must also contain some SiC.

Young carbon-rich PNe in the LMC and SMC often show unusually strong emission features at ∼11.5 μm in their spectra (Bernard-Salas et al. 2009). Sloan et al. (2014) showed that the shape of these features was consistent with SiC dust, modified by the presence of emission from polycyclic aromatic hydrocarbons (PAHs). From abundance arguments, one would expect weaker SiC emission in more metal-poor objects, but the opposite is true, with carbon-rich Magellanic PNe showing stronger SiC emission than in the Galaxy. Sloan et al. (2014) suggested that photoprocessing of carbonaceous grains would preferentially remove amorphous carbon from the surface, resulting in grains coated by SiC. Such a scenario

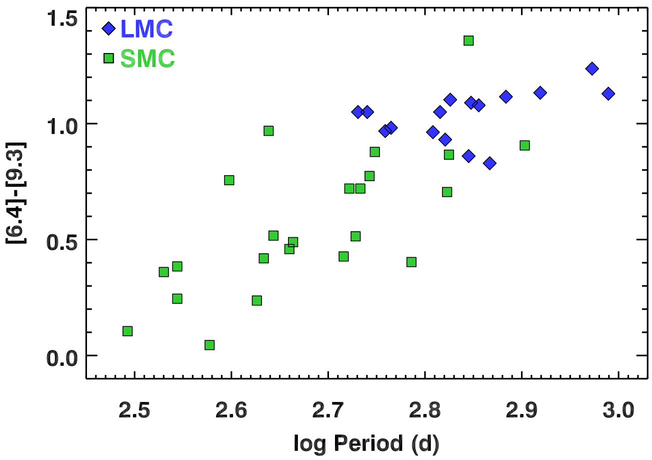

FIG. 16.— The samples of Magellanic carbon stars studied by van Loon et al. (2006, 2008) plotted on the [6.4]−[9.3] versus period plane. The SMC sample shows less dust than the LMC sample because it generally probes a sample with lower pulsation periods. Both samples follow the same trend of increasing dust content with increasing pulsation period.

would require some intermixing of SiC and amorphous carbon in the outer layers of the grains.

The available observational evidence points to layered grains with a structure more complicated than depicted in Figure 15. The strength of the SiC and MgS features with increasing [6.4]−[9.3] color points to two tracks as shown, but the presence of SiC absorption in the most embedded sources and the strength of the SiC feature in young PNe requires some SiC in the layers of the grains within one optical depth of the surface.

5.5. *Completeness*

The pointed nature of spectroscopic samples introduces biases, which can make it challenging to compare different populations. This work has focused on using properties like the pulsation period of the star or the [6.4]−[9.3] color, which is a proxy for the amount of dust, as the independent variable in order to compare sources with similar properties when examining other properties such as the strength of emission features from SiC or MgS dust. A key result is that the amount of dust produced by a star in the Galaxy, LMC, or SMC, depends primarily on its pulsation period and initial mass. The effect of metallicity is unclear with the current sample. While we do see hints of less dust in more metal-poor stars when controlling for period and mass, this decrease is not statistically significant in the IRS samples.

In contrast, van Loon et al. (2008) found a clearer difference in the dust content of their sample of carbon stars in the SMC, compared to a similar study in the LMC (van Loon et al. 2006). They drew this conclusion from a spectroscopic study of the absorption bands from C_2H_2 at 3.1 and 3.8 μm, finding that dust veiling affected the bands more in the LMC than in the SMC. Figure 16 plots the [6.4]−[9.3] color for the stars in common between their sample and ours as a function of pulsation period and shows that while the carbon stars in the LMC have more dust on average than their counterparts in the SMC, the two samples have different distributions in pulsation period, as well. None of the carbon stars in the LMC in common with the IRS sample have a period less than 500 days, compared to over half the SMC sample. Given the differences in the LMC and SMC samples, one would expect the stars in the LMC to show more dust, simply because they are pulsating with longer periods.

The IRS-based studies have concentrated on comparing like with like, which means comparing the dust content in stars with similar pulsation periods. Previous studies with the IRS on *Spitzer* have found little dependence of the dust content on metallicity in carbon stars. The larger sample considered here has not changed that result.

However, the evidence is building that the populations of carbon stars in LMC and SMC differ. Figure 16 shows that the 3 μm samples contain more longer-period pulsators and dustier carbon stars in the LMC than the SMC. The IRS samples show a similar difference in the two galaxies. In the SMC sample, the reddest [6.4]−[9.3] color is 1.4, so that only one SMC source out of 40, NGC 419 MIR 1, is classified as CE5, compared to 20 CE5 and CA5 sources out of 144 in the LMC, 15 of which are redder than NGC 419 MIR 1, with [6.4]−[9.3] colors extending past 3.0. At first glance, this could easily be a selection effect, as is often the case for spectroscopic samples, since the carbon-rich component of at least three IRS programs focused exclusively on the most embedded objects in the LMC. However, analogous objects do not appear to be present in the SMC. Our searches for deeply embedded carbon stars in the SMC using photometry from *Spitzer* and *WISE* have been unsuccessful. Searches using mid-IR photometry from *Spitzer* confirm this result (Dell'Agli et al. 2015; Srinivasan et al. 2016), and searches in the far-IR with *Herschel* have also not uncovered any deeply embedded AGB stars in the SMC (Jones et al. 2015). These missing objects are likely to be massive carbon stars not present in the SMC due to a lower rate of recent star formation (e.g. Ventura et al. 2016).

This deficiency of embedded stars in the SMC combined with how these sources move off the carbon sequence in near-IR color-magnitude space solves a problem first noticed by Lagadec et al. (2010). They derived a relation between absolute magnitude at K_s and $J-K_s$ as a means of estimating the distances to carbon stars, but they found much more scatter in the LMC sample than the SMC and used the latter galaxy to derive a relation. Figure 12 shows that the off-sequence embedded carbon stars that appear only in the LMC sample are responsible for this apparent scatter. This new finding presents a new problem for the use of color-magnitude relations to find the distance to carbon stars, because a given star might be off sequence. A possible solution would be to develop and use color-magnitude relationships at multiple wavelengths to estimate distance and to remove outliers at shorter wavelengths. Alternatively, off-sequence stars could be identified from their reduced variability.

5.6. *The dust-production trigger*

The dichotomy between the carbon stars on the molecular and dust sequences described by Sloan et al. (2015b) points to pulsation as the trigger for dust production. The carbon stars producing dust are almost entirely Mira variables, while the carbon stars on the molecular sequence are either pulsating in one or more overtones, or they are pulsating weakly in the fundamental mode. The link between strong pulsation and carbon-rich dust production is clear, even if which is the cause and which is the effect is not.

Abundance arguments suggest that dredge-up is the trigger. As described in the introduction, similar quantities of dredged-up carbon will lead to a higher amount of free carbon in a more metal-poor star (Matsuura et al. 2005; Sloan et al. 2012). The DPR should be related to the free carbon abundance, and yet we clearly do not observe higher DPRs in more metal-poor carbon stars. Sloan et al. (2012) suggested that once the free carbon abundance crossed a critical threshold, dust production would spike, stripping the stellar envelope and ending its evolution on the AGB. Lagadec & Zijlstra (2008) argued similarly, suggesting that the final dredge-up on the AGB would initiate a superwind. Crossing a free-carbon threshold is the more likely trigger.

Dredge-ups affect atmospheric opacity and generate more consequences than just free-carbon abundance. Higher opacities will increase the stellar radius, lowering the escape velocity and making dust-production and mass-loss easier. An expanded and more opaque atmosphere may also be more unstable to pulsations, which would in turn push material out at velocities closer to the now lowered escape velocity. In other words, the higher pulsation amplitudes and increased dust production may both result from the same underlying cause, the last critical dredge-up on the AGB.

What is intriguing about the sample of IRS-observed Magellanic carbon stars is that it may include some sources on the other side of that final superwind. Because of the selection biases that defined this sample, it cannot provide meaningful relative statistics of carbon stars in different phases of their lifetimes on the AGB. But it can inform the photometric studies needed to study these fundamentally important phases of stellar evolution.

6. SUMMARY

The IRS on the *Spitzer Space Telescope* obtained spectra of 144 carbon-rich AGB stars in the LMC and 40 in the SMC. Comparison to Galactic samples reveals no strong dependence of the amount of dust produced with metallicity. Using the bolometric magnitudes to estimate initial mass and accounting for the different mass distributions hints at a subtle decrease in dust-production rate from the LMC to the SMC, but the result is not statistically significant (1.3 σ).

The amount of SiC dust accompanying the amorphous carbon does depend on metallicity, with strong SiC features observed in most of the Galactic sample and roughly half of the LMC sample. Most of the carbon stars in the SMC show much weaker SiC emission. Some of the SMC stars are exceptions and show stronger SiC emission, but the reason is unknown. Generally, as the optical depth of the dust increases, the SiC emission rises to a peak and then shifts into self-absorption. The LMC is unique among the three samples considered here in that several sources show the SiC feature strongly in absorption.

The strength of the MgS feature at $\sim$30 μm also depends on metallicity, with lower metallicity leading to the appearance of the feature in more optically thick dust shells. This behavior is consistent with previous arguments that the MgS condenses as a layer onto pre-existing grains.

Photometry in the near-IR and at 3.6 and 4.5 μm reveals some radiation from the central stars in many of the more embedded carbon stars. This excess blue emission shifts these sources off the usual carbon sequence seen in most infrared color-color and color-magnitude diagrams. The photometric behavior of these off-sequence stars is consistent with either a patchy dust shell or scattered light in a system with less dust above its poles, possibly a disk.

The pulsation amplitudes generally increase as the dust grows optically thick. However, the most embedded sources in our sample are relatively non-variable, show SiC absorption in their spectra, and also show signs that they are revealing their central star. This behavior is consistent with evolution off the AGB. Their observed properties are also consistent with interacting binary systems, which complicates their interpretation.

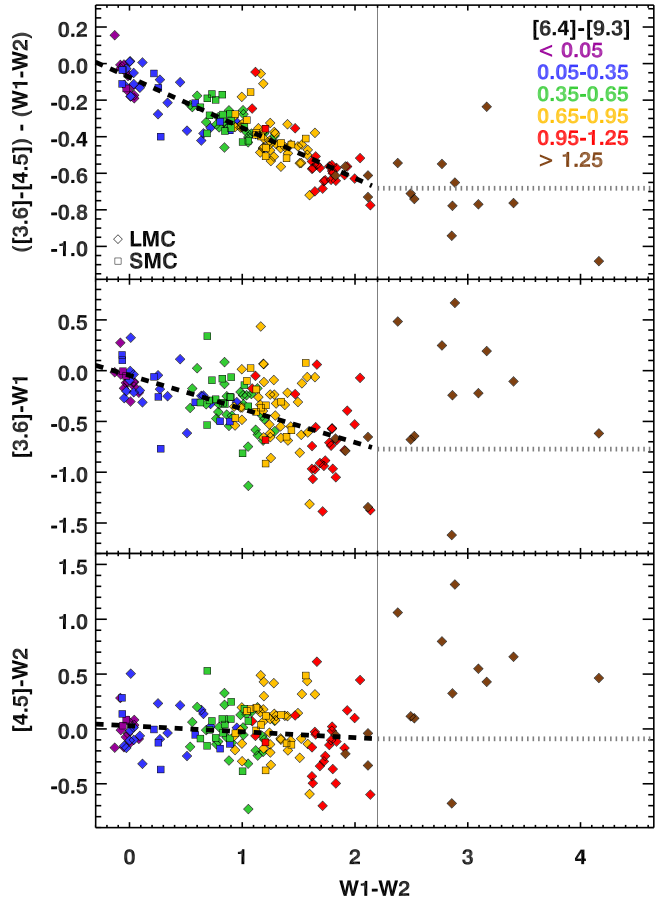

FIG. 17.— Relations between IRAC and *WISE* colors and magnitudes, as a function of W1−W2 color, for carbon stars. Lines are fitted to the data with W1−W2 < 2.2.

TABLE 8
COLOR AND MAGNITUDE CORRECTIONS FOR CARBON STARS

Relation	y-intercept	Slope
([3.6]−[4.5]) − (W1−W2) versus W1−W2	−0.0752	−0.2759
[3.6] − W1 versus W1−W2	−0.0469	−0.3298
[4.5] − W2 versus W1−W2	0.0283	−0.0539

NOTE. — These corrections are only valid for W1−W2 < 2.2.

APPENDIX A — PHOTOMETRIC RELATIONS FOR CARBON STARS

The repeated infrared photometric surveys of the Magellanic Clouds provide multiple epochs in the IRAC and *WISE* filter systems. Because the *WISE* filters at 3.4 and 4.6 μm overlap the IRAC filters at 3.6 and 4.5 μm, it is possible to develop color-based transformations so that we can convert the *WISE* data to the IRAC system. The result is up to ten or more epochs over baselines of several years for some of the targets in our sample.

Figure 17 plots the differences between the IRAC and *WISE* systems as a function of the W1−W2 color ([3.4]−[4.6]). The top panel shows that for carbon stars, the difference between

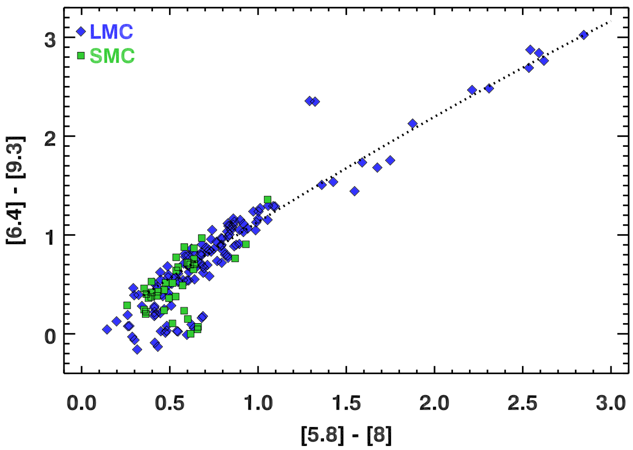

FIG. 18.— The relationship between [6.4]−[9.3] and [5.8]−[8] colors and a quadratic fitted to data with [6.4]−[9.3] > 0.35. The two data points at [6.4]−[9.3] ∼ 2.3 and [5.8]−[8] ∼ 1.3 are badly mispointed, resulting in artificially red [6.4]−[9.3] colors, which have been replaced in the data tables using estimates from the fitted relation (see text).

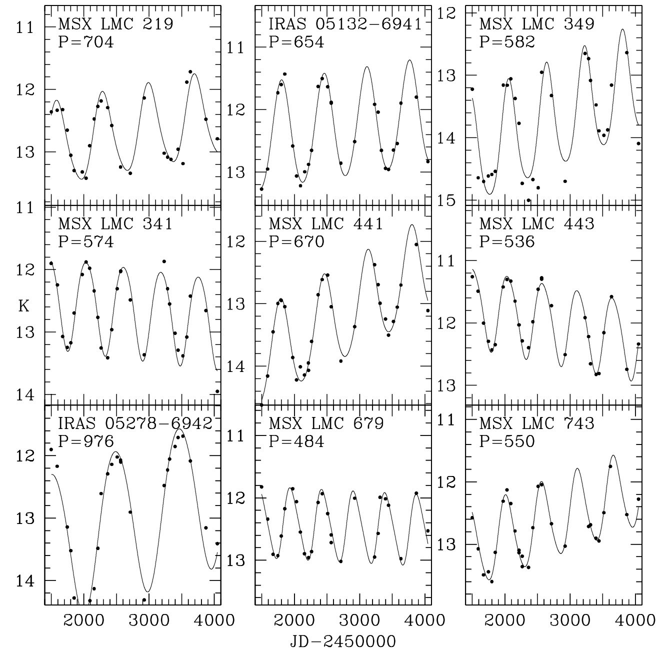

FIG. 19.— The light curves at K for the nine objects with newly reported pulsation periods. The solid points are the measured K values and the lines are fits to the light curves using the periods displayed in the individual panels. The range on the K axis is set to 3.2 magnitudes for all objects so that the differences in amplitudes are readily apparent.

IRAC [3.4]−[4.5] and *WISE* colors is well behaved. We could fit the entire sequence with a quadratic, but instead fit a line for W1−W2 < 2.2.

The lower two panels in Figure 17 illustrate the need for a cut-off at W1−W2 = 2.2. To the blue, the relations of [3.6] to W1 and [4.5] to W2 are clear enough, although with significant noise due to our limited sampling and the variability of the sources. This variability is suppressed in the top panel because the color changes much less than the magnitudes over the pulsation cycle. In the lower two panels, however, the data to the red of W1−W2 = 2.2 do not conform to the behavior of the bluer sources, with all but one data point falling above any line fitted to the blue data. An examination of Figure 14 hints at what must be happening. All of the stars with W1−W2 > 2.2 are classified as CE5 or CA5. From CE0 to CE4, the pulsation amplitude increases steadily, but most of the CE5s are on the other side of the peak amplitude. These stars are likely to be near the end of their AGB lifetimes and may be exhibiting non-spherical dust geometries. For lack of a better solution for the redder sources, we will assume that the corrections are flat past W1−W2 = 2.2 when combining *WISE* and IRAC data to determine mean magnitudes at 3.6 and 4.5 μm.

Because some sources are missing data in the different filters involved, the corrections determined for individual magnitudes do not quite produce the correction for color when combined algebraically. We have modified the magnitude corrections slightly so that they do. Table 8 gives the color-based corrections for all three panels in Figure 17. The shift between [4.5] and W2 is flatter than between [3.6] and W1 because the longer-wavelength filters overlap more.

Figure 18 illustrates the relationship between the IRAC [5.8]−[8] color and the [6.4]−[9.3] color derived from the IRS spectra. We excluded the two outliers with [5.8]−[8] ∼ 1.3 when fitting a quadratic to the data. The polynomial coefficients are −0.0282, 1.2074, −0.0476.[19] The standard deviation of the data about this function is 0.1085.

The two outliers are IRAS 04589 and IRAS 05306, both from Program 37088. The IRS observations were centered on a nearby 2MASS star and were somewhat mispointed for the intended target, leading to a loss of 75–80% of the flux in SL compared to LL. As a result, the targets did not appear as point sources in the spectral images, the optimal extraction broke down, and we used the tapered-column extraction method for these sources. The truncation of starlight by the spectroscopic slit in such a case is a function of wavelength, leading to an artifically reddened spectrum and a false measurement of the [6.4]−[9.3] color. For this reason, we replaced the [6.4]−[9.3] color for these two sources in all data tables and figures with values estimated from their [5.8]−[8] color.[20]

[19] Polynomical coefficients are listed with the y-interecept first.

TABLE 9
MULTI-EPOCH K-BAND PHOTOMETRY

Target	JD−2450000	K (mag.)
MSX LMC 219	1501	12.36
	1591	12.34
	1675	12.32
	1746	12.65
	1800	13.05
	1852	13.30
	1976	13.32
	2035	13.42
	2090	12.90
	2158	12.47

NOTE. — Table 9 is published in its entirety in the electronic edition of the Astrophysical Journal. A portion is shown here for guidance regarding its form and content.

[20] IRAS 04589 and IRAS 05306 have [5.8]−[8] colors of 1.292 and 1.323, respectively, giving estimated [6.4]−[9.3] colors of 1.452 and 1.486, compared to measurements of 2.356 and 2.349 from the mispointed spectra.

APPENDIX B — NEW PULSATION PERIODS FROM *K*-BAND PHOTOMETRY

Some of the targets for Spitzer program 3505 (PI P. Wood) were very red and had no light curves available in the MACHO or OGLE monitoring programs.[21] P. Wood led a long-term program to monitor many embedded evolved stars in the Magellanic Clouds using CASPIR, the Cryogenic Array Spectrometer Imager (McGregor et al. 1994), in the near-IR on the 2.3m telescope of the Australian National University at Siding Spring Observatory. Groenewegen et al. (2007) describe the observational and data reduction procedures, and Kamath et al. (2010) give the *K*- and *L*-band light curves of NGC 419 IR 1, NGC 419 MIR 1, NGC 1978 IR 1, and NGC 1978 MIR 1. Figure 19 presents the light curves at *K* for nine additional objects. The fitted light curves in the figure were made using a Fourier series of a single frequency and its first harmonic together with a term allowing a linear variation of *K* with time.

These objects clearly show large pulsation amplitudes of 1.1 to 2.5 magnitudes in *K* as well as long-term variations in *K* of up to 1 magnitude. The latter variations are short segments of long-term variations (e.g. Whitelock et al. 2003) that are probably due to the episodic nature of dust-ejection mechanisms (e.g. Winters et al. 1994). The large variations evident in the *K* light curves highlight the fact that variability will introduce a significant scatter in quantities such as $M_{\rm bol}$ when it is computed from SEDs constructed from single-epoch photometry taken in different bands at different times. Similarly, colors computed using magnitudes obtained at different times for the two bands involved will also show a significant scatter due to variability.

Table 1 identifies the nine new periods determined from *K*-band monitoring with the reference "App. B." Table 9 gives the multi-epoch *K*-band photometry.

APPENDIX C — NEW PULSATION PERIODS FROM 3–5 μm PHOTOMETRY

All the objects in this study have been observed multiple times at 3.6 and 4.5 μm by *Spitzer* and at 3.4 and 4.6 μm by *WISE* (see Section 2.4). We examined if sufficient epochs were available from the two spacecraft to generate mid-IR light curves and from these determine pulsation periods.

In order to maximize the number of points in each light curve, we converted the data at 3.4 and 4.6 μm from *WISE* to the *Spitzer* wavelengths using the transformations from Appendix A. Table 10 presents the multi-epoch photometry at 3.6 and 4.5 μm, including the converted *WISE* photometry, for all of the Magellanic carbon stars in our sample.

A Fourier fit consisting of a single frequency was made to the resulting light curves at 3.6 and 4.5 μm. We found that reliable results were only possible for light curves with at least eight individual epochs and a range in the photometry exceeding $\sim$0.5 magnitudes. In addition, the periods determined independently at 3.6 and 4.5 μm had to agree to better than 5%.

With the above constraints, we were able to fit the light curves of 42 objects. Of these objects, 37 had periods previously determined from more extensive light curves available at shorter wavelengths, such as those from OGLE or those discussed in Appendix B. Comparing the average of the periods from 3.6 and 4.5 μm with the previously known periods showed that 31 of the 37 periods agreed to better than 5%, a success rate of 84%.

In our sample of fitted periods we found five sources with previously unknown periods. Figure 20 plots their light curves. The averages of the periods from 3.6 and 4.5 μm appear in Table 1, with the reference for the periods given as "App. C." Based on our comparison of periods in the literature for the 37 other sources, we would expect that at least four of these five new periods are reliable to better than 5%.

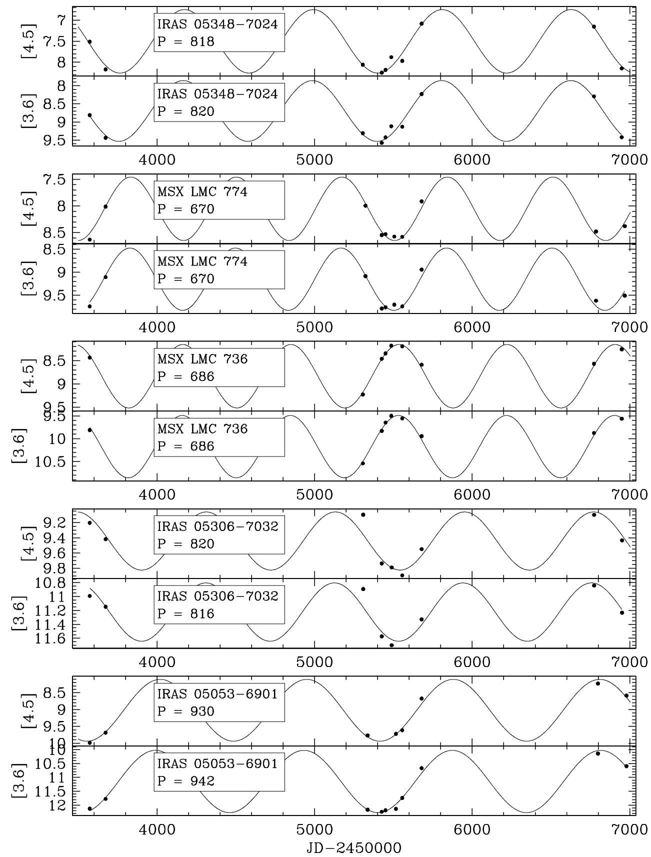

FIG. 20.— The light curves at 3.6 and 4.5 μm of five objects with previously unknown periods. The solid points are the measured values and the lines are sine functions fitted to the light curves using the periods displayed in the panels.

We thank the anonymous referee for helpful and constructive comments. G. C. S. was supported by NASA through Contract Number 1257184 issued by the Jet Propulsion Laboratory, California Institute of Technology under NASA contract 1407 and the NSF through Award 1108645. F. K. received support from the Ministry of Science and Technology (MoST) of Taiwan, grant MOST104-2628-M-001-004-MY3. This research relied on the following resources: NASA's Astrophysics Data System, the Infrared Science Archive at the Infrared Processing and Analysis Center, operated by JPL, and the Simbad and VizieR databases, operated at the Centre de Données astronomiques de Strasbourg.

[21] The MACHO project searched for gravitational lensing events from massive compact halo objects in the direction of the Magellanic Clouds. Fraser et al. (2005) show how this monitoring facilitated the study of long-period variables. The OGLE project has operated similarly.

TABLE 10
MULTI-EPOCH 3–5 μM PHOTOMETRY

Target	RA (J2000)	Decl. (J2000)	MJD	[3.6]	[4.5]	Data source[a]
GM 780	8.905055	−73.165641	54633	9.115 ± 0.059	8.609 ± 0.048	IRAC
	8.905572	−73.165577	54728	9.180 ± 0.034	8.686 ± 0.047	IRAC
	8.905168	−73.165589	55316	9.132 ± 0.025	8.672 ± 0.020	(*WISE*)
	8.905168	−73.165589	55498	8.465 ± 0.035	8.040 ± 0.038	(*WISE*)
	8.905188	−73.165607	56781	8.171 ± 0.019	7.764 ± 0.018	(*WISE*)
	8.905212	−73.165612	56961	8.364 ± 0.025	7.959 ± 0.017	(*WISE*)
MSX SMC 091	9.236177	−72.421510	54633	9.293 ± 0.046	8.721 ± 0.036	IRAC
	9.236628	−72.421501	54728	9.328 ± 0.060	8.752 ± 0.053	IRAC
	9.236252	−72.421493	55318	10.131 ± 0.021	9.452 ± 0.036	(*WISE*)
	9.236252	−72.421493	55499	9.406 ± 0.024	8.782 ± 0.056	(*WISE*)

NOTE. — Table 10 is published in its entirety in the electronic edition of the Astrophysical Journal. A portion is shown here for guidance regarding its form and content.
[a] *WISE* data are corrected as described in Appendix A.

REFERENCES

Bernard-Salas, J., Peeters, E., Sloan, G.C., et al. 2006, ApJ, 652, L29
Bernard-Salas, J., Peeters, E., Sloan, G.C., et al. 2009, ApJ, 699, 1541
Blum, R. D., Mould, J. R., Olsen, K. A., et al. 2006, AJ, 132, 2034
Bolatto, A. D., Simon, J. D., Stanimirović, S., et al. 2007, ApJ, 655, 212
Boyer, M. L., Srinivasan, S., Riebel, D., et al. 2012, ApJ, 748, 40
Buchanan, C. L., Kastner, J. H., Forrest, W. J., et al. 2006, AJ, 132, 1890
Cioni, M.-R., Loup, C., Habing, H. J., et al. 2000, A&AS, 144, 235
Cutri, R. M., Skrutskie, M. F., van Dyk, S., et al. 2006, 2MASS 6X Point Source Working Database/Catalog, VizieR Catalog II/281
de Graauw, T., Haser, L. N., Beintema, D. A., et al. 1996, A&A, 315, L49
Dell'Agli, F., Garcá-Hernández, D. A., Ventura, P., et al. 2015, MNRAS, 454, 4235
Feast, M. W. 2013, in Planets, Stars and Stellar Systems Vol. 5, Galactic Structure and Stellar Populations, ed. T. D. Oswalt & G. Gilmore, 829 (Dordrecht: Springer)
Fraser, O. J., Hawley, S. L., Cook, K. H., & Keller, S. C. 2005, AJ, 129, 768
Gardiner, L. T., & Hawkins, M. R. S. 1991, MNRAS, 251, 174
Girardi, L., Rubele, S., & Kerber, L. 2009, MNRAS, 394, L74
Glatt, K., Grebel, E. K., Sabbi, E., et al. 2008, AJ, 136, 1703
Goebel, J. H., & Moseley, S. H. 1985, ApJ, 290, L35
Gordon, K. D., Meixner, M., Meade, M. R., et al. 2011, AJ, 142, 102
Groenwegen, M. A. T., Sloan, G. C., Soszyński, I., & Petersen, E. A. 2009, A&A, 506, 1277
Groenwegen, M. A. T., Wood, P. R., Sloan, G. C., et al. 2007, MNRAS, 376, 313
Gruendl, R. A., Chu, Y.-H., Seale, J. P., et al. 2008, ApJ, 688, L9
Gullieuszik, M., Groenwegen, M. A. T., Cioni, M.-R. L., et al. 2012, A&A, 537, 105
Houck, J. R., Roellig, T. L., & van Cleve, J., et al. 2004, ApJS, 154, 18
Jones, B., Merrill, K. M., Puetter, R. C., & Willner, S. P. 1977, AJ, 83, 1437
Jones, D. 2015, in The Physics of Evolved Stars: A Conference Dedicated to the Memory of Olivier Chesneau, ed. E. Lagadec, F. Millour & T. Lanz, EAS Publications Series, 7172, 113
Jones, O. C. Meixner, M., Sargent, B. A., et al. 2015, ApJ, 811, 145
Kamath, D., Wood, P. R., Soszyński, I., & Lebzelter, T. 2010, MNRAS, 408, 522
Kato, D., Nagashima, Ch., Nagayama, T., et al. 2007, PASJ, 59, 615
Kemper, F., Woods, P. M., Antoniou, V., et al. 2010, PASP, 122, 683
Kervella, P., Montargès, M., Lagadec, E., et al. 2015, A&A, 578, 77
Kervella, P., Montargès, M., Ridgway, S. T., et al. 2014, A&A564 88
Kessler, M. F., Steinz, J. A., Anderegg, M. E., et al. 1996, A&A, 315, L27
Kraemer, K. E., Sloan, G. C., Bernard-Salas, J., et al. 2006, ApJ, 652, L25
Kraemer, K. E., Sloan, G. C., Price, S. D., & Walker, H. J. 2002, ApJS, 140, 389
Kraemer, K. E., Sloan, G. C., Wood, P. R., et al. 2005, ApJ, 631, L147
Lagadec, E., & Chesneau, O. 2014, in Why Galaxies Care about AGB Stars III: A Closer Look in Space and Time, ed. F. Kerschbaum, R. F. Wing, and J. Hron, ASPC, 497, 145 (San Francisco, ASP)
Lagadec, E., & Zijlstra, A. A. 2008, MNRAS, 390, L59
Lagadec, E., Zijlstra, A. A., Mauron, N., et al. 2010, MNRAS, 403, 1331
Lagadec, E., Zijlstra, A. A., Sloan, G. C., et al. 2007, MNRAS, 376, 1270
Lebofsky, M. J., & Rieke, G. H. 1977, AJ, 82, 646
Lebouteiller, V., Bernard-Salas, J., Sloan, G. C., & Barry, D. J. 2010, PASP, 122, 188
Leisenring, J. M., Kemper, F., & Sloan, G. C. 2008, ApJ, 681, 1557
Lombaert, R., de Vries, B. L., de Koter, A., et al. 2012, A&A, 544, L18
Maercker, M., Mohamed, S., Vlemmings, W. H. T., et al. 2012, Nature, 490, 232
Mainzer, A., Bauer, J., Cutri, R. M., et al. 2014, ApJ, 792, 30
Matsuura, M., Barlow, M. J., Zijlstra, A. A., et al. 2009, MNRAS, 396, 918
Matsuura, M., Bernard-Salas, J., Lloyd Evans, T., et al. 2014, MNRAS, 439, 1472
Matsuura, M., Wood, P. R., Sloan, G. C., et al. 2006, MNRAS, 371, 415
Matsuura, M., Zijlstra, A. A., van Loon, J. Th., et al. A&A, 434, 691
McGregor, P. J., Hart, J., Hoadley, D., & Bloxham, G. 1994, in Infrared Astronomy with Arrays, ed. I McLean (Dordrecht: Kluwer), 299
Meixner, M., Gordon, K. D., Indebetouw, R., et al. 2006, AJ, 132, 2268
Nidever, D. L., Monachesi, A., Bell, E. F., et al. 2013, ApJ, 779, 145
Nishida, S., Tanabé, T., Nakada, Y., et al. 2000, MNRAS, 313, 136
Pietrzyński, G., Graczyk, D., Gieren, W., et al. 2013, Nature, 495, 76
Piatti, A. E. 2012, MNRAS, 422, 1109
Piatti, A. E., & Giesler, D. 2013, ApJ, 145, 17
Price, S. D., Egan, M. P., Carey, S. J., Mizuno, D. R., & Kuchar, T. A. 2001, AJ, 121, 2819
Raimondo, G., Cioni, M.-R. L., Rejkuba, M., Silva, D. R. 2005, A&A, 438, 521
Riebel, D., Boyer, M. L., Srinivasan, S., et al. 2015, ApJ, 807, 1
Riebel, D., Srinivasan, S., Sargent, B., & Meixner, M. 2015, ApJ, 753, 71
Rubele, S., Girardi, L., Kerber, L., et al. 2015, MNRAS, 449, 639
Skrutskie, M. F., Cutri, R. M., Stiening, R., et al. 2006, AJ, 131, 1163
Sloan, G.C., & Egan, M. P. 1995, ApJ, 444, 452
Sloan, G. C., Herter, T. L., Charmandaris, V., et al. 2015a, AJ, 149, 11
Sloan, G. C., Kraemer, K. E., Matsuura, M., et al. 2006, ApJ, 645, 1118
Sloan, G. C., Kraemer, K. E., Wood, P. R., et al. 2008, ApJ, 686, 1056
Sloan, G. C., Lagadec, E., Kraemer, K. E., et al. 2015, in Why Galaxies Care about AGB Stars III, ed. F. Kerschbaum, J. Hron, & R. Wing, ASP Conf. Series, 497, 429
Sloan, G. C., Lagadec, E., Zijlstra, A. A., et al. 2014, ApJ, 791, 28
Sloan, G. C., Matsuura, M., Lagadec, E., et al. 2012, ApJ, 752, 140
Sloan, G. C., & Price, S. D. 1995, ApJ, 451, 758
Soker, N., & Livio, M. 1989, ApJ, 339, 268
Soszyński, Udalski, A., Szymański, M. K., et al. 2009, AcA, 59, 335
Soszyński, Udalski, A., Szymański, M. K., et al. 2011, AcA, 61, 217
Srinivasan, S., Sargent, B. A., & Meixner, M. 2011, A&A, 532, 54
Srinivasan, S., Boyer, M. L., Kemper, F., et al. 2016, MNRAS, 457, 2814
Ulaczyk, K., Szymański, M. K., Udalski, A., et al. 2013, AcA 63, 1
van Loon, J. Th., Cohen, M., Oliveira, J. M., et al. 2008, A&A, 487, 1055
van Loon, J. Th., Marshall, J. R., Cohen, M., et al. 2006, A&A, 447, 971
van Loon, J. Th., Marshall, J. R., & Zijlstra, A. A. 2005, A&A, 442, 597
Vassiliadis, E., & Wood, P. R. 1993, ApJ, 413, 641
Ventura, P., Karakas, A. I., Dell'Agli, F., et al. MNRAS, 457, 1456
Werner, M. W., Roellig, T. L., Low, F. J., et al. 2004, ApJS, 154, 1
Whitelock P. A., Feast M. W., Menzies J. W., Catchpole R. M. 1989, MNRAS, 238, 769
Whitelock, P. A., Feast, M. W., Marang, F., Groenewegen, M. A. T. 2006, MNRAS, 369, 751
Whitelock, P. A., Feast, M. W., van Loon, J. Th., & Zijlstra, A. A. 2003, MNRAS, 342, 86
Winters, J. M., Fleischer, A. J., Gauger, A., & Sedlmayr, E. 1994, A&A, 290, 623
Woitke, P. 2006, A&A, 452, 537
Wright, E. L., Eisenhardt, P. R. M., Mainzer, A. K., et al. 2010, AJ, 140, 1868
Zaritsky, D., Harris, J., Thompson, I. B., Grebel, E. K., & Massey, P. 2002, AJ, 123, 855
Zaritsky, D., Harris, J., Thompson, I. B., & Grebel, E. K. 2004, AJ, 128, 1606
Zhang, K., Jiang, B. W., & Li, A. 2009, ApJ, 702, 680
Zijlstra, A. A., Matsuura, M., Wood, P. R., et al. 2006, MNRAS, 370, 1961

TABLE 1
THE *Spitzer* SAMPLE OF MAGELLANIC CARBON STARS

Target	Alias	RA (J2000)	Decl. (J2000)	reference	Period (days)	reference[a]	Program identifier[b]
GM 780		8.905255	−73.165604	2MASS	611	OGLE	3505
MSX SMC 091		9.236293	−72.421547	2MASS	···	···	3277
MSX SMC 062		10.670455	−72.951599	2MASS	550	OGLE	3277
MSX SMC 054		10.774604	−73.361282	2MASS	396	OGLE	3277
2MASS J004326		10.860405	−73.445366	2MASS	330	R05	50240
MSX SMC 044		10.914901	−73.249336	2MASS	440	OGLE	3277
MSX SMC 105		11.258941	−72.873428	2MASS	668	OGLE	3277
MSX SMC 036		11.474785	−73.394775	2MASS	553	OGLE	3277
GB S06	MSX SMC 060	11.668442	−73.279793	2MASS	435	OGLE	3277
MSX SMC 200		11.711623	−71.794250	2MASS	426	OGLE	3277
MSX SMC 033		11.773011	−73.359169	2MASS	535	OGLE	3277
IRAS F00454−7257		11.828853	−72.676147	2MASS	144	OGLE	30332
MSX SMC 066		12.218778	−73.149124	2MASS	520	OGLE	3277
IRAS F00471−7352		12.247813	−73.594093	2MASS	685	OGLE	50240
LIN 131	CV 78	12.265996	−73.088852	2MASS	434	OGLE	200
RAW 594		12.535428	−72.838959	2MASS	139	OGLE	50240
MSX SMC 163		12.753117	−72.421829	2MASS	665	OGLE	3277
LEGC A144	MSX SMC 142	12.918636	−72.958054	2MASS	294	OGLE	3277
MSX SMC 125		12.959122	−72.847115	2MASS	458	OGLE	3277
MSX SMC 162		13.167399	−72.791023	2MASS	529	OGLE	3277
MSX SMC 202		13.292226	−72.198532	2MASS	491	OGLE	3277
MSX SMC 159		13.592872	−72.724907	2MASS	560	S06	3277
LEGC 105		13.695222	−73.227135	2MASS	350	OGLE	3505
ISO 00548		13.711488	−73.102051	2MASS	430	OGLE	3505
ISO 00549		13.725440	−73.055054	2MASS	541	OGLE	3505
RAW 960		13.977697	−73.193413	2MASS	315	OGLE	3505
MSX SMC 209		14.068300	−72.278152	2MASS	527	OGLE	3277
NGC 330 BAL 555	S3MC 204803	14.073058	−72.451187	2MASS	194	OGLE	50240
IRAS 00554−7351		14.266462	−73.587410	2MASS	800	W89	3505
MSX SMC 198		14.295754	−72.516663	2MASS	508	OGLE	3277
ISO 00573		14.335619	−73.212784	2MASS	350	OGLE	3505
MSX SMC 093		14.847344	−73.933624	2MASS	457	OGLE	3277
ISO 01019		15.477425	−72.972885	2MASS	339	OGLE	3505
MSX SMC 232		16.513772	−72.375626	2MASS	462	OGLE	3277
NGC 419 LE 16		17.004758	−72.888153	2MASS	423	G09	3505
NGC 419 IR 1		17.054022	−72.878883	2MASS	461	OGLE	3505
NGC 419 MIR 1		17.072878	−72.885926	IRAC	738	K10	3505
NGC 419 LE 35		17.072881	−72.883705	2MASS	173	OGLE	3505
NGC 419 LE 27		17.086129	−72.881104	2MASS	311	OGLE	3505
NGC 419 LE 18		17.103977	−72.882484	2MASS	378	G09	3505
IRAS 04628−6937	MSX LMC 1007	67.125786	−69.513962	2MASS	662	W03	3426
IRAS F04331−6932	MSX LMC 1008	68.239070	−69.442535	2MASS	···	···	30788
IRAS F04340−7016	MSX LMC 1077	68.432034	−70.164024	2MASS	442	OGLE	30788
IRAS F04353−6702	MSX LMC 1017	68.850409	−66.947029	2MASS	···	···	30788
IRAS F04375−7247	MSX LMC 1067	69.185329	−72.700279	2MASS	···	···	30788
IRAS 04374−6831	MSX LMC 1042	69.344705	−68.417595	2MASS	700	W03	3426
IRAS F04433−7018	MSX LMC 1075	70.738865	−70.207153	2MASS	478	OGLE	30788
2MASS J044627		71.613029	−68.796371	2MASS	389	OGLE	40159
IRAS 04473−6829	MSX LMC 1120	71.817052	−68.407120	2MASS	624	OGLE	3426
IRAS 04496−6958	MSX LMC 1130	72.327023	−69.887367	2MASS	736	OGLE	1094
MSX LMC 1128		72.668923	−68.971970	2MASS	441	OGLE	40159
MSX LMC 1308		72.795686	−69.337410	2MASS	499	OGLE	3591
MSX LMC 1205		72.814508	−68.694534	2MASS	566	OGLE	3591
IRAS 04518−6852	MSX LMC 1201	72.919061	−68.792947	IRAC	···	···	40159
MSX LMC 1213		73.084083	−68.725029	2MASS	···	···	3591
KDM 764		73.135511	−67.049835	2MASS	445	OGLE	40159
2MASS J045328		73.369657	−66.059555	2MASS	···	···	40159
IRAS 04535−6616	MSX LMC 1111	73.434367	−66.196140	IRAC	···	···	40159
IRAS 04539−6821	MSX LMC 1198	73.443188	−68.270279	2MASS	···	···	30788
IRAS F04537−6509	MSX LMC 1100	73.506689	−65.081139	2MASS	···	···	30788
MSX LMC 1209		73.828662	−68.775192	2MASS	565	OGLE	3591
IRAS 04557−6753	MSX LMC 1238	73.912433	−67.819649	2MASS	765	Z06	3505
IRAS 04567−6857	MSX LMC 1298	74.133960	−68.880844	2MASS	663	OGLE	3591
IRAS 04589−6825		74.691749	−68.343759	IRAC	···	···	30788
KDM 1238		74.729285	−69.188507	2MASS	133	OGLE	40159
IRAS F05013−7213	MSX LMC 178	75.134442	−72.150650	2MASS	···	···	30788
IRAS 05010−6739	MSX LMC 1282	75.253636	−67.589897	2MASS	664	OGLE	3426
IRAS 05009−6616	MSX LMC 1278	75.268440	−66.211220	2MASS	658	W03	3505
IRAS 05026−6809	GCS J050221	75.631173	−68.093324	IRAC	···	···	50338
KDM 1656		75.819280	−65.829178	2MASS	···	···	40159
W60 B14	KDM 1691	75.903917	−68.560699	2MASS	519	OGLE	40159
LMC-BM 12-14		75.972527	−70.463219	2MASS	220	OGLE	40159
IRAS 05042−6827	GCS J050405	76.023300	−68.394524	IRAC	···	···	40650
NGC 1818 WBT 64		76.032248	−66.418282	2MASS	···	···	40159

TABLE 1 — *Continued*

Target	Alias	RA (J2000)	Decl. (J2000)	reference	Period (days)	reference[a]	Program identifier[b]
NGC 1835 LE 1		76.263446	−69.407394	2MASS	217	OGLE	40159
IRAS 05053−6901	MSX LMC 84	76.270124	−68.963437	IRAC	936	App. C	50338
LMC-BM 13-2		76.481988	−67.369438	2MASS	206	OGLE	40159
2MASS J050607		76.531431	−71.696739	2MASS	···	···	40159
KDM 1961	NGC 1831 HOD E20	76.552487	−64.927116	2MASS	···	···	40159
KDM 1966		76.579074	−64.936180	2MASS	···	···	40159
2MASS J050620		76.583859	−64.916275	2MASS	···	···	40159
2MASS J050629		76.623347	−68.926346	2MASS	144	OGLE	40159
IRAS 05070−7020	MSX LMC 200	76.646286	−70.280609	2MASS	···	···	30788
SHV 0507252		76.789164	−68.980392	2MASS	507	OGLE	40159
SAGE MC J050752		76.970546	−68.212914	2MASS	302	OGLE	40159
MSX LMC 92		77.106622	−68.899971	2MASS	529	OGLE	50338
2MASS J050826		77.109899	−68.520844	2MASS	400	OGLE	40159
KDM 2187		77.151827	−69.720970	2MASS	758	OGLE	40159
IRAS 05103−6959	MSX LMC 95	77.499982	−69.936028	2MASS	598	OGLE	3426
IRAS 05107−6953	MSX LMC 87	77.581750	−69.830956	2MASS	624	OGLE	3426
2MASS J051028		77.618120	−68.742050	2MASS	465	OGLE	40159
IRAS 05112−6755	MSX LMC 44	77.793643	−67.869591	2MASS	830	W03	3505
IRAS 05113−6739	MSX LMC 47	77.807866	−67.604485	2MASS	717	OGLE	3505
MSX LMC 219		77.831348	−68.707748	2MASS	704	App. B	3505
TRM 72	MSX LMC 29	77.911028	−66.852730	2MASS	548	OGLE	3505
IRAS 05125−7035	MSX LMC 196	78.003244	−70.540009	2MASS	···	···	1094
MSX LMC 220		78.133621	−69.261230	2MASS	749	G09	3426
IRAS 05132−6941	MSX LMC 223	78.212787	−69.630630	2MASS	654	App. B	3505
IRAS 05133−6937		78.257332	−69.564177	IRAC	···	···	40159
OGLE J051306		78.276768	−69.162842	2MASS	356	OGLE	40159
MSX LMC 218		78.318373	−68.736107	2MASS	656	OGLE	3426
MSX LMC 349		79.362249	−68.916168	2MASS	582	App. B	3505
SAGE MC J051803		79.513592	−68.830750	IRAC	349	OGLE	40159
IRAS 05187−7033	GCS J051811	79.548784	−70.507500	IRAC	···	···	40650
IRAS 05191−6936	GCS J051848	79.701456	−69.559660	IRAC	···	···	40650
IRAS 05190−6758	MSX LMC 307	79.734427	−67.751221	2MASS	939	W03	3505
2MASS J051908		79.785394	−69.387268	2MASS	188	OGLE	40159
TRM 78	MSX LMC 310	80.080751	−66.596619	2MASS	544	W03	3505
MSX LMC 341		80.251562	−69.348686	2MASS	574	App. B	3505
OGLE J052242		80.674959	−69.257217	2MASS	417	OGLE	40159
BE 74	MSX LMC 663	80.683327	−69.641136	2MASS	422	G09	3505
MSX LMC 494		80.787690	−69.296368	IRAC	439	OGLE	3505
IRAS F05236−6655	MSX LMC 513	80.909700	−66.890182	2MASS	···	···	30788
2MASS J052405		81.022188	−68.300705	2MASS	330	OGLE	40159
MSX LMC 441		81.160918	−70.399208	2MASS	670	App. B	3505
IRAS F05254−7149	MSX LMC 428	81.182031	−71.790688	2MASS	···	···	30788
OGLE J052445		81.189200	−69.268143	2MASS	403	OGLE	40159
MSX LMC 443		81.273702	−70.169617	2MASS	536	App. B	3505
LI-LMC 1028	MSX LMC 438	81.331302	−71.067429	2MASS	557	OGLE	3426
IRAS 05260−7010	GCS J052540	81.419533	−70.140846	IRAC	···	···	40650
MSX LMC 474		81.466034	−68.776192	2MASS	642	OGLE	50338
WBP 17		81.582833	−69.693703	2MASS	314	OGLE	200
MSX LMC 774		81.596238	−69.188965	2MASS	670	App. C	3591
MSX LMC 634		81.648745	−69.139648	2MASS	486	OGLE	3591
WBP 29		81.670642	−69.386490	2MASS	247	OGLE	200
MSX LMC 601		81.711790	−69.526909	2MASS	550	OGLE	3505
WBP 42		81.769710	−69.637840	2MASS	403	OGLE	200
IRAS 05278−6942	MSX LMC 635	81.850499	−69.662491	2MASS	976	App. B	3505
SHV 0528350		82.024630	−70.131546	2MASS	476	OGLE	40159
MSX LMC 754		82.047840	−70.566299	2MASS	467	OGLE	3505
KDM 4257		82.107582	−69.779846	2MASS	134	OGLE	40159
NGC 1978 IR 1		82.167367	−66.231735	2MASS	491	N00	3505
NGC 1978 IR 4		82.185398	−66.234436	2MASS	523	G07	3505
IRAS 05295−7121	MSX LMC 692	82.194234	−71.320145	2MASS	643	OGLE	3505
NGC 1978 MIR 1		82.196649	−66.237106	2MASS	378	K10	3505
MSX LMC 679		82.202570	−69.800369	2MASS	484	App. B	3505
GRRV 38	LI-LMC 1137	82.281662	−66.970833	2MASS	503	G07	3505
IRAS 05305−7251	GCS J052937	82.407860	−72.831365	IRAC	···	···	40650
IRAS 05300−6651		82.516215	−66.823395	2MASS	···	···	200
IRAS 05306−7032		82.525881	−70.511437	IRAC	818	App. C	30788
2MASS J053044		82.687496	−68.358032	2MASS	426	OGLE	40159
MSX LMC 841		82.804646	−66.161438	2MASS	···	···	3591
MSX LMC 768		82.920407	−69.655502	2MASS	627	OGLE	3591
KDM 4665		82.995565	−72.743355	2MASS	···	···	40159
MSX LMC 782		83.013810	−69.291786	2MASS	485	OGLE	3591
KDM 4718		83.110531	−73.168571	2MASS	···	···	40159
KDM 4774		83.229197	−67.613098	2MASS	···	···	40159
MSX LMC 783		83.231141	−69.340736	2MASS	518	OGLE	3591
LMC-BM 32-9	MSX LMC 775	83.234091	−68.213539	2MASS	282	OGLE	3426

TABLE 1 — *Continued*

Target	Alias	RA (J2000)	Decl. (J2000)	reference	Period (days)	reference[a]	Program identifier[b]
MSX LMC 736		83.278350	−70.509682	2MASS	686	App. C	40159
2MASS J053318		83.327462	−66.011154	2MASS	⋯	⋯	40159
IRAS 05348−7024	MSX LMC 733	83.566623	−70.381241	2MASS	819	App. C	200
2MASS J053441		83.672587	−69.441864	2MASS	503	OGLE	40159
MSX LMC 743		83.723906	−70.490211	2MASS	550	App. B	3505
MSX LMC 787		83.734212	−69.154587	2MASS	⋯	⋯	3591
MSX LMC 950		83.764785	−69.879295	2MASS	558	OGLE	3591
MSX LMC 749		83.861930	−69.874420	2MASS	541	OGLE	3505
IRAS F05355−6521	MSX LMC 862	83.915505	−65.332336	2MASS	⋯	⋯	30788
IRAS 05360−6648	MSX LMC 872	84.005163	−66.777687	2MASS	538	W03	3505
IRAS F05373−7243	MSX LMC 721	84.100548	−72.692360	2MASS	⋯	⋯	30788
MSX LMC 967		84.152963	−69.789612	2MASS	532	OGLE	3505
OGLE J053930		84.874939	−69.965492	2MASS	399	OGLE	40159
MSX LMC 971		84.966024	−70.021393	2MASS	⋯	⋯	3591
MSX LMC 1400		85.085724	−66.245636	2MASS	⋯	⋯	3426
IRAS 05410−6954	MSX LMC 937	85.150270	−69.880508	2MASS	676	OGLE	3591
MSX LMC 974		85.242430	−69.886848	2MASS	521	OGLE	3591
IRAS 05416−6906	MSX LMC 1438	85.336396	−69.078785	IRAC	⋯	⋯	40159
KDM 5841		85.870020	−69.712158	2MASS	210	OGLE	40159
MSX LMC 1384		85.900123	−70.176430	2MASS	562	OGLE	3426
IRAS 05446−6945	MSX LMC 1383	86.056967	−69.738449	2MASS	⋯	⋯	3591
2MASS J054437		86.157794	−67.616005	2MASS	⋯	⋯	40159
2MASS J054546		86.443103	−67.544250	2MASS	⋯	⋯	40159
NGC 2121 LE 6		87.070039	−71.477577	2MASS	385	OGLE	40159
MSX LMC 1492		87.287000	−71.535255	2MASS	555	OGLE	3426
IRAS 05506−7053	MSX LMC 1453	87.485502	−70.886597	2MASS	⋯	⋯	30788
LI-LMC 1758	MSX LMC 1488	87.528169	−71.767410	2MASS	⋯	⋯	3426
IRAS 05509−6956	MSX LMC 1469	87.608775	−69.934248	IRAC	⋯	⋯	50338
KDM 6486		87.652749	−68.481178	2MASS	663	OGLE	40159
IRAS 05516−7124	MSX LMC 1487	87.707976	−71.393227	2MASS	⋯	⋯	30788
PMP 337		88.212756	−69.477654	2MASS	281	OGLE	40159
IRAS 05568−6753	MSX LMC 1592	89.161512	−67.892742	IRAC	⋯	⋯	3426
IRAS 06025−6712	MSX LMC 1652	90.629403	−67.213043	2MASS	⋯	⋯	3426
IRAS 06028−6722	MSX LMC 1651	90.687935	−67.378685	2MASS	⋯	⋯	1094
IRAS F06108−7045	MSX LMC 1638	92.544460	−70.767586	2MASS	⋯	⋯	30788

[a] OGLE = Soszyński et al. (2009, 2011, Optical Gravitational Lensing Experiment); GO7 = Groenewegen et al. (2007); G09 = Groenewegen et al. (2009); K10 = Kamath et al. (2010); N00 = Nishida et al. (2000); R05 = Raimondo et al. (2005); S06 = Sloan et al. (2006); W89 = Whitelock et al. (1989); W03 = Whitelock et al. (2003); Z06 = Zijlstra et al. (2006); App. B and C = the appendices in this paper.
[b] See Table 2.

TABLE 3
OPTICAL AND NEAR-INFRARED PHOTOMETRY

Target	*U* (mag.)	*B* (mag.)	*V* (mag.)	*I* (mag.)	*J* (mag.)	*H* (mag.)	*K* (mag.)
GM 780	⋯	⋯	16.760 ± ⋯	14.235 ± 0.040	12.098 ± 0.740	10.658 ± 0.564	9.934 ± 0.402
MSX SMC 091	⋯	⋯	⋯	15.781 ± 0.060	13.764 ± 0.374	12.259 ± 0.284	10.829 ± 0.191
MSX SMC 062	⋯	⋯	⋯	16.985 ± ⋯	13.261 ± 1.398	11.418 ± 0.159	10.281 ± 0.769
MSX SMC 054	⋯	⋯	21.430 ± ⋯	20.383 ± ⋯	16.536 ± 0.854	14.449 ± 0.182	12.281 ± 0.369
2MASS J004326	⋯	⋯	18.658 ± ⋯	15.170 ± 0.040	13.041 ± 0.117	11.857 ± 0.108	10.970 ± 0.151
MSX SMC 044	19.762 ± 0.135	19.230 ± 0.039	19.920 ± 0.045	16.406 ± 1.882	13.154 ± 1.336	12.178 ± 1.822	10.492 ± 0.943
MSX SMC 105	⋯	22.447 ± 0.391	21.099 ± 0.303	18.370 ± 0.081	15.151 ± 0.446	13.082 ± 0.382	11.245 ± 0.290
MSX SMC 036	⋯	⋯	⋯	19.462 ± 0.090	15.170 ± 1.013	13.553 ± 0.898	11.743 ± 0.632
GB S06	⋯	⋯	20.137 ± ⋯	18.114 ± ⋯	15.348 ± 0.364	13.146 ± 0.283	11.211 ± 0.242
MSX SMC 200	⋯	⋯	21.203 ± ⋯	17.557 ± 0.200	14.612 ± 0.899	12.724 ± 0.804	11.371 ± 0.413
MSX SMC 033	⋯	20.430 ± 0.072	22.031 ± 0.104	17.053 ± 0.060	13.770 ± 0.546	12.127 ± 0.446	10.512 ± 0.352
IRAS F00454−7257	⋯	⋯	⋯	⋯	13.785 ± 1.442	13.491 ± 0.626	11.616 ± 0.562
MSX SMC 066	⋯	⋯	19.631 ± ⋯	16.634 ± 0.120	14.505 ± 0.715	12.745 ± 0.732	11.075 ± 0.540
IRAS F00471−7352	18.041 ± 0.058	18.604 ± 0.063	21.965 ± 0.043	18.507 ± 0.075	14.997 ± 0.849	12.623 ± 0.364	10.959 ± 0.514
LIN 131	⋯	16.143 ± 0.024	15.424 ± 0.058	13.332 ± 0.442	11.632 ± 0.203	10.746 ± 0.385	10.174 ± 0.387
RAW 594	⋯	⋯	18.039 ± ⋯	14.812 ± 0.040	12.964 ± 0.084	11.899 ± 0.030	11.252 ± 0.049
MSX SMC 163	⋯	⋯	⋯	17.444 ± 0.150	14.591 ± 0.213	12.613 ± 0.226	10.983 ± 0.148
LEGC A144	⋯	⋯	19.064 ± ⋯	16.401 ± 0.050	13.582 ± 0.738	12.264 ± 0.666	11.119 ± 0.426
MSX SMC 125	⋯	⋯	18.334 ± ⋯	15.487 ± ⋯	13.387 ± 0.158	11.835 ± 0.154	10.535 ± 0.186
MSX SMC 162	⋯	⋯	19.716 ± ⋯	16.248 ± 0.050	13.235 ± 0.886	11.730 ± 0.884	10.406 ± 0.577
MSX SMC 202	20.066 ± 0.163	19.247 ± 0.048	17.654 ± 0.049	15.177 ± 0.210	12.585 ± 0.506	11.131 ± 0.497	10.162 ± 0.295
MSX SMC 159	⋯	19.834 ± 0.066	19.443 ± 0.116	18.591 ± 0.059	16.191 ± 0.141	13.772 ± 0.099	11.733 ± 0.089
LEGC 105	⋯	⋯	18.366 ± ⋯	15.702 ± 0.060	13.729 ± 0.488	12.215 ± 0.549	11.094 ± 0.366
ISO 00548	⋯	⋯	19.272 ± ⋯	16.181 ± 0.070	14.353 ± 0.255	12.691 ± 0.301	11.240 ± 0.244
ISO 00549	⋯	⋯	22.107 ± ⋯	18.022 ± ⋯	15.089 ± 0.839	13.090 ± 0.837	11.273 ± 0.673
RAW 960	⋯	⋯	18.029 ± ⋯	14.990 ± 0.030	13.228 ± 0.352	12.084 ± 0.157	11.016 ± 0.153
MSX SMC 209	⋯	⋯	21.690 ± ⋯	17.737 ± 0.130	14.622 ± 1.040	12.782 ± 0.981	11.161 ± 0.633
NGC 330 BAL 555	⋯	18.944 ± 0.080	17.232 ± 0.052	14.323 ± 0.027	12.588 ± 0.181	11.461 ± 0.160	10.803 ± 0.107

TABLE 3 — *Continued*

Target	*U* (mag.)	*B* (mag.)	*V* (mag.)	*I* (mag.)	*J* (mag.)	*H* (mag.)	*K* (mag.)
IRAS 00554−7351	···	···	···	20.239 ± ···	16.796 ± 1.446	14.059 ± 0.664	11.741 ± 0.499
MSX SMC 198	20.687 ± 0.467	20.781 ± 0.256	19.834 ± 0.619	17.805 ± 1.139	14.982 ± 1.845	13.365 ± 1.863	11.363 ± 0.503
ISO 00573	···	21.016 ± 0.103	18.276 ± 0.036	15.540 ± 0.112	13.077 ± 0.619	12.065 ± 0.404	10.880 ± 0.421
MSX SMC 093	···	···	18.763 ± ···	15.611 ± 0.040	13.360 ± 0.633	11.976 ± 0.560	10.673 ± 0.466
ISO 01019	···	···	20.115 ± ···	17.150 ± 0.070	14.382 ± 0.516	13.047 ± 0.167	11.500 ± 0.297
MSX SMC 232	···	···	···	18.873 ± 0.100	15.005 ± 1.058	13.505 ± 0.728	11.687 ± 0.560
NGC 419 LE 16	···	···	19.616 ± ···	15.899 ± 0.060	13.325 ± 0.407	12.019 ± 0.425	10.956 ± 0.292
NGC 419 IR 1	18.585 ± 0.165	18.637 ± 0.118	18.450 ± 0.127	16.534 ± 0.180	13.697 ± 0.475	12.237 ± 0.477	10.935 ± 0.255
NGC 419 MIR 1	···	···	···	···	···	15.380 ± 0.080	14.665 ± 0.516
NGC 419 LE 35	···	···	17.239 ± ···	14.382 ± 0.040	12.339 ± 0.189	11.429 ± 0.106	10.715 ± 0.111
NGC 419 LE 27	16.523 ± 0.188	17.523 ± 0.110	17.006 ± 0.103	14.324 ± 0.098	12.588 ± 0.164	11.589 ± 0.109	10.912 ± 0.085
NGC 419 LE 18	···	···	18.205 ± ···	14.823 ± 0.040	12.928 ± 0.049	11.717 ± 0.075	10.989 ± 0.067
IRAS 04628−6937	···	···	···	···	15.421 ± 0.738	13.051 ± 0.905	11.002 ± 0.691
IRAS F04331−6932	···	···	···	···	18.727 ± 0.852	17.483 ± 0.057	14.738 ± 0.776
IRAS F04340−7016	···	···	···	18.767 ± ···	16.016 ± 0.059	13.815 ± 0.013	12.054 ± 0.269
IRAS F04353−6702	···	···	···	···	16.289 ± 1.213	14.195 ± 1.158	12.065 ± 0.741
IRAS F04375−7247	···	···	···	···	18.094 ± 0.025	15.523 ± 0.285	12.885 ± 0.064
IRAS 04374−6831	···	···	···	···	16.741 ± 0.753	14.169 ± 0.754	12.180 ± 0.703
IRAS F04433−7018	···	···	···	18.668 ± 0.170	15.387 ± 0.741	13.480 ± 0.632	11.541 ± 0.506
2MASS J044627	20.152 ± 0.205	20.746 ± 0.074	19.386 ± 0.055	16.361 ± 0.133	13.753 ± 0.767	12.154 ± 0.830	10.777 ± 0.602
IRAS 04473−6829	19.517 ± 0.110	19.460 ± 0.047	19.195 ± 0.041	17.426 ± 1.245	14.080 ± 0.856	12.359 ± 0.650	10.434 ± 0.766
IRAS 04496−6958	20.060 ± 0.157	20.027 ± 0.102	18.791 ± 0.037	15.060 ± ···	12.087 ± 0.457	10.375 ± 0.414	9.111 ± 0.295
MSX LMC 1128	···	21.105 ± 0.115	20.981 ± 0.076	16.123 ± 0.218	13.096 ± 0.289	11.701 ± 0.153	10.413 ± 0.186
MSX LMC 1308	···	···	21.901 ± ···	17.754 ± ···	13.223 ± 0.846	11.585 ± 0.642	10.458 ± 0.444
MSX LMC 1205	···	···	···	18.000 ± ···	14.264 ± 0.662	12.284 ± 0.569	10.926 ± 0.917
IRAS 04518−6852	···	···	···	···	···	···	···
MSX LMC 1213	···	···	···	···	17.529 ± 0.539	14.649 ± 0.457	12.422 ± 0.340
KDM 764	···	19.973 ± 0.989	17.240 ± 1.240	13.897 ± 2.306	11.913 ± 0.136	10.773 ± 0.078	9.934 ± 0.116
2MASS J045328	···	···	···	14.446 ± 0.030	12.616 ± 0.130	11.404 ± 0.110	10.426 ± 0.119
IRAS 04535−6616	···	···	···	···	···	···	16.180 ± 0.070
IRAS 04539−6821	18.262 ± 0.067	18.585 ± 0.036	18.873 ± 0.284	18.420 ± 0.084	17.832 ± 0.210	15.685 ± 0.358	13.163 ± 0.304
IRAS F04537−6509	···	···	···	16.711 ± 0.090	14.073 ± 1.398	12.501 ± 1.469	10.760 ± 0.989
MSX LMC 1209	···	···	···	20.534 ± ···	16.477 ± 0.128	14.292 ± 0.539	12.145 ± 0.482
IRAS 04557−6753	20.078 ± 0.140	19.746 ± 0.064	19.511 ± 0.098	18.865 ± 0.127	16.779 ± 0.663	14.627 ± 0.155	12.403 ± 0.100
IRAS 04567−6857	···	···	···	19.477 ± ···	15.079 ± 0.486	12.928 ± 0.367	10.911 ± 0.243
IRAS 04589−6825	···	···	···	···	···	···	···
KDM 1238	21.348 ± 0.424	19.337 ± 0.051	16.576 ± 0.103	13.920 ± 0.085	12.217 ± 0.138	11.164 ± 0.059	10.656 ± 0.026
IRAS F05013−7213	···	···	···	···	18.161 ± 0.508	15.083 ± 0.573	12.494 ± 0.608
IRAS 05010−6739	20.911 ± 0.323	21.135 ± 0.164	20.773 ± 0.081	17.448 ± 0.210	16.320 ± 0.479	13.958 ± 0.497	11.482 ± 0.572
IRAS 05009−6616	···	···	···	···	16.199 ± 1.511	15.146 ± 0.660	12.174 ± 0.916
IRAS 05026−6809	···	···	···	···	···	···	···
KDM 1656	19.681 ± 0.154	18.771 ± 0.051	16.275 ± 0.037	13.423 ± 0.126	11.592 ± 0.093	10.442 ± 0.115	9.757 ± 0.121
W60 B14	20.167 ± 0.317	19.514 ± 0.050	16.312 ± 0.031	13.371 ± 0.247	11.475 ± 0.142	10.208 ± 0.085	9.573 ± 0.102
LMC-BM 12-14	19.201 ± 0.104	18.667 ± 0.068	16.152 ± 0.141	13.336 ± 0.046	11.673 ± 0.293	10.611 ± 0.230	9.947 ± 0.166
IRAS 05042−6827	···	···	···	···	···	···	···
NGC 1818 WBT 64	···	18.399 ± 0.030	16.128 ± 0.024	13.945 ± 0.071	12.380 ± 0.126	11.346 ± 0.017	10.860 ± 0.023
NGC 1835 LE 1	···	···	16.770 ± ···	14.040 ± 0.030	12.276 ± 0.193	11.284 ± 0.183	10.640 ± 0.155
IRAS 05053−6901	···	···	···	···	···	···	17.500 ± 0.260
LMC-BM 13-2	···	···	19.635 ± ···	16.731 ± 0.070	13.886 ± 0.484	12.486 ± 0.407	11.507 ± 0.260
2MASS J050607	···	···	···	14.489 ± 0.030	13.066 ± 0.752	11.940 ± 0.614	10.727 ± 0.496
KDM 1961	···	···	···	14.650 ± 0.030	12.918 ± 0.058	11.969 ± 0.001	11.551 ± 0.047
KDM 1966	···	···	···	14.351 ± 0.030	12.718 ± 0.052	11.732 ± 0.075	11.285 ± 0.044
2MASS J050620	···	···	···	13.639 ± 0.030	11.845 ± 0.065	10.558 ± 0.197	10.120 ± 0.064
2MASS J050629	···	···	17.773 ± 0.076	14.848 ± 0.011	12.931 ± 0.070	11.658 ± 0.079	11.011 ± 0.035
IRAS 05070−7020	···	···	···	···	18.312 ± 0.648	16.065 ± 0.798	13.626 ± 0.651
SHV 0507252	···	···	18.286 ± ···	14.769 ± 0.030	11.998 ± 0.461	10.894 ± 0.211	9.776 ± 0.316
SAGE MC J050752	···	···	21.738 ± ···	17.963 ± 0.140	14.534 ± 0.642	12.923 ± 0.641	11.531 ± 0.396
MSX LMC 92	···	···	22.302 ± ···	17.988 ± ···	14.519 ± 1.380	12.641 ± 1.001	11.097 ± 0.872
2MASS J050826	···	21.877 ± 0.345	20.103 ± 0.128	16.777 ± 1.367	13.189 ± 1.791	12.772 ± 1.027	10.786 ± 1.082
KDM 2187	20.841 ± 0.472	20.320 ± 0.049	17.018 ± 0.045	14.681 ± 0.007	12.895 ± 0.152	11.845 ± 0.073	11.378 ± 0.045
IRAS 05103−6959	···	···	21.017 ± ···	16.758 ± 0.070	13.801 ± 0.769	12.148 ± 0.659	10.355 ± 0.596
IRAS 05107−6953	···	···	21.926 ± ···	17.416 ± ···	13.681 ± 1.257	12.069 ± 0.926	11.265 ± 0.258
2MASS J051028	···	···	···	19.855 ± ···	15.873 ± 0.526	13.665 ± 0.545	11.956 ± 0.536
IRAS 05112−6755	20.764 ± 0.237	20.375 ± 0.058	19.149 ± 0.062	18.113 ± 0.033	16.647 ± 0.443	14.517 ± 0.826	11.921 ± 0.500
IRAS 05113−6739	···	···	···	19.548 ± ···	17.300 ± 0.343	14.790 ± 0.015	12.606 ± 0.103
MSX LMC 219	···	···	···	···	15.914 ± 1.336	14.858 ± 0.182	12.940 ± 0.599
TRM 72	20.519 ± 0.203	20.357 ± 0.060	19.962 ± 0.059	17.961 ± 0.134	14.749 ± 0.833	12.738 ± 0.792	11.056 ± 0.586
IRAS 05125−7035	···	···	···	···	18.427 ± 0.694	17.504 ± 0.842	15.107 ± 0.748
MSX LMC 220	···	20.042 ± 0.076	19.198 ± 0.067	16.981 ± 0.585	14.446 ± 0.595	12.783 ± 0.082	10.835 ± 0.303
IRAS 05132−6941	···	···	···	···	17.729 ± 0.420	15.347 ± 0.702	12.908 ± 0.619
IRAS 05133−6937	···	···	···	···	17.407 ± 0.807	16.389 ± 0.071	16.632 ± 0.643
OGLE J051306	···	···	···	17.586 ± 0.140	14.364 ± 0.405	12.514 ± 0.507	11.069 ± 0.308
MSX LMC 218	19.609 ± 0.118	19.291 ± 0.081	19.025 ± 0.084	16.533 ± 0.458	14.155 ± 0.488	12.577 ± 0.229	10.588 ± 0.526
MSX LMC 349	···	···	···	···	17.339 ± 0.141	16.284 ± 0.480	13.738 ± 0.854
SAGE MC J051803	···	···	18.892 ± 0.544	15.607 ± 0.390	13.881 ± 0.434	12.423 ± 0.345	11.199 ± 0.267
IRAS 05187−7033	···	20.975 ± 0.160	20.876 ± 0.112	20.111 ± 0.161	···	···	···

TABLE 3 — *Continued*

Target	*U* (mag.)	*B* (mag.)	*V* (mag.)	*I* (mag.)	*J* (mag.)	*H* (mag.)	*K* (mag.)
IRAS 05191−6936	···	···	···	···	···	···	···
IRAS 05190−6758	···	···	···	···	18.373 ± 0.257	15.631 ± 1.196	12.721 ± 0.846
2MASS J051908	20.859 ± 0.502	19.867 ± 0.108	16.774 ± 0.544	13.781 ± 0.149	11.959 ± 0.107	10.861 ± 0.150	10.172 ± 0.109
TRM 78	···	···	···	14.825 ± 0.040	13.659 ± 1.549	13.225 ± 0.463	10.643 ± 0.969
MSX LMC 341	···	···	···	···	17.852 ± 0.437	15.249 ± 0.680	12.516 ± 0.615
OGLE J052242	···	21.271 ± 0.173	20.011 ± 0.184	17.413 ± 0.072	14.963 ± 0.666	13.065 ± 0.435	11.445 ± 0.304
BE 74	15.795 ± 0.139	16.496 ± 0.051	15.152 ± 0.164	14.071 ± 0.072	12.648 ± 0.088	11.511 ± 0.196	10.420 ± 0.226
MSX LMC 494	···	20.934 ± 0.186	21.967 ± 0.107	16.628 ± 0.080	13.278 ± 0.523	11.913 ± 0.245	10.830 ± 0.394
IRAS F05236−6655	20.505 ± 0.186	19.444 ± 0.046	18.526 ± 0.050	17.103 ± 0.166	15.132 ± 0.457	13.291 ± 0.321	11.362 ± 0.328
2MASS J052405	···	···	20.563 ± ···	16.895 ± 0.070	14.118 ± 0.657	12.670 ± 0.548	11.251 ± 0.364
MSX LMC 441	···	···	···	···	17.486 ± 0.572	16.440 ± 0.103	13.592 ± 0.587
IRAS F05254−7149	···	20.838 ± 0.188	20.409 ± 0.093	19.753 ± 0.098	16.045 ± 1.321	13.643 ± 1.128	11.773 ± 0.856
OGLE J052445	···	21.098 ± 0.110	18.632 ± 0.052	15.736 ± 0.242	12.715 ± 0.568	11.465 ± 0.542	10.151 ± 0.375
MSX LMC 443	···	···	···	···	15.258 ± 1.651	14.246 ± 0.574	11.733 ± 0.727
LI-LMC 1028	···	···	···	18.454 ± ···	15.511 ± 0.629	13.248 ± 0.643	11.046 ± 0.603
IRAS 05260−7010	20.687 ± 0.311	20.236 ± 0.119	19.095 ± 0.099	18.356 ± 0.093	···	···	···
MSX LMC 474	···	23.070 ± 0.508	22.297 ± 0.426	19.280 ± ···	16.634 ± 0.493	14.412 ± 1.043	12.154 ± 1.113
WBP 17	···	20.616 ± 0.293	16.768 ± 0.275	14.179 ± 0.457	12.174 ± 0.203	11.196 ± 0.179	10.672 ± 0.146
MSX LMC 774	···	···	···	···	16.824 ± 0.617	14.337 ± 0.746	11.934 ± 0.621
MSX LMC 634	···	21.974 ± 0.266	21.352 ± 0.220	17.423 ± 0.176	14.748 ± 0.790	12.798 ± 0.552	11.186 ± 0.392
WBP 29	···	19.953 ± 0.077	16.297 ± 0.680	14.057 ± 0.342	12.344 ± 0.495	11.512 ± 0.463	10.925 ± 0.248
MSX LMC 601	···	···	···	18.093 ± ···	14.675 ± 0.917	12.589 ± 0.928	11.072 ± 0.575
WBP 42	···	···	18.241 ± 0.779	15.073 ± 0.107	13.087 ± 0.480	11.762 ± 0.358	10.668 ± 0.229
IRAS 05278−6942	20.530 ± 0.310	20.518 ± 0.167	20.351 ± 0.141	19.464 ± 0.124	17.645 ± 0.165	15.931 ± 0.634	12.608 ± 0.967
SHV 0528350	···	···	17.891 ± 0.258	14.252 ± 0.301	12.036 ± 0.218	10.842 ± 0.111	9.828 ± 0.142
MSX LMC 754	···	···	···	17.258 ± 0.060	14.445 ± 0.989	13.002 ± 0.535	11.065 ± 0.584
KDM 4257	20.585 ± 0.313	17.266 ± 0.095	16.234 ± 0.203	13.680 ± 0.191	11.951 ± 0.093	10.947 ± 0.105	10.477 ± 0.102
NGC 1978 IR 1	···	···	···	···	14.424 ± 1.717	13.273 ± 1.013	11.152 ± 0.995
NGC 1978 IR 4	16.352 ± 0.241	16.525 ± 0.148	15.604 ± 0.159	12.578 ± 0.878	11.539 ± 0.038	10.292 ± 0.139	9.673 ± 0.019
IRAS 05295−7121	···	···	···	20.591 ± ···	15.924 ± 0.895	14.058 ± 0.502	11.484 ± 0.719
NGC 1978 MIR 1	···	···	···	···	16.670 ± 0.050	15.351 ± 0.665	12.382 ± ···
MSX LMC 679	···	···	···	···	16.232 ± 0.785	14.412 ± 0.306	12.275 ± 0.267
GRRV 38	···	19.823 ± 0.079	18.140 ± 0.034	14.391 ± 0.151	12.376 ± 0.208	11.022 ± 0.106	9.872 ± 0.148
IRAS 05305−7251	···	···	···	···	···	···	···
IRAS 05300−6651	···	21.859 ± 0.145	21.296 ± 0.116	···	17.392 ± 0.708	14.750 ± 0.484	12.248 ± 0.415
IRAS 05306−7032	···	20.593 ± 0.086	20.458 ± 0.113	···	18.160 ± ···	18.056 ± 0.826	15.623 ± 0.518
2MASS J053044	···	···	19.660 ± ···	16.196 ± 0.050	13.468 ± 0.731	12.134 ± 0.622	10.866 ± 0.458
MSX LMC 841	···	···	···	17.542 ± 0.150	15.177 ± 0.462	13.198 ± 0.271	11.342 ± 0.204
MSX LMC 768	···	···	···	19.906 ± ···	15.858 ± 0.441	13.720 ± 1.042	11.434 ± 0.825
KDM 4665	···	···	···	14.109 ± 0.040	12.540 ± 0.114	11.488 ± 0.054	11.045 ± 0.073
MSX LMC 782	17.562 ± 0.047	18.091 ± 0.080	18.037 ± 0.192	19.429 ± 0.075	14.897 ± 0.384	13.291 ± 0.188	11.525 ± 0.212
KDM 4718	···	···	···	13.798 ± 0.040	12.090 ± 0.089	10.977 ± 0.063	10.387 ± 0.065
KDM 4774	19.481 ± 0.094	18.177 ± 0.024	16.281 ± 0.077	13.632 ± 0.023	11.981 ± 0.144	10.921 ± 0.048	10.381 ± 0.078
MSX LMC 783	···	21.496 ± 0.146	20.841 ± 0.148	18.313 ± ···	15.122 ± 0.593	12.946 ± 0.610	11.269 ± 0.372
LMC-BM 32-9	20.895 ± 0.222	20.806 ± 0.084	20.412 ± 0.243	16.242 ± 0.050	12.602 ± 0.568	10.959 ± 0.538	9.415 ± 0.115
MSX LMC 736	···	17.875 ± 0.069	16.526 ± 0.268	14.730 ± 0.064	13.733 ± 0.046	13.088 ± 0.039	12.645 ± 0.267
2MASS J053318	···	···	···	···	14.729 ± 0.777	13.045 ± 0.617	11.513 ± 0.518
IRAS 05348−7024	···	···	···	···	17.190 ± 0.562	14.852 ± 0.962	12.327 ± 0.648
2MASS J053441	···	22.778 ± 0.447	21.654 ± 0.107	17.635 ± 1.506	13.050 ± 1.170	11.352 ± 1.020	10.228 ± 0.577
MSX LMC 743	···	···	···	···	14.581 ± 2.964	13.902 ± 1.649	13.250 ± 0.331
MSX LMC 787	···	21.112 ± 0.194	20.227 ± 0.586	18.572 ± 0.070	16.727 ± 0.489	14.172 ± 0.562	11.875 ± 0.447
MSX LMC 950	···	···	···	19.349 ± ···	15.560 ± 0.937	13.225 ± 0.878	11.364 ± 0.799
MSX LMC 749	20.560 ± 0.232	20.297 ± 0.076	19.972 ± 0.103	17.658 ± 0.266	15.128 ± 0.333	13.023 ± 0.211	11.179 ± 0.179
IRAS F05355−6521	21.012 ± 0.459	20.639 ± 0.090	19.839 ± 0.058	···	14.498 ± 1.407	12.553 ± 1.257	10.840 ± 1.098
IRAS 05360−6648	···	···	···	···	18.260 ± 0.359	15.579 ± 0.807	12.992 ± 0.695
IRAS F05373−7243	···	···	···	···	18.378 ± 0.619	17.126 ± 0.332	13.876 ± 0.125
MSX LMC 967	19.733 ± 0.163	18.499 ± 0.045	22.334 ± 0.058	17.739 ± 0.255	13.751 ± 0.351	12.239 ± 0.243	10.958 ± 0.286
OGLE J053930	···	21.486 ± 0.136	21.420 ± 0.124	17.024 ± 0.537	14.489 ± 0.683	12.873 ± 0.521	11.114 ± 0.515
MSX LMC 971	···	21.308 ± 0.121	19.846 ± 0.090	18.614 ± 0.067	17.778 ± 0.165	15.637 ± 0.872	12.953 ± 0.922
MSX LMC 1400	18.368 ± 0.047	18.730 ± 0.028	18.684 ± 0.031	18.697 ± 0.066	16.978 ± 0.481	14.227 ± 0.367	11.864 ± 0.277
IRAS 05410−6954	21.528 ± 0.447	21.237 ± 0.416	20.448 ± 0.102	19.209 ± 0.124	15.229 ± 0.781	12.950 ± 1.038	10.957 ± 0.669
MSX LMC 974	···	···	···	18.367 ± ···	14.795 ± 0.387	12.729 ± 0.200	11.124 ± 0.155
IRAS 05416−6906	···	···	···	···	···	···	16.970 ± 0.180
KDM 5841	···	19.964 ± 0.054	17.657 ± 0.042	14.881 ± 0.134	13.040 ± 0.138	11.812 ± 0.098	11.164 ± 0.074
MSX LMC 1384	···	···	···	19.445 ± ···	16.310 ± 0.534	13.806 ± 0.514	11.689 ± 0.433
IRAS 05446−6945	···	···	···	···	18.318 ± 0.350	15.950 ± 0.649	13.441 ± 0.594
2MASS J054437	···	···	···	16.954 ± 0.090	14.144 ± 0.171	12.402 ± 0.083	11.054 ± 0.135
2MASS J054546	···	···	···	17.794 ± 0.150	15.939 ± 0.198	14.593 ± 0.269	13.311 ± 0.274
NGC 2121 LE 6	···	19.961 ± 0.115	17.972 ± 0.154	14.717 ± 0.775	12.627 ± 0.295	11.184 ± 0.170	10.258 ± 0.095
MSX LMC 1492	···	22.602 ± 0.195	18.843 ± 0.040	15.163 ± 0.180	12.849 ± 0.696	11.197 ± 0.658	9.728 ± 0.377
IRAS 05506−7053	···	···	···	···	17.667 ± 0.571	15.691 ± 1.429	12.943 ± 1.136
LI-LMC 1758	···	···	···	···	15.784 ± 0.535	13.427 ± 0.600	11.631 ± 0.482
IRAS 05509−6956	···	···	···	···	···	···	···
KDM 6486	21.607 ± 0.443	19.309 ± 0.047	17.145 ± 0.029	14.627 ± 0.031	12.963 ± 0.031	12.009 ± 0.062	11.541 ± 0.032
IRAS 05516−7124	···	···	···	···	18.444 ± 0.551	15.603 ± 0.828	13.133 ± 0.838
PMP 337	···	19.235 ± 0.043	16.454 ± 0.024	13.960 ± 0.093	12.249 ± 0.054	11.212 ± 0.103	10.649 ± 0.071

TABLE 3 — *Continued*

Target	*U* (mag.)	*B* (mag.)	*V* (mag.)	*I* (mag.)	*J* (mag.)	*H* (mag.)	*K* (mag.)
IRAS 05568−6753	···	···	···	···	19.405 ± ···	17.435 ± ···	15.873 ± 0.121
IRAS 06025−6712	···	···	···	···	17.887 ± 0.059	14.944 ± 0.764	12.336 ± 0.737
IRAS 06028−6722	···	22.637 ± 0.303	21.897 ± 0.219	···	18.352 ± 0.115	16.215 ± 0.323	12.725 ± 0.769
IRAS F06108−7045	···	···	···	···	17.644 ± 0.328	14.877 ± 0.068	12.426 ± 0.225

TABLE 4
MID-INFRARED PHOTOMETRY AND BOLOMETRIC MAGNITUDES

Target	[3.6] (mag.)	[4.5] (mag.)	[5.8] (mag.)	[8.0] (mag.)	[24] (mag.)	M_{bol} (mag.)
GM 780	8.738 ± 0.454	8.288 ± 0.413	8.283 ± 0.064	7.916 ± 0.066	6.771 ± 0.368	−5.90
MSX SMC 091	9.602 ± 0.366	8.976 ± 0.322	8.260 ± 0.008	7.864 ± 0.029	7.328 ± 0.060	−4.88
MSX SMC 062	8.941 ± 0.266	8.375 ± 0.304	7.639 ± 0.026	7.092 ± 0.023	6.272 ± 0.178	−5.50
MSX SMC 054	9.940 ± 0.327	9.037 ± 0.313	8.408 ± 0.201	7.771 ± 0.142	6.595 ± 0.142	−4.58
2MASS J004326	10.495 ± 0.400	10.476 ± 0.257	10.196 ± 0.095	9.615 ± 0.061	9.316 ± 0.056	−4.56
MSX SMC 044	9.300 ± 0.256	8.661 ± 0.230	8.189 ± 0.191	7.713 ± 0.155	7.216 ± 0.077	−5.29
MSX SMC 105	9.312 ± 0.129	8.544 ± 0.151	8.007 ± 0.079	7.370 ± 0.078	5.928 ± 0.220	−5.04
MSX SMC 036	9.698 ± 0.314	8.790 ± 0.274	8.051 ± 0.199	7.515 ± 0.160	6.529 ± 0.131	−4.62
GB S06	8.666 ± 0.259	7.927 ± 0.373	6.922 ± 0.157	6.241 ± 0.182	4.874 ± 0.098	−5.62
MSX SMC 200	9.298 ± 0.180	8.806 ± 0.198	8.362 ± 0.062	7.894 ± 0.030	7.276 ± 0.206	−4.81
MSX SMC 033	8.601 ± 0.304	7.941 ± 0.255	7.439 ± 0.164	6.923 ± 0.146	6.421 ± 0.163	−5.69
IRAS F00454−7257	8.808 ± 0.342	7.969 ± 0.306	7.251 ± 0.338	6.381 ± 0.319	4.953 ± 0.306	−5.10
MSX SMC 066	8.805 ± 0.167	8.271 ± 0.158	7.779 ± 0.038	7.345 ± 0.041	6.715 ± 0.015	−5.46
IRAS F00471−7352	8.414 ± 0.415	7.625 ± 0.353	6.725 ± 0.116	6.109 ± 0.136	5.015 ± 0.281	−6.04
LIN 131	9.865 ± 0.374	9.732 ± 0.322	9.298 ± 0.379	9.040 ± 0.353	8.354 ± 0.370	−5.72
RAW 594	10.522 ± 0.044	10.624 ± 0.054	10.504 ± 0.048	9.886 ± 0.054	9.647 ± 0.105	−4.50
MSX SMC 163	9.176 ± 0.298	8.441 ± 0.287	7.900 ± 0.220	7.261 ± 0.151	5.979 ± 0.186	−5.25
LEGC A144	9.874 ± 0.267	9.443 ± 0.264	9.327 ± 0.083	8.794 ± 0.181	8.562 ± 0.205	−4.55
MSX SMC 125	8.588 ± 0.366	8.048 ± 0.338	7.373 ± 0.170	7.008 ± 0.132	···	−5.94
MSX SMC 162	8.689 ± 0.243	8.133 ± 0.200	7.731 ± 0.176	7.352 ± 0.179	7.250 ± 0.118	−5.47
MSX SMC 202	8.947 ± 0.108	8.553 ± 0.123	8.077 ± 0.120	7.682 ± 0.151	7.634 ± 0.051	−5.56
MSX SMC 159	9.572 ± 0.433	8.589 ± 0.370	7.575 ± 0.020	6.993 ± 0.027	5.976 ± 0.285	−4.79
LEGC 105	9.809 ± 0.227	9.310 ± 0.226	8.913 ± 0.202	8.487 ± 0.169	8.219 ± 0.077	−4.73
ISO 00548	9.356 ± 0.300	8.815 ± 0.302	8.241 ± 0.286	7.844 ± 0.253	7.418 ± 0.135	−4.97
ISO 00549	8.948 ± 0.356	8.222 ± 0.308	7.532 ± 0.346	6.926 ± 0.285	6.097 ± 0.022	−5.20
RAW 960	10.257 ± 0.242	9.925 ± 0.191	9.503 ± 0.223	9.140 ± 0.215	8.979 ± 0.109	−4.59
MSX SMC 209	9.178 ± 0.275	8.410 ± 0.257	7.765 ± 0.318	7.166 ± 0.225	6.243 ± 0.120	−5.30
NGC 330 BAL 555	10.017 ± 0.108	10.200 ± 0.131	10.281 ± 0.050	9.621 ± 0.079	9.368 ± 0.011	−4.92
IRAS 00554−7351	9.078 ± 0.513	7.989 ± 0.456	7.436 ± 0.024	6.505 ± 0.028	4.552 ± 0.404	−6.01
MSX SMC 198	9.540 ± 0.301	8.887 ± 0.274	8.522 ± 0.297	7.986 ± 0.276	7.158 ± 0.206	−4.72
ISO 00573	9.951 ± 0.209	9.457 ± 0.200	9.180 ± 0.075	8.826 ± 0.066	8.347 ± 0.047	−4.76
MSX SMC 093	9.328 ± 0.237	8.945 ± 0.187	8.543 ± 0.132	8.189 ± 0.087	7.877 ± 0.140	−5.02
ISO 01019	10.196 ± 0.257	9.596 ± 0.210	8.984 ± 0.224	8.489 ± 0.153	8.132 ± 0.039	−4.34
MSX SMC 232	9.865 ± 0.239	9.120 ± 0.261	8.284 ± 0.228	7.650 ± 0.180	6.964 ± 0.189	−4.55
NGC 419 LE 16	9.949 ± 0.119	9.834 ± 0.127	9.532 ± 0.185	9.065 ± 0.160	8.764 ± 0.159	−4.66
NGC 419 IR 1	9.019 ± 0.168	8.437 ± 0.185	8.023 ± 0.037	7.451 ± 0.095	6.766 ± 0.212	−5.24
NGC 419 MIR 1	10.730 ± 0.613	9.208 ± 0.566	7.880 ± 0.477	6.826 ± 0.396	4.618 ± 0.148	−4.73
NGC 419 LE 35	10.188 ± 0.058	10.395 ± 0.041	10.460 ± 0.038	9.858 ± 0.007	···	−4.98
NGC 419 LE 27	10.276 ± 0.068	10.381 ± 0.055	10.300 ± 0.031	9.785 ± 0.027	···	−4.85
NGC 419 LE 18	10.240 ± 0.033	10.377 ± 0.050	10.419 ± 0.064	9.762 ± 0.058	9.793 ± 0.112	−4.66
IRAS 04628−6937	9.022 ± 0.514	8.021 ± 0.436	6.933 ± 0.516	6.168 ± 0.413	4.666 ± 0.286	−5.36
IRAS F04331−6932	10.005 ± 0.461	8.559 ± 0.385	7.702 ± 0.272	6.648 ± 0.222	4.634 ± 0.148	−5.02
IRAS F04340−7016	9.278 ± 0.285	8.595 ± 0.279	7.924 ± 0.229	7.377 ± 0.201	6.367 ± 0.193	−4.63
IRAS F04353−6702	9.896 ± 0.480	8.701 ± 0.428	···	···	5.355 ± 0.010	−4.51
IRAS F04375−7247	9.101 ± 0.467	8.042 ± 0.432	···	···	···	−4.99
IRAS 04374−6831	9.270 ± 0.305	8.252 ± 0.296	7.511 ± 0.283	6.761 ± 0.234	5.101 ± 0.189	−5.29
IRAS F04433−7018	9.172 ± 0.372	8.422 ± 0.355	7.646 ± 0.020	7.040 ± 0.014	6.089 ± 0.021	−4.80
2MASS J044627	9.527 ± 0.329	8.990 ± 0.296	8.710 ± 0.240	8.264 ± 0.213	7.326 ± 0.099	−4.48
IRAS 04473−6829	7.980 ± 0.368	7.185 ± 0.309	6.323 ± 0.132	5.717 ± 0.117	4.640 ± 0.041	−5.83
IRAS 04496−6958	7.621 ± 0.194	6.985 ± 0.198	6.324 ± 0.109	5.691 ± 0.075	4.001 ± 0.069	−6.50
MSX LMC 1128	9.186 ± 0.192	8.805 ± 0.198	8.572 ± 0.048	8.142 ± 0.078	7.615 ± 0.036	−4.84
MSX LMC 1308	8.646 ± 0.465	7.970 ± 0.450	6.887 ± 0.037	6.339 ± 0.017	5.553 ± 0.012	−5.47
MSX LMC 1205	8.686 ± 0.347	7.863 ± 0.319	6.972 ± 0.272	6.278 ± 0.236	5.093 ± 0.182	−5.60
IRAS 04518−6852	11.928 ± 0.680	9.794 ± 0.598	8.614 ± 0.085	7.024 ± 0.037	4.196 ± 0.012	−5.07
MSX LMC 1213	9.751 ± 0.436	8.700 ± 0.385	8.083 ± 0.130	7.315 ± 0.100	5.805 ± 0.066	−4.78
KDM 764	9.268 ± 0.057	9.365 ± 0.032	9.346 ± 0.019	8.800 ± 0.019	8.456 ± 0.008	−5.25
2MASS J045328	9.685 ± 0.207	9.434 ± 0.137	8.967 ± 0.012	8.459 ± 0.014	8.173 ± 0.002	−4.81
IRAS 04535−6616	10.464 ± 0.750	8.886 ± 0.718	8.192 ± 0.060	6.766 ± 0.043	4.217 ± 0.074	−5.04
IRAS 04539−6821	9.181 ± 0.320	7.983 ± 0.262	7.017 ± 0.156	6.179 ± 0.138	4.622 ± 0.124	−4.97
IRAS F04537−6509	8.912 ± 0.341	8.182 ± 0.291	···	···	5.917 ± 0.014	−5.23
MSX LMC 1209	9.209 ± 0.356	8.276 ± 0.316	7.412 ± 0.213	6.734 ± 0.204	5.376 ± 0.116	−4.75
IRAS 04557−6753	9.080 ± 0.548	7.960 ± 0.475	6.646 ± 0.055	5.818 ± 0.076	4.104 ± 0.075	−5.12

TABLE 4 — *Continued*

Target	[3.6] (mag.)	[4.5] (mag.)	[5.8] (mag.)	[8.0] (mag.)	[24] (mag.)	$M_{\rm bol}$ (mag.)
IRAS 04567−6857	8.016 ± 0.368	7.223 ± 0.351	6.479 ± 0.354	5.755 ± 0.284	4.574 ± 0.223	−6.21
IRAS 04589−6825	11.440 ± 0.674	9.350 ± 0.532	7.475 ± 0.101	6.183 ± 0.083	3.684 ± 0.032	−5.06
KDM 1238	10.090 ± 0.095	10.172 ± 0.126	9.971 ± 0.010	9.556 ± 0.020	9.507 ± 0.007	−4.76
IRAS F05013−7213	9.416 ± 0.407	8.405 ± 0.374	7.530 ± 0.347	6.851 ± 0.295	5.300 ± 0.241	−4.93
IRAS 05010−6739	8.555 ± 0.430	7.755 ± 0.381	7.212 ± 0.107	6.385 ± 0.081	4.995 ± 0.011	−5.79
IRAS 05009−6616	8.793 ± 0.392	7.712 ± 0.345	6.787 ± 0.164	5.994 ± 0.137	4.612 ± 0.165	−5.47
IRAS 05026−6809	16.077 ± 0.021	12.761 ± 0.121	9.946 ± 0.067	7.326 ± 0.042	3.073 ± 0.011	−5.02
KDM 1656	9.003 ± 0.054	8.939 ± 0.122	8.900 ± 0.015	8.264 ± 0.023	8.233 ± 0.013	−5.57
W60 B14	8.937 ± 0.080	9.031 ± 0.069	8.921 ± 0.050	8.439 ± 0.008	7.850 ± 0.049	−5.69
LMC-BM 12-14	9.265 ± 0.062	9.349 ± 0.052	9.213 ± 0.006	8.738 ± 0.021	8.332 ± 0.092	−5.40
IRAS 05042−6827	16.509 ± 0.093	13.107 ± 0.182	10.266 ± 0.005	7.723 ± 0.031	3.640 ± 0.001	−4.49
NGC 1818 WBT 64	10.363 ± 0.085	10.225 ± 0.078	9.877 ± 0.078	9.535 ± 0.065	8.969 ± 0.009	−4.62
NGC 1835 LE 1	9.995 ± 0.155	10.101 ± 0.134	10.103 ± 0.007	9.654 ± 0.013	9.560 ± 0.124	−4.72
IRAS 05053−6901	11.576 ± 0.794	9.283 ± 0.674	8.134 ± 0.231	6.587 ± 0.185	3.822 ± 0.159	−5.70
LMC-BM 13-2	9.964 ± 0.163	9.682 ± 0.113	9.422 ± 0.009	9.010 ± 0.028	8.454 ± 0.056	−3.96
2MASS J050607	9.899 ± 0.239	9.501 ± 0.232	9.154 ± 0.378	8.861 ± 0.301	8.331 ± 0.095	−4.50
KDM 1961	10.930 ± 0.027	11.036 ± 0.112	10.743 ± 0.018	10.599 ± 0.061	···	−4.01
KDM 1966	10.873 ± 0.043	10.990 ± 0.052	10.792 ± 0.045	10.492 ± 0.035	···	−4.22
2MASS J050620	9.363 ± 0.051	9.428 ± 0.033	9.352 ± 0.035	8.755 ± 0.040	8.652 ± 0.033	−5.32
2MASS J050629	10.317 ± 0.117	10.467 ± 0.093	10.546 ± 0.038	9.858 ± 0.045	···	−4.25
IRAS 05070−7020	10.079 ± 0.454	8.842 ± 0.441	7.651 ± 0.576	6.565 ± 0.520	4.033 ± 0.346	−5.19
SHV 0507252	8.797 ± 0.145	8.395 ± 0.113	8.206 ± 0.030	7.760 ± 0.022	7.561 ± 0.014	−5.49
SAGE MC J050752	10.006 ± 0.235	9.358 ± 0.244	8.681 ± 0.259	8.194 ± 0.223	7.479 ± 0.127	−3.93
MSX LMC 92	8.830 ± 0.268	8.035 ± 0.229	7.261 ± 0.273	6.548 ± 0.226	5.371 ± 0.158	−5.28
2MASS J050826	9.160 ± 0.200	8.666 ± 0.236	8.365 ± 0.132	7.905 ± 0.083	7.363 ± 0.045	−4.82
KDM 2187	10.813 ± 0.101	10.841 ± 0.084	10.645 ± 0.185	10.162 ± 0.094	9.363 ± 0.129	−4.06
IRAS 05103−6959	8.450 ± 0.481	7.716 ± 0.486	6.683 ± 0.216	6.104 ± 0.192	5.029 ± 0.127	−5.64
IRAS 05107−6953	8.682 ± 0.431	7.898 ± 0.399	7.407 ± 0.202	6.594 ± 0.164	5.188 ± 0.111	−5.53
2MASS J051028	9.634 ± 0.352	8.749 ± 0.301	8.227 ± 0.093	7.553 ± 0.124	6.425 ± 0.139	−4.33
IRAS 05112−6755	8.328 ± 0.436	7.186 ± 0.386	6.113 ± 0.005	5.247 ± 0.031	3.472 ± 0.004	−5.80
IRAS 05113−6739	8.909 ± 0.434	7.823 ± 0.408	6.599 ± 0.114	5.747 ± 0.111	4.171 ± 0.026	−5.30
MSX LMC 219	9.371 ± 0.446	8.241 ± 0.389	6.825 ± 0.089	5.993 ± 0.099	4.348 ± 0.052	−4.91
TRM 72	8.804 ± 0.541	7.939 ± 0.404	7.447 ± 0.334	6.617 ± 0.308	5.364 ± 0.155	−5.41
IRAS 05125−7035	10.102 ± 0.325	8.277 ± 0.269	6.957 ± 0.198	5.596 ± 0.161	3.152 ± 0.120	−5.69
MSX LMC 220	8.024 ± 0.304	7.161 ± 0.289	6.380 ± 0.316	5.665 ± 0.265	4.563 ± 0.170	−5.85
IRAS 05132−6941	9.053 ± 0.598	8.100 ± 0.375	6.967 ± 0.426	6.073 ± 0.385	4.565 ± 0.235	−5.08
IRAS 05133−6937	15.869 ± 0.077	13.866 ± 0.213	10.696 ± 0.127	7.850 ± 0.093	3.322 ± 0.040	−4.71
OGLE J051306	9.693 ± 0.385	8.964 ± 0.360	8.083 ± 0.233	7.591 ± 0.209	6.826 ± 0.138	−4.56
MSX LMC 218	8.104 ± 0.459	7.370 ± 0.419	6.550 ± 0.027	6.004 ± 0.080	4.978 ± 0.088	−5.65
MSX LMC 349	9.609 ± 0.458	8.400 ± 0.414	7.545 ± 0.581	6.715 ± 0.534	4.934 ± 0.368	−4.88
SAGE MC J051803	9.799 ± 0.245	9.476 ± 0.253	8.834 ± 0.226	8.427 ± 0.153	7.847 ± 0.148	−4.18
IRAS 05187−7033	14.518 ± 0.641	11.883 ± 0.397	9.876 ± 0.086	7.663 ± 0.074	2.786 ± 0.052	−5.15
IRAS 05191−6936	15.193 ± 0.139	12.663 ± 0.283	9.703 ± 0.091	7.168 ± 0.030	3.341 ± 0.004	−4.87
IRAS 05190−6758	9.181 ± 0.697	7.727 ± 0.595	6.201 ± 0.038	5.198 ± 0.036	3.165 ± 0.085	−5.61
2MASS J051908	9.570 ± 0.124	9.716 ± 0.074	9.599 ± 0.016	9.059 ± 0.003	8.526 ± 0.035	−5.10
TRM 78	8.716 ± 0.379	8.020 ± 0.381	7.307 ± 0.243	6.720 ± 0.214	5.696 ± 0.129	−5.16
MSX LMC 341	9.458 ± 0.522	8.288 ± 0.435	7.363 ± 0.431	6.572 ± 0.383	4.914 ± 0.192	−4.79
OGLE J052242	9.406 ± 0.367	8.705 ± 0.307	8.328 ± 0.260	7.753 ± 0.226	6.828 ± 0.165	−4.62
BE 74	8.771 ± 0.082	8.147 ± 0.055	7.539 ± 0.021	6.937 ± 0.025	5.062 ± 0.035	−5.49
MSX LMC 494	9.330 ± 0.346	8.618 ± 0.311	8.174 ± 0.150	7.578 ± 0.181	6.507 ± 0.062	−4.87
IRAS F05236−6655	9.340 ± 0.555	8.317 ± 0.454	7.188 ± 0.029	6.580 ± 0.057	5.312 ± 0.019	−5.20
2MASS J052405	9.595 ± 0.287	9.113 ± 0.278	8.716 ± 0.126	8.268 ± 0.099	7.598 ± 0.058	−4.23
MSX LMC 441	9.738 ± 0.356	8.520 ± 0.318	7.293 ± 0.397	6.394 ± 0.329	4.628 ± 0.148	−4.90
IRAS F05254−7149	9.296 ± 0.393	8.175 ± 0.391	7.672 ± 0.155	6.731 ± 0.124	4.925 ± 0.012	−5.12
OGLE J052445	9.257 ± 0.275	8.802 ± 0.247	8.122 ± 0.069	7.824 ± 0.085	7.051 ± 0.101	−5.00
MSX LMC 443	9.456 ± 0.474	8.439 ± 0.414	7.276 ± 0.109	6.594 ± 0.123	5.129 ± 0.072	−4.67
LI-LMC 1028	8.641 ± 0.339	7.783 ± 0.290	7.032 ± 0.159	6.355 ± 0.116	5.407 ± 0.071	−5.52
IRAS 05260−7010	16.152 ± 0.292	13.315 ± 0.167	10.436 ± 0.037	7.844 ± 0.057	3.805 ± 0.051	−4.26
MSX LMC 474	8.702 ± 0.397	7.780 ± 0.358	7.029 ± 0.052	6.164 ± 0.049	4.685 ± 0.052	−5.47
WBP 17	10.259 ± 0.105	10.293 ± 0.092	10.139 ± 0.221	9.824 ± 0.146	9.487 ± 0.142	−4.70
MSX LMC 774	9.498 ± 0.326	8.364 ± 0.279	7.322 ± 0.362	6.462 ± 0.260	4.729 ± 0.150	−4.98
MSX LMC 634	9.017 ± 0.286	8.226 ± 0.265	7.550 ± 0.197	6.941 ± 0.199	6.143 ± 0.133	−5.00
WBP 29	10.543 ± 0.150	10.467 ± 0.233	10.093 ± 0.117	9.822 ± 0.148	···	−4.52
MSX LMC 601	8.636 ± 0.279	7.890 ± 0.258	7.102 ± 0.351	6.395 ± 0.270	5.265 ± 0.169	−5.20
WBP 42	9.431 ± 0.127	9.098 ± 0.154	8.893 ± 0.075	8.570 ± 0.076	8.355 ± 0.006	−4.65
IRAS 05278−6942	8.424 ± 0.378	7.124 ± 0.329	6.042 ± 0.218	5.052 ± 0.185	3.129 ± 0.102	−6.44
SHV 0528350	9.175 ± 0.144	9.033 ± 0.120	8.754 ± 0.047	8.286 ± 0.035	6.532 ± 0.083	−5.30
MSX LMC 754	8.966 ± 0.309	8.370 ± 0.284	7.770 ± 0.299	7.240 ± 0.289	6.349 ± 0.183	−4.82
KDM 4257	9.853 ± 0.046	9.864 ± 0.060	9.773 ± 0.030	9.355 ± 0.043	8.898 ± 0.057	−5.00
NGC 1978 IR 1	8.819 ± 0.305	8.243 ± 0.309	7.476 ± 0.019	6.986 ± 0.015	6.392 ± 0.198	−4.96
NGC 1978 IR 4	8.795 ± 0.219	8.913 ± 0.275	9.167 ± 0.017	8.486 ± 0.010	8.178 ± 0.042	−5.77
IRAS 05295−7121	9.111 ± 0.442	8.032 ± 0.392	7.071 ± 0.354	6.274 ± 0.327	4.671 ± 0.221	−5.15
NGC 1978 MIR 1	9.723 ± 0.489	8.792 ± 0.362	7.976 ± 0.524	7.242 ± 0.421	5.776 ± 0.012	−4.66
MSX LMC 679	9.779 ± 0.429	8.706 ± 0.414	8.141 ± 0.221	7.265 ± 0.159	5.499 ± 0.097	−4.80
GRRV 38	8.688 ± 0.238	8.324 ± 0.219	8.181 ± 0.266	7.920 ± 0.270	7.136 ± 0.134	−5.39
IRAS 05305−7251	13.315 ± 0.461	10.624 ± 0.478	8.984 ± 0.252	7.108 ± 0.221	3.868 ± 0.190	−4.73

TABLE 4 — *Continued*

Target	[3.6] (mag.)	[4.5] (mag.)	[5.8] (mag.)	[8.0] (mag.)	[24] (mag.)	M_{bol} (mag.)
IRAS 05300−6651	9.208 ± 0.448	8.050 ± 0.400	6.971 ± 0.375	6.146 ± 0.285	4.469 ± 0.194	−5.21
IRAS 05306−7032	11.214 ± 0.310	9.469 ± 0.298	7.881 ± 0.133	6.558 ± 0.124	4.100 ± 0.057	−4.26
2MASS J053044	8.886 ± 0.247	8.402 ± 0.274	8.256 ± 0.084	7.755 ± 0.083	7.189 ± 0.055	−4.96
MSX LMC 841	8.965 ± 0.258	8.230 ± 0.231	7.753 ± 0.052	7.067 ± 0.047	5.923 ± 0.045	−5.11
MSX LMC 768	8.493 ± 0.351	7.606 ± 0.353	6.773 ± 0.291	5.973 ± 0.246	4.488 ± 0.163	−5.83
KDM 4665	10.702 ± 0.099	10.782 ± 0.118	10.454 ± 0.056	10.191 ± 0.017	9.343 ± 0.128	−4.45
MSX LMC 782	9.144 ± 0.372	8.367 ± 0.341	7.482 ± 0.305	6.897 ± 0.267	5.668 ± 0.211	−4.81
KDM 4718	9.884 ± 0.037	10.001 ± 0.038	9.978 ± 0.056	9.546 ± 0.015	9.186 ± 0.114	−5.00
KDM 4774	9.845 ± 0.058	9.891 ± 0.091	9.532 ± 0.026	9.119 ± 0.028	8.273 ± 0.021	−5.03
MSX LMC 783	9.016 ± 0.298	8.293 ± 0.354	7.932 ± 0.042	7.283 ± 0.027	6.013 ± 0.064	−5.04
LMC-BM 32-9	7.742 ± 0.094	7.123 ± 0.086	6.686 ± 0.068	6.273 ± 0.055	6.194 ± 0.061	−6.17
MSX LMC 736	9.811 ± 0.037	8.436 ± 0.045	7.323 ± 0.027	6.266 ± 0.034	···	−4.85
2MASS J053318	9.724 ± 0.245	9.126 ± 0.248	8.484 ± 0.066	7.873 ± 0.056	6.807 ± 0.068	−4.26
IRAS 05348−7024	9.074 ± 0.480	7.840 ± 0.436	6.734 ± 0.367	5.748 ± 0.326	4.041 ± 0.242	−5.60
2MASS J053441	8.777 ± 0.214	8.134 ± 0.181	7.780 ± 0.043	7.269 ± 0.029	6.739 ± 0.005	−5.24
MSX LMC 743	9.380 ± 0.370	8.316 ± 0.336	7.222 ± 0.091	6.482 ± 0.069	4.928 ± 0.108	−4.75
MSX LMC 787	9.166 ± 0.535	8.262 ± 0.481	7.228 ± 0.348	6.494 ± 0.303	4.846 ± 0.197	−4.97
MSX LMC 950	8.921 ± 0.442	8.037 ± 0.399	7.604 ± 0.395	6.881 ± 0.343	5.652 ± 0.228	−4.98
MSX LMC 749	8.925 ± 0.273	8.121 ± 0.261	7.300 ± 0.161	6.611 ± 0.098	5.539 ± 0.113	−5.36
IRAS F05355−6521	8.934 ± 0.336	8.261 ± 0.305	7.844 ± 0.291	7.297 ± 0.217	6.275 ± 0.019	−5.11
IRAS 05360−6648	9.770 ± 0.509	8.513 ± 0.440	7.481 ± 0.338	6.633 ± 0.305	5.008 ± 0.012	−4.73
IRAS F05373−7243	9.600 ± 0.435	8.424 ± 0.378	7.648 ± 0.254	6.754 ± 0.211	5.201 ± 0.115	−5.13
MSX LMC 967	8.735 ± 0.324	7.979 ± 0.307	7.553 ± 0.135	6.913 ± 0.118	5.801 ± 0.091	−5.34
OGLE J053930	9.222 ± 0.264	8.688 ± 0.243	8.263 ± 0.268	7.771 ± 0.223	7.026 ± 0.115	−4.57
MSX LMC 971	10.077 ± 0.357	8.727 ± 0.331	7.836 ± 0.198	6.835 ± 0.180	5.008 ± 0.129	−4.68
MSX LMC 1400	9.301 ± 0.339	8.209 ± 0.322	7.014 ± 0.200	6.171 ± 0.210	4.490 ± 0.156	−5.09
IRAS 05410−6954	8.600 ± 0.419	7.624 ± 0.391	6.326 ± 0.511	5.535 ± 0.431	4.101 ± 0.252	−5.71
MSX LMC 974	8.798 ± 0.325	8.026 ± 0.246	7.326 ± 0.133	6.671 ± 0.097	5.622 ± 0.042	−5.14
IRAS 05416−6906	12.131 ± 0.605	9.748 ± 0.538	8.385 ± 0.214	6.709 ± 0.123	3.782 ± 0.106	−5.25
KDM 5841	10.416 ± 0.092	10.475 ± 0.079	10.271 ± 0.016	9.648 ± 0.006	8.296 ± 0.038	−4.14
MSX LMC 1384	8.712 ± 0.128	7.912 ± 0.176	7.297 ± 0.228	6.674 ± 0.223	5.237 ± 0.139	−5.04
IRAS 05446−6945	9.714 ± 0.450	8.373 ± 0.411	6.847 ± 0.194	5.835 ± 0.168	3.863 ± 0.080	−5.04
2MASS J054437	9.637 ± 0.319	8.972 ± 0.294	8.329 ± 0.155	7.836 ± 0.128	7.130 ± 0.090	−4.59
2MASS J054546	11.314 ± 0.124	10.558 ± 0.062	9.824 ± 0.011	8.906 ± 0.016	6.803 ± 0.011	−3.05
NGC 2121 LE 6	9.161 ± 0.178	8.832 ± 0.173	8.676 ± 0.074	8.264 ± 0.036	8.112 ± 0.053	−5.03
MSX LMC 1492	7.960 ± 0.292	7.425 ± 0.246	6.867 ± 0.061	6.413 ± 0.044	6.056 ± 0.013	−5.94
IRAS 05506−7053	9.221 ± 0.774	7.741 ± 0.631	6.462 ± 0.719	5.366 ± 0.589	3.611 ± 0.006	−5.88
LI-LMC 1758	8.933 ± 0.377	8.098 ± 0.374	7.685 ± 0.023	6.891 ± 0.025	5.375 ± 0.015	−5.40
IRAS 05509−6956	14.790 ± 0.553	11.442 ± 0.606	9.301 ± 0.139	6.992 ± 0.072	3.106 ± 0.025	−5.04
KDM 6486	11.061 ± 0.047	11.098 ± 0.072	10.860 ± 0.048	10.662 ± 0.028	···	−3.93
IRAS 05516−7124	9.494 ± 0.446	8.270 ± 0.388	7.036 ± 0.027	6.119 ± 0.034	4.500 ± 0.008	−5.26
PMP 337	10.252 ± 0.065	10.344 ± 0.059	10.185 ± 0.074	9.898 ± 0.088	10.000 ± 0.210	−4.71
IRAS 05568−6753	10.902 ± 0.803	8.687 ± 0.769	7.807 ± 0.210	6.058 ± 0.177	3.142 ± 0.108	−6.03
IRAS 06025−6712	8.335 ± 0.570	7.030 ± 0.500	5.744 ± 0.110	4.884 ± 0.072	3.167 ± 0.074	−5.99
IRAS 06028−6722	8.771 ± 0.459	7.401 ± 0.384	6.454 ± 0.293	5.481 ± 0.269	3.571 ± 0.189	−5.72
IRAS F06108−7045	9.396 ± 0.331	8.288 ± 0.292	···	···	···	−4.96

TABLE 5
SPECTROSCOPIC DATA — IRS SAMPLE

Target	Eq. Width of C_2H_2 at 7.5 um	F_{SiC} / continuum	[6.4]−[9.3] (mag.)	[16.5]−[21.5] (mag.)	F_{MgS} / continuum	IR spectral classification
GM 780	0.162 ± 0.010	0.316 ± 0.006	0.403 ± 0.008	0.165 ± 0.024	···	CE2
MSX SMC 091	0.146 ± 0.015	0.147 ± 0.007	0.528 ± 0.007	0.073 ± 0.025	···	CE2
MSX SMC 062	0.117 ± 0.006	0.062 ± 0.003	0.675 ± 0.008	0.174 ± 0.024	···	CE3
MSX SMC 054	0.177 ± 0.006	0.179 ± 0.003	0.756 ± 0.004	0.101 ± 0.016	0.191 ± 0.021	CE3
2MASS J004326	0.196 ± 0.007	0.080 ± 0.006	0.234 ± 0.019	···	···	CE1
MSX SMC 044	0.050 ± 0.005	0.024 ± 0.004	0.517 ± 0.006	−0.101 ± 0.046	···	CE2
MSX SMC 105	0.184 ± 0.008	0.157 ± 0.005	0.866 ± 0.003	0.226 ± 0.022	0.254 ± 0.029	CE3
MSX SMC 036	0.234 ± 0.006	0.088 ± 0.004	0.774 ± 0.005	0.286 ± 0.017	0.279 ± 0.021	CE3
GB S06	0.113 ± 0.005	0.058 ± 0.002	0.969 ± 0.003	0.284 ± 0.020	0.358 ± 0.025	CE4
MSX SMC 200	0.032 ± 0.007	0.010 ± 0.003	0.443 ± 0.008	0.067 ± 0.029	···	CE2
MSX SMC 033	0.055 ± 0.004	0.040 ± 0.002	0.514 ± 0.009	−0.122 ± 0.022	···	CE2
IRAS F00454−7257	0.003 ± 0.024	0.117 ± 0.006	0.763 ± 0.025	···	···	CE3
MSX SMC 066	0.083 ± 0.003	0.036 ± 0.002	0.427 ± 0.010	−0.440 ± 0.093	···	CE2
IRAS F00471−7352	0.125 ± 0.003	0.116 ± 0.003	0.701 ± 0.008	0.240 ± 0.009	0.120 ± 0.011	CE3
LIN 131	−0.001 ± 0.010	0.181 ± 0.009	0.288 ± 0.014	0.526 ± 0.045	···	CE1
RAW 594	−0.075 ± 0.008	−0.001 ± 0.010	0.000 ± 0.016	···	···	CE0
MSX SMC 163	0.132 ± 0.005	0.169 ± 0.004	0.705 ± 0.004	0.198 ± 0.010	0.143 ± 0.014	CE3
LEGC A144	0.142 ± 0.016	0.006 ± 0.012	0.377 ± 0.014	0.297 ± 0.094	···	CE2
MSX SMC 125	0.089 ± 0.011	0.062 ± 0.012	0.225 ± 0.015	1.408 ± 0.037	···	CE1
MSX SMC 162	0.140 ± 0.006	0.051 ± 0.003	0.361 ± 0.010	−0.109 ± 0.029	···	CE2

TABLE 5 — *Continued*

Target	Eq. Width of C_2H_2 at 7.5 um	F_{SiC} / continuum	[6.4]−[9.3] (mag.)	[16.5]−[21.5] (mag.)	F_{MgS} / continuum	IR spectral classification
MSX SMC 202	0.153 ± 0.006	0.013 ± 0.005	0.373 ± 0.017	−0.070 ± 0.019	···	CE2
MSX SMC 159	0.150 ± 0.006	0.183 ± 0.004	0.878 ± 0.005	0.289 ± 0.012	0.502 ± 0.017	CE3
LEGC 105	0.124 ± 0.004	0.036 ± 0.003	0.384 ± 0.012	0.030 ± 0.023	···	CE2
ISO 00548	0.129 ± 0.005	0.064 ± 0.003	0.419 ± 0.012	−0.135 ± 0.020	···	CE2
ISO 00549	0.070 ± 0.006	0.050 ± 0.009	0.720 ± 0.005	0.179 ± 0.006	···	CE3
RAW 960	0.246 ± 0.012	0.066 ± 0.005	0.200 ± 0.017	−0.067 ± 0.039	···	CE1
MSX SMC 209	0.095 ± 0.005	0.030 ± 0.002	0.720 ± 0.006	0.146 ± 0.017	···	CE3
NGC 330 BAL 555	0.151 ± 0.006	0.066 ± 0.011	0.071 ± 0.021	···	···	CE1
IRAS 00554−7351	0.088 ± 0.005	0.115 ± 0.006	0.906 ± 0.003	0.270 ± 0.011	0.266 ± 0.014	CE3
MSX SMC 198	0.105 ± 0.005	0.054 ± 0.003	0.640 ± 0.010	0.076 ± 0.011	···	CE2
ISO 00573	0.145 ± 0.006	0.067 ± 0.009	0.245 ± 0.012	−0.020 ± 0.037	···	CE1
MSX SMC 093	0.265 ± 0.006	0.020 ± 0.003	0.459 ± 0.012	0.164 ± 0.018	···	CE2
ISO 01019	0.144 ± 0.005	0.047 ± 0.006	0.360 ± 0.010	−0.082 ± 0.016	···	CE2
MSX SMC 232	0.085 ± 0.006	0.034 ± 0.003	0.652 ± 0.006	0.076 ± 0.020	···	CE3
NGC 419 LE 16	0.146 ± 0.007	0.081 ± 0.004	0.237 ± 0.012	−0.292 ± 0.031	···	CE1
NGC 419 IR 1	0.155 ± 0.004	0.047 ± 0.002	0.489 ± 0.009	0.069 ± 0.015	···	CE2
NGC 419 MIR 1	0.180 ± 0.005	0.086 ± 0.005	1.358 ± 0.011	0.326 ± 0.005	0.424 ± 0.006	CE5
NGC 419 LE 35	0.185 ± 0.027	0.039 ± 0.013	0.150 ± 0.030	···	···	CE1
NGC 419 LE 27	0.068 ± 0.009	0.008 ± 0.010	0.105 ± 0.020	···	···	CE1
NGC 419 LE 18	0.097 ± 0.010	0.060 ± 0.011	0.045 ± 0.017	0.091 ± 0.082	···	CE0
IRAS 04628−6937	0.072 ± 0.005	0.099 ± 0.012	0.931 ± 0.004	0.424 ± 0.008	−0.034 ± 0.010	CE3
IRAS F04331−6932	0.097 ± 0.005	0.163 ± 0.006	1.153 ± 0.008	0.376 ± 0.007	0.577 ± 0.009	CE4
IRAS F04340−7016	0.046 ± 0.005	0.227 ± 0.004	0.608 ± 0.008	0.209 ± 0.019	0.262 ± 0.025	CE2
IRAS F04353−6702	0.192 ± 0.006	0.086 ± 0.003	1.052 ± 0.006	0.347 ± 0.007	0.457 ± 0.009	CE4
IRAS F04375−7247	0.143 ± 0.004	0.128 ± 0.004	1.061 ± 0.006	0.335 ± 0.010	0.325 ± 0.013	CE4
IRAS 04374−6831	0.174 ± 0.003	0.142 ± 0.004	0.860 ± 0.003	0.453 ± 0.004	0.015 ± 0.006	CE3
IRAS F04433−7018	0.128 ± 0.007	0.174 ± 0.004	0.540 ± 0.004	0.152 ± 0.016	0.187 ± 0.022	CE2
2MASS J044627	0.179 ± 0.008	0.248 ± 0.005	0.622 ± 0.012	0.304 ± 0.009	0.048 ± 0.013	CE2
IRAS 04473−6829	0.065 ± 0.003	0.144 ± 0.005	0.793 ± 0.002	0.348 ± 0.004	0.023 ± 0.005	CE3
IRAS 04496−6958	0.227 ± 0.005	0.053 ± 0.004	0.829 ± 0.002	0.295 ± 0.012	−0.011 ± 0.015	CE3
MSX LMC 1128	0.118 ± 0.008	0.065 ± 0.005	0.475 ± 0.012	0.055 ± 0.015	−0.127 ± 0.026	CE2
MSX LMC 1308	0.151 ± 0.012	0.059 ± 0.005	0.538 ± 0.006	0.095 ± 0.014	−0.034 ± 0.019	CE2
MSX LMC 1205	0.101 ± 0.004	0.069 ± 0.004	0.666 ± 0.005	0.156 ± 0.013	0.077 ± 0.017	CE3
IRAS 04518−6852	0.089 ± 0.010	0.037 ± 0.003	1.734 ± 0.020	0.434 ± 0.011	0.527 ± 0.015	CE5
MSX LMC 1213	0.117 ± 0.008	0.220 ± 0.006	0.737 ± 0.004	0.243 ± 0.014	0.567 ± 0.018	CE3
KDM 764	0.206 ± 0.009	0.111 ± 0.006	0.023 ± 0.013	···	···	CE0
2MASS J045328	0.013 ± 0.010	0.114 ± 0.012	0.285 ± 0.017	···	···	CE1
IRAS 04535−6616	0.099 ± 0.007	0.095 ± 0.004	1.537 ± 0.016	0.399 ± 0.004	0.481 ± 0.005	CE5
IRAS 04539−6821	0.054 ± 0.006	0.101 ± 0.005	1.004 ± 0.006	0.250 ± 0.012	0.316 ± 0.015	CE4
IRAS F04537−6509	0.152 ± 0.005	0.149 ± 0.004	0.619 ± 0.006	0.120 ± 0.013	0.135 ± 0.018	CE2
MSX LMC 1209	0.144 ± 0.008	0.178 ± 0.006	0.822 ± 0.005	0.173 ± 0.018	0.360 ± 0.023	CE3
IRAS 04557−6753	0.141 ± 0.006	0.135 ± 0.005	1.116 ± 0.007	0.337 ± 0.006	0.426 ± 0.008	CE4
IRAS 04567−6857	0.046 ± 0.007	0.108 ± 0.003	0.583 ± 0.004	0.095 ± 0.016	0.206 ± 0.019	CE2
IRAS 04589−6825	0.140 ± 0.045	0.111 ± 0.017	2.356 ± 0.041 [a]	0.468 ± 0.026	0.481 ± 0.033	CE5
KDM 1238	0.094 ± 0.007	-0.000 ± 0.011	−0.090 ± 0.014	···	···	CE0
IRAS F05013−7213	0.107 ± 0.003	0.208 ± 0.004	0.792 ± 0.002	0.332 ± 0.008	0.471 ± 0.010	CE3
IRAS 05010−6739	0.024 ± 0.003	0.064 ± 0.002	0.792 ± 0.003	0.315 ± 0.008	−0.071 ± 0.010	CE3
IRAS 05009−6616	0.067 ± 0.005	0.150 ± 0.005	0.901 ± 0.005	0.259 ± 0.011	0.241 ± 0.013	CE3
IRAS 05026−6809	0.174 ± 0.021	−0.150 ± 0.003	2.763 ± 0.031	0.625 ± 0.008	···	CA5
KDM 1656	0.010 ± 0.019	0.073 ± 0.010	0.058 ± 0.031	···	···	CE1
W60 B14	0.177 ± 0.005	0.242 ± 0.007	0.031 ± 0.025	···	···	CE0
LMC-BM 12-14	0.105 ± 0.008	0.139 ± 0.009	0.011 ± 0.023	···	···	CE0
IRAS 05042−6827	0.227 ± 0.028	−0.124 ± 0.004	2.874 ± 0.083	0.592 ± 0.009	···	CA5
NGC 1818 WBT 64	0.026 ± 0.008	0.380 ± 0.012	0.281 ± 0.007	···	···	CE1
NGC 1835 LE 1	0.052 ± 0.005	−0.012 ± 0.011	0.026 ± 0.012	···	···	CE0
IRAS 05053−6901	0.069 ± 0.005	0.094 ± 0.005	1.443 ± 0.013	0.407 ± 0.007	0.504 ± 0.009	CE5
LMC-BM 13-2	0.048 ± 0.005	0.387 ± 0.006	0.262 ± 0.009	···	···	CE1
2MASS J050607	0.191 ± 0.006	0.223 ± 0.012	0.462 ± 0.004	···	···	CE2
KDM 1961	0.085 ± 0.012	−0.044 ± 0.019	0.044 ± 0.014	···	···	CE0
KDM 1966	0.021 ± 0.010	0.058 ± 0.010	−0.063 ± 0.020	···	···	CE0
2MASS J050620	0.114 ± 0.008	0.087 ± 0.010	−0.010 ± 0.021	···	···	CE0
2MASS J050629	0.187 ± 0.010	0.130 ± 0.014	0.178 ± 0.024	···	···	CE1
IRAS 05070−7020	0.123 ± 0.003	0.082 ± 0.003	1.292 ± 0.009	0.439 ± 0.006	0.258 ± 0.007	CE5
SHV 0507252	0.028 ± 0.009	0.013 ± 0.008	0.209 ± 0.019	−0.056 ± 0.022	···	CE1
SAGE MC J050752	0.052 ± 0.011	0.139 ± 0.008	0.683 ± 0.016	0.121 ± 0.020	···	CE3
MSX LMC 92	0.077 ± 0.006	0.070 ± 0.002	0.696 ± 0.005	0.129 ± 0.014	0.054 ± 0.019	CE3
2MASS J050826	0.026 ± 0.007	0.059 ± 0.005	0.381 ± 0.011	−0.027 ± 0.021	−0.010 ± 0.006	CE2
KDM 2187	0.246 ± 0.012	0.236 ± 0.015	0.080 ± 0.024	···	···	CE1
IRAS 05103−6959	0.106 ± 0.003	0.241 ± 0.005	0.711 ± 0.003	0.357 ± 0.002	−0.008 ± 0.003	CE3
IRAS 05107−6953	0.061 ± 0.003	0.092 ± 0.003	0.800 ± 0.002	0.362 ± 0.009	−0.044 ± 0.011	CE3
2MASS J051028	0.115 ± 0.011	0.195 ± 0.006	0.798 ± 0.008	0.271 ± 0.014	0.081 ± 0.019	CE3
IRAS 05112−6755	0.108 ± 0.005	0.104 ± 0.003	1.133 ± 0.007	0.335 ± 0.007	0.303 ± 0.008	CE4
IRAS 05113−6739	0.107 ± 0.010	0.094 ± 0.005	1.079 ± 0.012	0.258 ± 0.010	0.229 ± 0.012	CE4
MSX LMC 219	0.117 ± 0.005	0.126 ± 0.003	1.090 ± 0.006	0.360 ± 0.004	0.339 ± 0.005	CE4
TRM 72	0.042 ± 0.005	0.076 ± 0.003	0.769 ± 0.005	0.107 ± 0.013	···	CE3
IRAS 05125−7035	0.050 ± 0.005	0.076 ± 0.003	1.507 ± 0.013	0.354 ± 0.005	0.476 ± 0.006	CE5

TABLE 5 — *Continued*

Target	Eq. Width of C_2H_2 at 7.5 um	F_{SiC} / continuum	[6.4]−[9.3] (mag.)	[16.5]−[21.5] (mag.)	F_{MgS} / continuum	IR spectral classification
MSX LMC 220	0.052 ± 0.006	0.058 ± 0.003	0.831 ± 0.004	0.334 ± 0.009	−0.112 ± 0.011	CE3
IRAS 05132−6941	0.089 ± 0.007	0.119 ± 0.006	1.050 ± 0.008	0.282 ± 0.012	0.206 ± 0.014	CE4
IRAS 05133−6937	0.193 ± 0.033	−0.153 ± 0.003	3.024 ± 0.042	0.658 ± 0.007	0.167 ± 0.009	CA5
OGLE J051306	0.043 ± 0.009	0.153 ± 0.005	0.598 ± 0.009	0.206 ± 0.023	0.674 ± 0.102	CE2
MSX LMC 218	0.084 ± 0.004	0.266 ± 0.012	0.632 ± 0.004	0.365 ± 0.007	0.041 ± 0.009	CE2
MSX LMC 349	0.078 ± 0.006	0.185 ± 0.005	0.982 ± 0.005	0.369 ± 0.009	0.659 ± 0.011	CE4
SAGE MC J051803	0.227 ± 0.012	0.099 ± 0.007	0.516 ± 0.012	0.132 ± 0.021	···	CE2
IRAS 05187−7033	0.046 ± 0.033	−0.012 ± 0.003	2.467 ± 0.031	0.786 ± 0.006	···	CA5
IRAS 05191−6936	0.135 ± 0.024	−0.068 ± 0.003	2.691 ± 0.035	0.607 ± 0.005	···	CA5
IRAS 05190−6758	0.133 ± 0.008	0.101 ± 0.006	1.237 ± 0.010	0.370 ± 0.005	0.361 ± 0.006	CE4
2MASS J051908	0.161 ± 0.010	0.076 ± 0.007	0.028 ± 0.012	···	···	CE0
TRM 78	0.059 ± 0.006	0.067 ± 0.004	0.779 ± 0.004	0.199 ± 0.015	···	CE3
MSX LMC 341	0.071 ± 0.007	0.162 ± 0.005	0.968 ± 0.005	0.315 ± 0.010	0.619 ± 0.012	CE4
OGLE J052242	0.093 ± 0.007	0.190 ± 0.006	0.543 ± 0.005	0.152 ± 0.019	0.158 ± 0.028	CE2
BE 74	−0.026 ± 0.005	0.024 ± 0.004	0.692 ± 0.006	0.465 ± 0.005	···	CE3
MSX LMC 494	0.108 ± 0.007	0.094 ± 0.002	0.538 ± 0.005	0.160 ± 0.015	···	CE2
IRAS F05236−6655	0.111 ± 0.005	0.207 ± 0.005	0.692 ± 0.002	0.205 ± 0.010	0.405 ± 0.015	CE3
2MASS J052405	−0.047 ± 0.009	0.076 ± 0.006	0.546 ± 0.010	0.139 ± 0.022	0.054 ± 0.031	CE2
MSX LMC 441	0.128 ± 0.006	0.140 ± 0.004	1.152 ± 0.008	0.352 ± 0.008	0.426 ± 0.010	CE4
IRAS F05254−7149	0.101 ± 0.005	0.126 ± 0.002	1.065 ± 0.002	0.334 ± 0.006	0.327 ± 0.008	CE4
OGLE J052445	0.110 ± 0.017	0.277 ± 0.012	0.390 ± 0.018	0.056 ± 0.030	···	CE2
MSX LMC 443	0.133 ± 0.005	0.189 ± 0.005	0.904 ± 0.003	0.325 ± 0.010	0.462 ± 0.012	CE3
LI-LMC 1028	0.015 ± 0.004	0.073 ± 0.002	0.712 ± 0.005	0.275 ± 0.007	−0.072 ± 0.008	CE3
IRAS 05260−7010	0.148 ± 0.031	−0.050 ± 0.004	2.841 ± 0.045	0.590 ± 0.008	···	CA5
MSX LMC 474	0.130 ± 0.005	0.074 ± 0.007	0.886 ± 0.006	0.272 ± 0.011	0.108 ± 0.013	CE3
WBP 17	0.255 ± 0.025	0.057 ± 0.032	−0.159 ± 0.039	0.085 ± 0.279	···	CE0
MSX LMC 774	0.120 ± 0.007	0.118 ± 0.004	1.103 ± 0.007	0.327 ± 0.006	0.264 ± 0.008	CE4
MSX LMC 634	0.037 ± 0.007	0.070 ± 0.003	0.625 ± 0.010	0.143 ± 0.016	−0.023 ± 0.028	CE2
WBP 29	0.343 ± 0.010	0.075 ± 0.015	0.079 ± 0.027	···	···	CE1
MSX LMC 601	0.014 ± 0.006	0.063 ± 0.004	0.875 ± 0.002	0.160 ± 0.013	···	CE3
WBP 42	0.262 ± 0.013	0.070 ± 0.006	0.394 ± 0.015	−0.033 ± 0.034	···	CE2
IRAS 05278−6942	0.074 ± 0.005	0.113 ± 0.006	1.128 ± 0.005	0.346 ± 0.008	0.412 ± 0.010	CE4
SHV 0528350	0.230 ± 0.007	0.093 ± 0.006	0.249 ± 0.016	0.825 ± 0.016	0.678 ± 0.020	CE1
MSX LMC 754	0.103 ± 0.007	0.178 ± 0.004	0.571 ± 0.005	0.213 ± 0.015	···	CE2
KDM 4257	0.057 ± 0.009	0.138 ± 0.008	0.195 ± 0.018	···	···	CE1
NGC 1978 IR 1	0.109 ± 0.005	0.108 ± 0.003	0.570 ± 0.006	0.142 ± 0.014	···	CE2
NGC 1978 IR 4	0.142 ± 0.014	0.119 ± 0.005	0.161 ± 0.027	−0.201 ± 0.040	···	CE1
IRAS 05295−7121	0.082 ± 0.005	0.091 ± 0.003	0.963 ± 0.008	0.312 ± 0.009	0.184 ± 0.011	CE4
NGC 1978 MIR 1	0.145 ± 0.006	0.170 ± 0.005	0.832 ± 0.003	0.318 ± 0.010	0.565 ± 0.012	CE3
MSX LMC 679	0.108 ± 0.004	0.159 ± 0.005	0.901 ± 0.003	0.337 ± 0.012	0.519 ± 0.014	CE3
GRRV 38	0.218 ± 0.014	0.179 ± 0.008	0.190 ± 0.015	0.267 ± 0.018	···	CE1
IRAS 05305−7251	0.181 ± 0.015	−0.079 ± 0.003	2.127 ± 0.024	0.464 ± 0.006	0.398 ± 0.013	CA5
IRAS 05300−6651	0.139 ± 0.006	0.098 ± 0.005	1.035 ± 0.004	0.301 ± 0.011	0.262 ± 0.014	CE4
IRAS 05306−7032	0.149 ± 0.033	0.134 ± 0.012	2.349 ± 0.037 [a]	0.427 ± 0.032	0.338 ± 0.039	CE5
2MASS J053044	0.083 ± 0.007	0.022 ± 0.005	0.361 ± 0.013	−0.065 ± 0.022	−0.131 ± 0.008	CE2
MSX LMC 841	0.065 ± 0.006	0.070 ± 0.005	0.682 ± 0.004	0.181 ± 0.018	0.095 ± 0.023	CE3
MSX LMC 768	0.060 ± 0.005	0.094 ± 0.004	0.843 ± 0.004	0.265 ± 0.009	0.125 ± 0.011	CE3
KDM 4665	0.037 ± 0.012	0.024 ± 0.011	0.077 ± 0.026	···	···	CE1
MSX LMC 782	0.119 ± 0.007	0.205 ± 0.005	0.810 ± 0.004	0.360 ± 0.021	1.392 ± 0.145	CE3
KDM 4718	0.092 ± 0.006	0.055 ± 0.008	−0.131 ± 0.013	···	···	CE0
KDM 4774	0.023 ± 0.013	0.151 ± 0.006	0.221 ± 0.026	···	···	CE1
MSX LMC 783	0.079 ± 0.008	0.156 ± 0.003	0.672 ± 0.006	0.272 ± 0.011	0.312 ± 0.016	CE3
LMC-BM 32-9	0.055 ± 0.004	0.010 ± 0.002	0.279 ± 0.013	0.005 ± 0.013	−0.129 ± 0.014	CE1
MSX LMC 736	0.101 ± 0.012	0.125 ± 0.004	1.295 ± 0.009	0.341 ± 0.015	0.634 ± 0.020	CE5
2MASS J053318	0.169 ± 0.012	0.054 ± 0.006	0.683 ± 0.007	0.164 ± 0.016	−0.004 ± 0.024	CE3
IRAS 05348−7024	0.008 ± 0.006	0.137 ± 0.004	1.048 ± 0.008	0.298 ± 0.010	0.249 ± 0.013	CE4
2MASS J053441	0.078 ± 0.007	0.032 ± 0.003	0.506 ± 0.012	0.022 ± 0.017	−0.034 ± 0.024	CE2
MSX LMC 743	0.165 ± 0.005	0.174 ± 0.005	1.050 ± 0.005	0.325 ± 0.011	0.394 ± 0.014	CE4
MSX LMC 787	0.154 ± 0.007	0.179 ± 0.007	0.957 ± 0.002	0.420 ± 0.011	1.059 ± 0.014	CE4
MSX LMC 950	0.099 ± 0.008	0.165 ± 0.004	0.847 ± 0.003	0.215 ± 0.011	0.220 ± 0.016	CE3
MSX LMC 749	0.095 ± 0.004	0.065 ± 0.005	0.618 ± 0.003	0.137 ± 0.013	···	CE2
IRAS F05355−6521	0.158 ± 0.005	0.211 ± 0.004	0.525 ± 0.005	0.225 ± 0.015	0.304 ± 0.020	CE2
IRAS 05360−6648	0.086 ± 0.005	0.181 ± 0.006	1.050 ± 0.005	0.333 ± 0.008	0.655 ± 0.011	CE4
IRAS F05373−7243	0.125 ± 0.004	0.142 ± 0.003	0.909 ± 0.004	0.254 ± 0.010	0.298 ± 0.013	CE3
MSX LMC 967	0.066 ± 0.006	0.088 ± 0.002	0.551 ± 0.005	0.151 ± 0.009	···	CE2
OGLE J053930	0.105 ± 0.007	0.154 ± 0.003	0.411 ± 0.013	0.125 ± 0.020	−0.042 ± 0.032	CE2
MSX LMC 971	0.138 ± 0.008	0.127 ± 0.005	1.166 ± 0.007	0.290 ± 0.009	0.405 ± 0.012	CE4
MSX LMC 1400	0.131 ± 0.004	0.115 ± 0.004	1.095 ± 0.006	0.484 ± 0.004	0.098 ± 0.005	CE4
IRAS 05410−6954	0.077 ± 0.007	0.135 ± 0.011	0.890 ± 0.006	0.266 ± 0.008	0.296 ± 0.011	CE3
MSX LMC 974	0.093 ± 0.013	0.063 ± 0.008	0.738 ± 0.007	0.188 ± 0.019	0.241 ± 0.029	CE3
IRAS 05416−6906	0.103 ± 0.005	0.052 ± 0.004	1.682 ± 0.017	0.490 ± 0.006	0.356 ± 0.009	CE5
KDM 5841	−0.013 ± 0.007	0.077 ± 0.014	0.094 ± 0.031	···	···	CE1
MSX LMC 1384	0.187 ± 0.004	0.198 ± 0.005	0.862 ± 0.001	0.425 ± 0.005	−0.076 ± 0.007	CE3
IRAS 05446−6945	0.073 ± 0.006	0.116 ± 0.005	1.272 ± 0.009	0.396 ± 0.005	0.606 ± 0.007	CE5
2MASS J054437	0.033 ± 0.006	0.101 ± 0.005	0.494 ± 0.009	0.089 ± 0.018	0.026 ± 0.024	CE2
2MASS J054546	0.038 ± 0.012	0.086 ± 0.008	1.112 ± 0.009	0.513 ± 0.010	−0.138 ± 0.014	CE4

TABLE 5 — *Continued*

Target	Eq. Width of C_2H_2 at 7.5 um	F_{SiC} / continuum	[6.4]−[9.3] (mag.)	[16.5]−[21.5] (mag.)	F_{MgS} / continuum	IR spectral classification
NGC 2121 LE 6	0.192 ± 0.005	0.070 ± 0.005	0.180 ± 0.018	···	···	CE1
MSX LMC 1492	0.036 ± 0.003	0.055 ± 0.002	0.403 ± 0.008	0.129 ± 0.011	−0.124 ± 0.014	CE2
IRAS 05506−7053	0.019 ± 0.005	0.137 ± 0.005	1.289 ± 0.009	0.354 ± 0.010	0.397 ± 0.012	CE5
LI-LMC 1758	0.130 ± 0.004	0.099 ± 0.004	0.719 ± 0.002	0.360 ± 0.009	−0.037 ± 0.011	CE3
IRAS 05509−6956	0.151 ± 0.014	−0.117 ± 0.005	2.483 ± 0.027	0.558 ± 0.008	0.300 ± 0.010	CA5
KDM 6486	0.030 ± 0.013	0.028 ± 0.018	0.126 ± 0.021	···	···	CE1
IRAS 05516−7124	0.065 ± 0.004	0.137 ± 0.004	1.030 ± 0.005	0.282 ± 0.008	0.294 ± 0.011	CE4
PMP 337	0.065 ± 0.010	−0.007 ± 0.009	−0.030 ± 0.014	···	···	CE0
IRAS 05568−6753	−0.005 ± 0.004	0.030 ± 0.003	1.755 ± 0.016	0.570 ± 0.008	0.165 ± 0.010	CE5
IRAS 06025−6712	0.105 ± 0.005	0.127 ± 0.004	1.166 ± 0.008	0.484 ± 0.005	0.320 ± 0.006	CE4
IRAS 06028−6722	0.106 ± 0.005	0.107 ± 0.004	1.238 ± 0.008	0.321 ± 0.008	0.379 ± 0.010	CE4
IRAS F06108−7045	0.120 ± 0.004	0.210 ± 0.004	0.920 ± 0.004	0.349 ± 0.009	0.697 ± 0.012	CE3

[a] [6.4]−[9.3] color replaced with an estimate based on [5.8]−[8].

TABLE 6
SPECTROSCOPIC DATA — SWS SAMPLE

Target	Alias	Eq. width of C_2H_2 at 7.5 um	F_{SiC} / continuum	[6.4]−[9.3] (mag.)	[16.5]−[21.5] (mag.)	F_{MgS} / continuum	IR spectral classification
WZ Cas	···	0.347 ± 0.007	−0.022 ± 0.002	0.029 ± 0.002	0.438 ± 0.004	···	CE0
VX And	···	0.238 ± 0.001	0.182 ± 0.001	0.123 ± 0.003	0.067 ± 0.010	···	CE1
HV Cas	···	0.090 ± 0.001	0.226 ± 0.001	0.353 ± 0.002	−0.139 ± 0.004	···	CE2
R Scl	···	0.290 ± 0.002	0.205 ± 0.001	0.273 ± 0.002	0.266 ± 0.002	0.292 ± 0.004	CE1
R For	···	0.125 ± 0.001	0.279 ± 0.001	0.361 ± 0.001	0.131 ± 0.003	···	CE2
AFGL 341	V596 Per	0.063 ± 0.001	0.073 ± 0.001	1.665 ± 0.005	0.407 ± 0.008	0.411 ± 0.010	CE5
CIT 5	V384 Per	0.065 ± 0.001	0.305 ± 0.002	0.682 ± 0.001	0.323 ± 0.002	0.186 ± 0.002	CE3
U Cam	···	0.078 ± 0.001	0.327 ± 0.001	0.107 ± 0.002	0.157 ± 0.004	···	CE1
W Ori	···	0.064 ± 0.001	0.229 ± 0.001	0.055 ± 0.001	−0.054 ± 0.004	0.137 ± 0.002	CE1
IRC −10095	V1187 Ori	0.277 ± 0.002	0.192 ± 0.001	0.163 ± 0.003	0.196 ± 0.008	0.784 ± 0.012	CE1
TU Tau	···	0.050 ± 0.002	0.218 ± 0.002	0.083 ± 0.004	0.036 ± 0.010	···	CE1
IRC −10122	V636 Mon	0.094 ± 0.001	0.288 ± 0.001	0.377 ± 0.002	0.147 ± 0.003	···	CE2
AFGL 940	···	−0.003 ± 0.001	0.207 ± 0.001	0.773 ± 0.001	0.096 ± 0.006	0.858 ± 0.009	CE3
SS Vir	···	0.264 ± 0.002	0.338 ± 0.001	0.357 ± 0.003	0.324 ± 0.019	···	CE2
Y CVn	···	0.146 ± 0.002	0.120 ± 0.001	0.152 ± 0.002	0.069 ± 0.006	···	CE1
RU Vir	···	0.054 ± 0.001	0.302 ± 0.001	0.512 ± 0.001	0.226 ± 0.002	0.114 ± 0.003	CE2
RY Dra	···	0.124 ± 0.001	0.104 ± 0.001	0.109 ± 0.002	−0.032 ± 0.004	···	CE1
C* 2178	···	0.113 ± 0.002	0.253 ± 0.002	0.415 ± 0.003	0.062 ± 0.009	···	CE2
CGCS 3592	II Lup	0.129 ± 0.006	0.111 ± 0.002	0.788 ± 0.000	0.290 ± 0.001	0.218 ± 0.002	CE3
V CrB	···	0.126 ± 0.002	0.403 ± 0.001	0.404 ± 0.001	0.136 ± 0.003	0.245 ± 0.008	CE2
C* 2429	V1079 Sco	0.127 ± 0.001	0.531 ± 0.002	0.192 ± 0.002	−0.149 ± 0.008	0.731 ± 0.004	CE1
IRC +20326	V833 Her	−0.037 ± 0.002	0.066 ± 0.001	0.888 ± 0.002	0.469 ± 0.001	0.401 ± 0.001	CE3
T Dra	···	0.089 ± 0.001	0.350 ± 0.001	0.506 ± 0.001	0.173 ± 0.003	0.143 ± 0.004	CE2
AFGL 2155	V1076 Her	0.007 ± 0.001	0.113 ± 0.001	1.290 ± 0.003	0.492 ± 0.001	0.338 ± 0.001	CE5
T Lyr	···	0.322 ± 0.006	0.146 ± 0.002	0.184 ± 0.001	−0.137 ± 0.003	···	CE1
IRC +00365	V1417 Aql	0.043 ± 0.001	0.195 ± 0.001	0.667 ± 0.001	0.323 ± 0.002	0.212 ± 0.002	CE3
S Sct	···	0.252 ± 0.002	0.128 ± 0.001	0.143 ± 0.002	0.090 ± 0.009	···	CE1
Case 181	V1418 Aql	0.026 ± 0.001	0.231 ± 0.001	0.613 ± 0.002	0.174 ± 0.002	0.259 ± 0.002	CE2
V Aql	···	0.160 ± 0.001	0.173 ± 0.001	0.110 ± 0.002	0.090 ± 0.003	0.353 ± 0.006	CE1
IRAS 19068+0544	···	0.024 ± 0.002	0.338 ± 0.002	0.483 ± 0.003	0.349 ± 0.005	0.523 ± 0.007	CE2
AFGL 2392	V1421 Aql	0.057 ± 0.001	0.357 ± 0.002	0.583 ± 0.002	0.190 ± 0.004	0.564 ± 0.005	CE2
TT Cyg	···	0.096 ± 0.005	0.047 ± 0.002	0.123 ± 0.003	0.537 ± 0.013	···	CE1
V Cyg	···	0.144 ± 0.001	0.346 ± 0.001	0.515 ± 0.001	0.177 ± 0.002	0.111 ± 0.003	CE2
AFGL 2699	V1899 Cyg	−0.056 ± 0.001	0.274 ± 0.002	0.939 ± 0.002	0.310 ± 0.003	0.244 ± 0.004	CE3
T Ind	···	0.104 ± 0.001	0.035 ± 0.001	0.161 ± 0.002	0.297 ± 0.005	···	CE1
S Cep	···	0.154 ± 0.001	0.238 ± 0.001	0.296 ± 0.002	0.074 ± 0.002	···	CE1
V460 Cyg	···	0.120 ± 0.001	0.083 ± 0.001	0.156 ± 0.001	−0.075 ± 0.006	···	CE1
DO 40123	PQ Cep	0.210 ± 0.001	0.290 ± 0.001	0.293 ± 0.002	0.154 ± 0.005	···	CE1
IRAS 21489+5301	···	0.053 ± 0.002	0.123 ± 0.001	1.357 ± 0.005	0.376 ± 0.004	0.439 ± 0.005	CE5
AFGL 3099	IZ Peg	0.049 ± 0.002	0.127 ± 0.001	1.211 ± 0.004	0.457 ± 0.003	0.437 ± 0.003	CE4
IRC +40540	LP And	0.022 ± 0.001	0.165 ± 0.001	1.163 ± 0.003	0.404 ± 0.001	0.398 ± 0.001	CE4
TX Psc	···	0.223 ± 0.002	−0.007 ± 0.001	0.097 ± 0.002	0.040 ± 0.004	···	CE1

TABLE 9
MULTI-EPOCH K-BAND PHOTOMETRY

Target	JD−2450000	*K*
MSX LMC 219	1501	12.36

TABLE 9 — *Continued*

Target	JD−2450000	K
	1591	12.34
	1675	12.32
	1746	12.65
	1800	13.05
	1852	13.30
	1976	13.32
	2035	13.42
	2090	12.90
	2158	12.47
	2215	12.27
	2265	12.18
	2364	12.29
	2429	12.58
	2563	13.24
	2713	13.34
	2924	12.14
	3229	13.02
	3283	13.09
	3334	13.12
	3443	12.96
	3518	13.19
	3577	11.88
	3633	11.72
	3870	12.48
	4047	12.79
MSX LMC 341	1500	11.90
	1594	12.24
	1675	13.07
	1746	13.25
	1800	13.17
	1852	12.70
	1976	12.08
	2034	11.88
	2090	11.98
	2158	12.34
	2215	12.76
	2265	13.26
	2364	13.41
	2429	12.96
	2511	12.31
	2563	12.03
	2565	12.02
	2713	12.49
	2924	13.37
	3229	11.87
	3283	12.31
	3314	12.55
	3398	13.02
	3443	13.29
	3517	13.38
	3577	13.08
	3633	12.42
	3870	12.66
	4047	13.95
IRAS 05278-6942	1499	11.90
	1591	12.17
	1747	13.14
	1800	13.52
	1852	14.28
	1975	14.51
	2032	14.52
	2094	14.32
	2158	14.13
	2216	13.49
	2265	12.61
	2364	12.29
	2428	12.14
	2510	12.02
	2563	12.07
	2565	12.10
	2713	12.90
	2924	14.31
	3229	12.48
	3283	12.23
	3314	12.06
	3398	11.85
	3443	11.71

TABLE 9 — *Continued*

Target	JD−2450000	*K*
	3517	11.69
	3633	12.08
	3870	13.16
	4047	13.41
IRAS 05132-6941	1499	13.27
	1591	12.95
	1747	11.73
	1800	11.60
	1852	11.43
	1975	12.58
	2034	13.06
	2094	13.22
	2158	13.00
	2216	12.88
	2265	12.65
	2364	11.63
	2428	11.50
	2510	11.63
	2563	11.90
	2565	11.88
	2713	12.86
	2924	12.51
	3229	11.92
	3283	12.04
	3334	12.65
	3398	12.94
	3443	12.96
	3517	12.65
	3577	12.54
	3633	11.90
	3870	11.80
	4047	12.83
MSX LMC 441	1499	14.62
	1591	14.16
	1674	13.45
	1747	13.00
	1800	12.95
	1852	13.05
	1975	13.86
	2032	14.22
	2092	14.01
	2156	14.14
	2215	13.95
	2216	14.07
	2265	13.60
	2364	12.86
	2428	12.61
	2510	12.54
	2565	13.05
	2713	13.92
	2924	13.37
	3229	12.38
	3283	12.69
	3314	12.99
	3398	13.24
	3443	13.50
	3517	13.29
	3577	13.05
	3633	12.70
	3870	12.05
	4047	13.11
MSX LMC 679	1499	11.82
	1592	12.34
	1674	12.91
	1747	12.93
	1800	12.61
	1852	12.17
	1975	11.85
	2032	12.06
	2092	12.55
	2156	12.89
	2216	12.96
	2265	12.86
	2364	12.07
	2428	11.93
	2510	12.25
	2563	12.59

TABLE 9 — *Continued*

Target	JD−2450000	K
	2565	12.72
	2713	13.02
	2924	12.01
	3229	12.95
	3283	12.57
	3314	11.99
	3398	12.02
	3443	12.12
	3633	12.98
	3870	11.93
	4047	12.53
MSX LMC 349	1501	13.22
	1591	14.64
	1675	14.70
	1746	14.61
	1800	14.59
	1852	14.54
	1976	13.16
	2035	13.16
	2090	13.06
	2158	13.37
	2215	13.77
	2265	14.73
	2364	15.00
	2429	14.67
	2511	14.80
	2565	12.95
	2713	13.32
	2924	14.70
	3229	12.65
	3283	12.73
	3314	13.08
	3398	13.47
	3443	13.89
	3517	13.96
	3577	13.87
	3633	13.16
	3870	12.64
	4047	14.09
MSX LMC 443	1502	11.26
	1590	11.49
	1674	12.00
	1747	12.29
	1800	12.43
	1852	12.35
	1975	11.42
	2032	11.31
	2092	11.33
	2156	11.65
	2215	12.03
	2216	12.03
	2265	12.29
	2364	12.40
	2428	11.98
	2510	11.46
	2563	11.30
	2565	11.28
	2713	11.72
	2924	12.51
	3229	11.91
	3283	12.22
	3314	12.65
	3398	12.83
	3443	12.81
	3517	12.16
	3633	11.58
	3870	12.74
	4047	12.34
MSX LMC 743	1499	12.58
	1591	13.07
	1674	13.49
	1747	13.44
	1800	13.60
	1852	13.13
	1975	12.31
	2032	12.13
	2092	12.35

TABLE 9 — *Continued*

Target	JD−2450000	*K*
	2156	12.79
	2215	13.14
	2216	13.10
	2265	13.19
	2266	13.36
	2364	13.37
	2428	12.74
	2510	12.07
	2565	12.05
	2713	12.67
	2924	13.03
	3283	12.71
	3314	12.69
	3397	12.90
	3443	12.95
	3517	12.49
	3619	11.75
	3870	12.53
	4047	12.28

TABLE 10
MULTI-EPOCH 3–5 μM PHOTOMETRY

Target	RA (J2000)	Decl. (J2000)	MJD	[3.6]	[4.5]	Data source[a]
GM 780	8.905055	−73.165641	54633	9.115 ± 0.059	8.609 ± 0.048	IRAC
	8.905572	−73.165577	54728	9.180 ± 0.034	8.686 ± 0.047	IRAC
	8.905168	−73.165589	55316	9.132 ± 0.025	8.672 ± 0.020	(*WISE*)
	8.905168	−73.165589	55498	8.465 ± 0.035	8.040 ± 0.038	(*WISE*)
	8.905188	−73.165607	56781	8.171 ± 0.019	7.764 ± 0.018	(*WISE*)
	8.905212	−73.165612	56961	8.364 ± 0.025	7.959 ± 0.017	(*WISE*)
MSX SMC 091	9.236177	−72.421510	54633	9.293 ± 0.046	8.721 ± 0.036	IRAC
	9.236628	−72.421501	54728	9.328 ± 0.060	8.752 ± 0.053	IRAC
	9.236252	−72.421493	55318	10.131 ± 0.021	9.452 ± 0.036	(*WISE*)
	9.236252	−72.421493	55499	9.406 ± 0.024	8.782 ± 0.056	(*WISE*)
	9.236314	−72.421510	56782	9.454 ± 0.018	8.830 ± 0.021	(*WISE*)
	9.236302	−72.421518	56963	10.000 ± 0.023	9.321 ± 0.017	(*WISE*)
MSX SMC 062	10.670211	−72.951654	53498	8.960 ± 0.024	8.258 ± 0.023	IRAC
	10.670270	−72.951421	54633	8.862 ± 0.062	8.195 ± 0.033	IRAC
	10.670810	−72.951571	54728	8.814 ± 0.038	8.195 ± 0.038	IRAC
	10.670493	−72.951599	55318	8.816 ± 0.024	8.217 ± 0.028	(*WISE*)
	10.670493	−72.951599	55499	9.439 ± 0.040	8.826 ± 0.036	(*WISE*)
	10.670400	−72.951600	55555	···	8.816 ± 0.035	IRAC
	10.670396	−72.951586	56782	9.093 ± 0.014	8.482 ± 0.018	(*WISE*)
	10.670378	−72.951594	56962	8.604 ± 0.019	8.010 ± 0.017	(*WISE*)
MSX SMC 054	10.774386	−73.361353	53498	9.998 ± 0.017	9.087 ± 0.019	IRAC
	10.774385	−73.361243	54633	10.284 ± 0.036	9.376 ± 0.036	IRAC
	10.774978	−73.361299	54728	9.857 ± 0.037	8.943 ± 0.039	IRAC
	10.774675	−73.361282	55316	9.732 ± 0.028	8.868 ± 0.023	(*WISE*)
	10.774675	−73.361282	55498	10.096 ± 0.028	9.211 ± 0.025	(*WISE*)
	10.774593	−73.361272	56781	9.355 ± 0.019	8.464 ± 0.022	(*WISE*)
	10.774621	−73.361289	56961	10.260 ± 0.016	9.307 ± 0.012	(*WISE*)
2MASS J004326	10.860192	−73.445405	53498	10.261 ± 0.014	10.332 ± 0.013	IRAC
	10.860244	−73.445326	54633	10.119 ± 0.026	10.263 ± 0.026	IRAC
	10.860742	−73.445374	54728	10.024 ± 0.067	10.177 ± 0.035	IRAC
	10.860367	−73.445351	55316	10.971 ± 0.019	10.786 ± 0.020	(*WISE*)
	10.860367	−73.445351	55498	11.053 ± 0.037	10.855 ± 0.039	(*WISE*)
	10.860416	−73.445365	56781	10.493 ± 0.019	10.432 ± 0.024	(*WISE*)
	10.860353	−73.445350	56961	10.545 ± 0.024	10.490 ± 0.018	(*WISE*)
MSX SMC 044	10.914629	−73.249422	53498	9.501 ± 0.021	8.837 ± 0.027	IRAC
	10.914656	−73.249185	54633	9.056 ± 0.046	8.515 ± 0.039	IRAC
	10.915246	−73.249335	54728	9.486 ± 0.068	8.841 ± 0.045	IRAC
	10.914838	−73.249315	55317	9.213 ± 0.024	8.690 ± 0.028	(*WISE*)
	10.914800	−73.249400	55452	···	8.317 ± 0.057	IRAC
	10.914838	−73.249315	55498	8.971 ± 0.036	8.452 ± 0.025	(*WISE*)
	10.914842	−73.249324	56781	9.208 ± 0.018	8.623 ± 0.018	(*WISE*)
	10.914882	−73.249342	56962	9.666 ± 0.017	9.011 ± 0.017	(*WISE*)
MSX SMC 105	11.258750	−72.873470	53498	9.377 ± 0.022	8.591 ± 0.018	IRAC
	11.258702	−72.873302	54633	9.291 ± 0.052	8.521 ± 0.034	IRAC
	11.259147	−72.873413	54728	9.421 ± 0.048	8.661 ± 0.040	IRAC
	11.258919	−72.873420	55318	9.231 ± 0.028	8.482 ± 0.024	(*WISE*)
	11.258900	−72.873400	55452	9.375 ± 0.092	8.728 ± 0.063	IRAC

TABLE 10 — *Continued*

Target	RA (J2000)	Decl. (J2000)	MJD	[3.6]	[4.5]	Data source[a]
	11.258919	−72.873420	55499	9.337 ± 0.039	8.574 ± 0.061	(*WISE*)
	11.258900	−72.873400	55555	9.248 ± 0.099	8.375 ± 0.046	IRAC
	11.258860	−72.873414	56782	9.486 ± 0.022	8.696 ± 0.022	(*WISE*)
	11.258918	−72.873434	56963	9.045 ± 0.019	8.271 ± 0.018	(*WISE*)
MSX SMC 036	11.474497	−73.394792	53498	9.847 ± 0.016	8.928 ± 0.022	IRAC
	11.474489	−73.394624	54633	9.614 ± 0.034	8.750 ± 0.054	IRAC
	11.474947	−73.394738	54728	9.386 ± 0.040	8.545 ± 0.043	IRAC
	11.474751	−73.394781	55317	9.384 ± 0.026	8.489 ± 0.021	(*WISE*)
	11.474751	−73.394781	55498	10.268 ± 0.042	9.288 ± 0.039	(*WISE*)
	11.474577	−73.394761	56781	9.836 ± 0.017	8.888 ± 0.020	(*WISE*)
	11.474643	−73.394780	56962	9.550 ± 0.018	8.639 ± 0.015	(*WISE*)
GB S06	11.668238	−73.279845	53498	8.515 ± 0.023	7.635 ± 0.015	IRAC
	11.668207	−73.279668	54633	8.645 ± 0.048	7.837 ± 0.032	IRAC
	11.668805	−73.279807	54728	8.430 ± 0.048	7.568 ± 0.044	IRAC
	11.668502	−73.279807	55317	8.427 ± 0.025	7.570 ± 0.027	(*WISE*)
	11.668400	−73.279800	55452	···	8.494 ± 0.110	IRAC
	11.668502	−73.279807	55499	8.810 ± 0.025	7.877 ± 0.035	(*WISE*)
	11.668408	−73.279806	56781	8.678 ± 0.020	7.961 ± 0.024	(*WISE*)
	11.668435	−73.279808	56962	9.160 ± 0.016	8.474 ± 0.016	(*WISE*)
MSX SMC 200	11.711460	−71.794244	54633	9.490 ± 0.036	8.906 ± 0.041	IRAC
	11.711763	−71.794252	54728	9.365 ± 0.039	8.819 ± 0.047	IRAC
	11.711657	−71.794155	55320	8.979 ± 0.073	8.462 ± 0.048	(*WISE*)
	11.711657	−71.794155	55501	9.224 ± 0.074	8.719 ± 0.084	(*WISE*)
	11.711713	−71.794238	56784	9.415 ± 0.014	9.034 ± 0.019	(*WISE*)
	11.711701	−71.794221	56966	9.314 ± 0.016	8.899 ± 0.016	(*WISE*)
MSX SMC 033	11.772898	−73.359184	53498	8.755 ± 0.020	8.171 ± 0.016	IRAC
	11.772877	−73.359065	54633	8.845 ± 0.032	8.146 ± 0.037	IRAC
	11.773538	−73.359232	54728	8.618 ± 0.043	7.887 ± 0.041	IRAC
	11.773152	−73.359167	55317	8.342 ± 0.016	7.660 ± 0.021	(*WISE*)
	11.773000	−73.359200	55452	···	7.981 ± 0.056	IRAC
	11.773151	−73.359167	55498	8.955 ± 0.032	8.219 ± 0.038	(*WISE*)
	11.773026	−73.359158	56781	8.620 ± 0.015	7.967 ± 0.018	(*WISE*)
	11.773079	−73.359171	56962	8.075 ± 0.017	7.496 ± 0.019	(*WISE*)
IRAS F00454−7257	11.828679	−72.676186	53498	8.538 ± 0.021	7.681 ± 0.025	IRAC
	11.828678	−72.676096	54633	9.361 ± 0.055	8.463 ± 0.041	IRAC
	11.829033	−72.676166	54728	9.156 ± 0.034	8.226 ± 0.024	IRAC
	11.829695	−72.676182	55318	8.794 ± 0.102	8.192 ± 0.042	(*WISE*)
	11.828800	−72.676100	55426	9.157 ± 0.062	8.311 ± 0.063	IRAC
	11.828800	−72.676100	55452	9.103 ± 0.071	8.074 ± 0.060	IRAC
	11.829695	−72.676182	55500	8.398 ± 0.052	7.609 ± 0.071	(*WISE*)
	11.828800	−72.676100	55555	8.776 ± 0.110	7.752 ± 0.039	IRAC
	11.828800	−72.676100	55729	8.656 ± 0.072	7.815 ± 0.042	IRAC
	11.829708	−72.676204	56783	8.631 ± 0.052	7.975 ± 0.046	(*WISE*)
	11.829493	−72.676186	56964	8.323 ± 0.037	7.561 ± 0.021	(*WISE*)
MSX SMC 066	12.218507	−73.149173	53498	8.740 ± 0.023	8.300 ± 0.019	IRAC
	12.218568	−73.149043	54633	8.848 ± 0.038	8.289 ± 0.044	IRAC
	12.219183	−73.149182	54728	8.836 ± 0.046	8.232 ± 0.036	IRAC
	12.218738	−73.149153	55318	8.608 ± 0.018	8.104 ± 0.025	(*WISE*)
	12.218600	−73.149100	55426	8.605 ± 0.052	8.046 ± 0.046	IRAC
	12.218600	−73.149100	55452	8.619 ± 0.075	8.105 ± 0.047	IRAC
	12.218738	−73.149153	55499	8.775 ± 0.042	8.255 ± 0.034	(*WISE*)
	12.218600	−73.149100	55555	9.007 ± 0.055	8.434 ± 0.055	IRAC
	12.218600	−73.149100	55729	9.023 ± 0.054	8.318 ± 0.049	IRAC
	12.218656	−73.149140	56782	9.056 ± 0.024	8.603 ± 0.049	(*WISE*)
	12.218719	−73.149152	56962	8.733 ± 0.016	8.299 ± 0.013	(*WISE*)
IRAS F00471−7352	12.247724	−73.594080	54633	8.020 ± 0.048	7.307 ± 0.032	IRAC
	12.247940	−73.594102	54728	8.181 ± 0.048	7.495 ± 0.035	IRAC
	12.247937	−73.594118	55316	8.150 ± 0.023	7.350 ± 0.022	(*WISE*)
	12.247800	−73.594100	55426	···	7.487 ± 0.043	IRAC
	12.247937	−73.594118	55498	8.643 ± 0.032	7.833 ± 0.042	(*WISE*)
	12.247873	−73.594102	56781	8.351 ± 0.016	7.576 ± 0.022	(*WISE*)
	12.247899	−73.594117	56961	9.138 ± 0.017	8.326 ± 0.014	(*WISE*)
LIN 131	12.265803	−73.088909	53498	9.308 ± 0.025	9.196 ± 0.011	IRAC
	12.265793	−73.088804	54633	10.244 ± 0.023	9.990 ± 0.030	IRAC
	12.266426	−73.088924	54728	9.806 ± 0.038	9.599 ± 0.024	IRAC
	12.266066	−73.088907	55318	9.475 ± 0.032	9.430 ± 0.023	(*WISE*)
	12.265800	−73.088900	55426	10.053 ± 0.045	9.878 ± 0.034	IRAC
	12.265800	−73.088900	55452	10.177 ± 0.037	10.038 ± 0.048	IRAC
	12.266065	−73.088907	55499	10.187 ± 0.024	10.029 ± 0.065	(*WISE*)
	12.265800	−73.088900	55555	10.157 ± 0.040	9.954 ± 0.036	IRAC
	12.265800	−73.088900	55729	9.459 ± 0.062	9.410 ± 0.044	IRAC
	12.265938	−73.088887	56782	10.212 ± 0.061	10.090 ± 0.024	(*WISE*)
	12.265958	−73.088890	56962	9.439 ± 0.017	9.435 ± 0.015	(*WISE*)
RAW 594	12.535264	−72.838982	53498	10.501 ± 0.017	10.619 ± 0.015	IRAC
	12.535099	−72.838879	54633	10.470 ± 0.030	10.559 ± 0.029	IRAC
	12.535608	−72.838946	54728	10.532 ± 0.026	10.656 ± 0.028	IRAC

TABLE 10 — *Continued*

Target	RA (J2000)	Decl. (J2000)	MJD	[3.6]	[4.5]	Data source[a]
	12.534786	−72.838976	55318	10.505 ± 0.033	10.581 ± 0.038	(*WISE*)
	12.535300	−72.839000	55426	10.574 ± 0.058	10.638 ± 0.041	IRAC
	12.535300	−72.839000	55452	10.522 ± 0.050	10.575 ± 0.042	IRAC
	12.534786	−72.838976	55500	10.467 ± 0.056	10.601 ± 0.051	(*WISE*)
	12.535300	−72.839000	55555	10.612 ± 0.058	10.735 ± 0.048	IRAC
	12.535300	−72.839000	55729	10.500 ± 0.051	10.580 ± 0.045	IRAC
	12.534963	−72.838952	56782	10.500 ± 0.067	10.626 ± 0.088	(*WISE*)
	12.534864	−72.838939	56964	10.557 ± 0.057	10.691 ± 0.035	(*WISE*)
MSX SMC 163	12.752842	−72.421804	54633	9.096 ± 0.054	8.416 ± 0.041	IRAC
	12.753605	−72.421846	54728	9.401 ± 0.048	8.717 ± 0.042	IRAC
	12.753102	−72.421852	55319	9.048 ± 0.028	8.348 ± 0.025	(*WISE*)
	12.753100	−72.421800	55426	9.413 ± 0.070	8.659 ± 0.047	IRAC
	12.753100	−72.421800	55452	9.384 ± 0.048	8.624 ± 0.048	IRAC
	12.753102	−72.421852	55500	9.369 ± 0.064	8.637 ± 0.047	(*WISE*)
	12.753100	−72.421800	55555	9.276 ± 0.082	8.470 ± 0.057	IRAC
	12.753100	−72.421800	55729	8.514 ± 0.059	7.805 ± 0.058	IRAC
	12.753070	−72.421827	56783	9.389 ± 0.022	8.617 ± 0.024	(*WISE*)
	12.753081	−72.421838	56965	8.868 ± 0.017	8.121 ± 0.017	(*WISE*)
LEGC A144	12.918454	−72.958043	53498	10.274 ± 0.019	9.800 ± 0.013	IRAC
	12.918278	−72.957963	54633	9.605 ± 0.041	9.258 ± 0.028	IRAC
	12.919057	−72.958079	54728	10.041 ± 0.034	9.637 ± 0.020	IRAC
	12.918526	−72.958014	55318	10.271 ± 0.041	9.809 ± 0.032	(*WISE*)
	12.918600	−72.958000	55426	9.712 ± 0.059	9.315 ± 0.037	IRAC
	12.918600	−72.958000	55452	9.747 ± 0.044	9.184 ± 0.042	IRAC
	12.918526	−72.958014	55499	9.723 ± 0.036	9.283 ± 0.046	(*WISE*)
	12.918600	−72.958000	55555	9.901 ± 0.044	9.580 ± 0.027	IRAC
	12.918600	−72.958000	55729	9.812 ± 0.039	9.329 ± 0.035	IRAC
	12.918617	−72.958028	56782	10.082 ± 0.016	9.657 ± 0.070	(*WISE*)
	12.918599	−72.958027	56963	9.450 ± 0.018	9.020 ± 0.024	(*WISE*)
MSX SMC 125	12.958801	−72.847149	53498	8.211 ± 0.020	7.756 ± 0.017	IRAC
	12.958731	−72.847074	54633	8.579 ± 0.035	8.011 ± 0.029	IRAC
	12.959354	−72.847154	54728	8.175 ± 0.032	7.680 ± 0.038	IRAC
	12.958936	−72.847122	55318	8.203 ± 0.023	7.669 ± 0.021	(*WISE*)
	12.958900	−72.847100	55426	8.848 ± 0.077	8.369 ± 0.051	IRAC
	12.958900	−72.847100	55452	9.011 ± 0.080	8.467 ± 0.059	IRAC
	12.958936	−72.847122	55500	8.966 ± 0.038	8.373 ± 0.045	(*WISE*)
	12.958900	−72.847100	55555	8.824 ± 0.056	8.203 ± 0.056	IRAC
	12.958900	−72.847100	55729	8.060 ± 0.098	7.549 ± 0.042	IRAC
	12.958859	−72.847096	56782	8.615 ± 0.068	8.054 ± 0.038	(*WISE*)
	12.958893	−72.847097	56964	8.981 ± 0.020	8.393 ± 0.027	(*WISE*)
MSX SMC 162	13.167329	−72.791055	53498	8.799 ± 0.016	8.326 ± 0.016	IRAC
	13.167151	−72.791032	54633	8.488 ± 0.053	8.075 ± 0.048	IRAC
	13.167761	−72.791044	54728	8.595 ± 0.046	8.092 ± 0.036	IRAC
	13.167411	−72.791040	55319	8.769 ± 0.024	8.150 ± 0.029	(*WISE*)
	13.167500	−72.791000	55426	9.036 ± 0.072	8.311 ± 0.038	IRAC
	13.167500	−72.791000	55452	8.920 ± 0.077	8.359 ± 0.081	IRAC
	13.167411	−72.791040	55500	8.827 ± 0.039	8.165 ± 0.045	(*WISE*)
	13.167500	−72.791000	55555	8.859 ± 0.072	8.265 ± 0.046	IRAC
	13.167500	−72.791000	55729	8.333 ± 0.057	7.780 ± 0.060	IRAC
	13.167386	−72.791033	56783	8.269 ± 0.066	7.772 ± 0.042	(*WISE*)
	13.167387	−72.791049	56964	8.688 ± 0.014	8.164 ± 0.015	(*WISE*)
MSX SMC 202	13.291972	−72.198598	53498	8.837 ± 0.052	···	IRAC
	13.291991	−72.198524	54633	8.775 ± 0.068	8.350 ± 0.033	IRAC
	13.292482	−72.198538	54728	8.873 ± 0.042	8.532 ± 0.038	IRAC
	13.292205	−72.198498	55319	8.985 ± 0.023	8.585 ± 0.017	(*WISE*)
	13.292200	−72.198500	55426	9.089 ± 0.092	8.628 ± 0.053	IRAC
	13.292200	−72.198500	55452	9.047 ± 0.080	8.636 ± 0.047	IRAC
	13.292205	−72.198498	55501	8.872 ± 0.029	8.467 ± 0.031	(*WISE*)
	13.292200	−72.198500	55555	···	8.371 ± 0.048	IRAC
	13.292200	−72.198500	55729	8.918 ± 0.046	8.605 ± 0.062	IRAC
	13.292207	−72.198512	56784	9.084 ± 0.014	8.736 ± 0.019	(*WISE*)
	13.292228	−72.198517	56965	8.990 ± 0.018	8.621 ± 0.019	(*WISE*)
MSX SMC 159	13.592734	−72.724966	53498	9.145 ± 0.021	8.289 ± 0.014	IRAC
	13.592650	−72.724944	54633	9.157 ± 0.044	8.234 ± 0.037	IRAC
	13.593043	−72.724927	54728	9.082 ± 0.040	8.200 ± 0.031	IRAC
	13.592966	−72.724998	55319	9.091 ± 0.024	8.181 ± 0.023	(*WISE*)
	13.592800	−72.725000	55426	9.631 ± 0.065	8.581 ± 0.066	IRAC
	13.592800	−72.725000	55452	9.820 ± 0.061	8.727 ± 0.053	IRAC
	13.592966	−72.724998	55500	9.888 ± 0.078	8.923 ± 0.022	(*WISE*)
	13.592800	−72.725000	55555	10.177 ± 0.042	9.151 ± 0.038	IRAC
	13.592800	−72.725000	55729	9.823 ± 0.068	8.701 ± 0.073	IRAC
	13.592837	−72.724961	56783	10.186 ± 0.021	9.151 ± 0.055	(*WISE*)
	13.592892	−72.724984	56965	9.294 ± 0.015	8.346 ± 0.015	(*WISE*)
LEGC 105	13.695106	−73.227172	53498	9.598 ± 0.017	9.119 ± 0.016	IRAC
	13.695220	−73.227146	54633	9.829 ± 0.030	9.475 ± 0.031	IRAC
	13.695528	−73.227154	54728	9.706 ± 0.044	9.306 ± 0.023	IRAC

TABLE 10 — *Continued*

Target	RA (J2000)	Decl. (J2000)	MJD	[3.6]	[4.5]	Data source[a]
	13.695184	−73.227181	55318	10.018 ± 0.071	9.564 ± 0.023	(*WISE*)
	13.695200	−73.227200	55426	10.036 ± 0.078	9.480 ± 0.035	IRAC
	13.695200	−73.227200	55452	9.882 ± 0.034	9.300 ± 0.028	IRAC
	13.695184	−73.227181	55499	9.565 ± 0.047	9.109 ± 0.040	(*WISE*)
	13.695200	−73.227200	55555	9.643 ± 0.062	9.101 ± 0.040	IRAC
	13.695200	−73.227200	55729	9.963 ± 0.049	9.536 ± 0.046	IRAC
	13.695277	−73.227186	56782	10.181 ± 0.015	9.526 ± 0.021	(*WISE*)
	13.695327	−73.227197	56963	9.479 ± 0.020	8.895 ± 0.019	(*WISE*)
ISO 00548	13.711280	−73.102079	53498	9.107 ± 0.033	8.488 ± 0.037	IRAC
	13.711309	−73.102032	54633	9.437 ± 0.054	8.997 ± 0.038	IRAC
	13.711691	−73.102093	54728	9.165 ± 0.041	8.696 ± 0.030	IRAC
	13.711559	−73.102053	55318	8.892 ± 0.027	8.374 ± 0.035	(*WISE*)
	13.711500	−73.102100	55426	9.456 ± 0.045	9.011 ± 0.058	IRAC
	13.711500	−73.102100	55452	9.717 ± 0.036	9.083 ± 0.039	IRAC
	13.711559	−73.102053	55499	9.582 ± 0.059	9.026 ± 0.054	(*WISE*)
	13.711500	−73.102100	55555	9.598 ± 0.054	8.953 ± 0.076	IRAC
	13.711500	−73.102100	55729	9.023 ± 0.061	8.426 ± 0.054	IRAC
	13.711416	−73.101948	56782	9.781 ± 0.037	9.269 ± 0.085	(*WISE*)
	13.711477	−73.102021	56963	9.158 ± 0.035	8.641 ± 0.016	(*WISE*)
ISO 00549	13.725477	−73.055079	54633	9.141 ± 0.048	8.451 ± 0.037	IRAC
	13.725658	−73.055093	54728	8.553 ± 0.031	7.920 ± 0.030	IRAC
	13.725546	−73.055116	55318	8.486 ± 0.020	7.796 ± 0.020	(*WISE*)
	13.725600	−73.055100	55426	9.103 ± 0.078	8.168 ± 0.059	IRAC
	13.725600	−73.055100	55452	9.201 ± 0.058	8.492 ± 0.058	IRAC
	13.725546	−73.055116	55499	9.344 ± 0.032	8.581 ± 0.055	(*WISE*)
	13.725600	−73.055100	55555	9.389 ± 0.052	8.696 ± 0.046	IRAC
	13.725600	−73.055100	55729	···	8.064 ± 0.051	IRAC
	13.725432	−73.055084	56782	8.661 ± 0.062	8.028 ± 0.057	(*WISE*)
	13.725465	−73.055092	56963	8.655 ± 0.015	8.027 ± 0.015	(*WISE*)
RAW 960	13.977518	−73.193462	53498	10.126 ± 0.037	9.831 ± 0.014	IRAC
	13.977530	−73.193454	54633	9.846 ± 0.028	9.574 ± 0.021	IRAC
	13.977819	−73.193468	54728	10.318 ± 0.036	9.943 ± 0.023	IRAC
	13.977608	−73.193508	55318	10.479 ± 0.031	10.101 ± 0.026	(*WISE*)
	13.977600	−73.193500	55426	10.496 ± 0.052	10.069 ± 0.049	IRAC
	13.977600	−73.193500	55452	10.448 ± 0.067	10.029 ± 0.051	IRAC
	13.977608	−73.193508	55499	10.157 ± 0.037	9.774 ± 0.041	(*WISE*)
	13.977600	−73.193500	55555	9.984 ± 0.044	···	IRAC
	13.977600	−73.193500	55729	10.394 ± 0.036	9.978 ± 0.039	IRAC
	13.977701	−73.193509	56782	10.018 ± 0.067	9.748 ± 0.087	(*WISE*)
	13.977669	−73.193503	56963	10.558 ± 0.014	10.201 ± 0.019	(*WISE*)
MSX SMC 209	14.068109	−72.278175	53498	9.317 ± 0.019	8.701 ± 0.054	IRAC
	14.067926	−72.278138	54633	9.322 ± 0.035	8.550 ± 0.034	IRAC
	14.068610	−72.278118	54728	8.809 ± 0.053	8.090 ± 0.044	IRAC
	14.068294	−72.278142	55319	8.695 ± 0.064	7.998 ± 0.028	(*WISE*)
	14.068200	−72.278100	55426	9.041 ± 0.058	8.294 ± 0.059	IRAC
	14.068200	−72.278100	55452	9.211 ± 0.073	8.425 ± 0.064	IRAC
	14.068294	−72.278142	55501	9.371 ± 0.030	8.584 ± 0.036	(*WISE*)
	14.068200	−72.278100	55555	9.573 ± 0.033	8.768 ± 0.066	IRAC
	14.068200	−72.278100	55729	9.239 ± 0.053	8.438 ± 0.051	IRAC
	14.068181	−72.278132	56784	9.442 ± 0.019	8.549 ± 0.024	(*WISE*)
	14.068236	−72.278153	56966	8.936 ± 0.021	8.108 ± 0.021	(*WISE*)
NGC 330 BAL 555	14.072894	−72.451228	53498	10.066 ± 0.015	10.237 ± 0.014	IRAC
	14.072894	−72.451176	54633	···	10.349 ± 0.031	IRAC
	14.073336	−72.451185	54728	···	10.324 ± 0.035	IRAC
	14.072149	−72.451212	55319	9.943 ± 0.032	10.077 ± 0.026	(*WISE*)
	14.073000	−72.451200	55426	10.161 ± 0.043	10.272 ± 0.042	IRAC
	14.073000	−72.451200	55452	10.128 ± 0.050	10.289 ± 0.046	IRAC
	14.072149	−72.451212	55501	9.895 ± 0.040	10.041 ± 0.067	(*WISE*)
	14.073000	−72.451200	55555	9.992 ± 0.036	10.298 ± 0.052	IRAC
	14.073000	−72.451200	55729	10.138 ± 0.053	10.273 ± 0.045	IRAC
	14.072189	−72.451230	56784	9.941 ± 0.037	10.047 ± 0.031	(*WISE*)
	14.072155	−72.451203	56965	9.890 ± 0.032	9.997 ± 0.021	(*WISE*)
IRAS 00554−7351	14.266263	−73.587399	54633	9.474 ± 0.038	8.400 ± 0.041	IRAC
	14.266646	−73.587413	54728	9.534 ± 0.067	8.303 ± 0.046	IRAC
	14.266475	−73.587439	55317	9.061 ± 0.021	7.972 ± 0.028	(*WISE*)
	14.266475	−73.587439	55499	9.457 ± 0.029	8.357 ± 0.032	(*WISE*)
	14.266375	−73.587420	56781	8.287 ± 0.014	7.279 ± 0.015	(*WISE*)
	14.266447	−73.587438	56962	8.652 ± 0.028	7.624 ± 0.022	(*WISE*)
MSX SMC 198	14.295595	−72.516686	53498	9.398 ± 0.020	8.768 ± 0.022	IRAC
	14.295523	−72.516655	54633	9.972 ± 0.027	9.310 ± 0.029	IRAC
	14.296189	−72.516685	54728	9.987 ± 0.041	9.292 ± 0.029	IRAC
	14.295722	−72.516656	55319	9.448 ± 0.048	8.789 ± 0.038	(*WISE*)
	14.295600	−72.516700	55426	9.170 ± 0.061	8.547 ± 0.057	IRAC
	14.295600	−72.516700	55452	9.182 ± 0.053	8.566 ± 0.073	IRAC
	14.295722	−72.516656	55501	9.253 ± 0.029	8.639 ± 0.046	(*WISE*)
	14.295600	−72.516700	55555	9.465 ± 0.060	8.874 ± 0.069	IRAC

TABLE 10 — *Continued*

Target	RA (J2000)	Decl. (J2000)	MJD	[3.6]	[4.5]	Data source[a]
	14.295600	−72.516700	55729	9.714 ± 0.074	9.105 ± 0.059	IRAC
	14.295731	−72.516652	56784	9.863 ± 0.015	9.093 ± 0.019	(*WISE*)
	14.295792	−72.516676	56965	9.484 ± 0.018	8.775 ± 0.017	(*WISE*)
ISO 00573	14.335409	−73.212771	54633	9.901 ± 0.045	9.530 ± 0.029	IRAC
	14.335756	−73.212793	54728	9.714 ± 0.031	9.423 ± 0.018	IRAC
	14.335607	−73.212817	55318	9.935 ± 0.021	9.407 ± 0.023	(*WISE*)
	14.335600	−73.212800	55426	9.687 ± 0.031	9.191 ± 0.032	IRAC
	14.335600	−73.212800	55452	9.796 ± 0.067	9.259 ± 0.067	IRAC
	14.335607	−73.212817	55499	10.045 ± 0.045	9.510 ± 0.048	(*WISE*)
	14.335600	−73.212800	55555	10.292 ± 0.054	9.689 ± 0.046	IRAC
	14.335600	−73.212800	55729	9.872 ± 0.047	9.255 ± 0.037	IRAC
	14.335561	−73.212790	56782	9.992 ± 0.022	9.473 ± 0.018	(*WISE*)
	14.335611	−73.212804	56963	10.281 ± 0.022	9.834 ± 0.018	(*WISE*)
MSX SMC 093	14.847142	−73.933604	54633	9.271 ± 0.036	8.933 ± 0.047	IRAC
	14.847543	−73.933602	54728	9.037 ± 0.048	8.764 ± 0.052	IRAC
	14.847375	−73.933615	55316	9.154 ± 0.029	8.753 ± 0.035	(*WISE*)
	14.847375	−73.933615	55498	9.303 ± 0.034	8.899 ± 0.043	(*WISE*)
	14.847327	−73.933609	56781	9.679 ± 0.017	9.230 ± 0.016	(*WISE*)
	14.847326	−73.933613	56961	9.527 ± 0.017	9.090 ± 0.013	(*WISE*)
ISO 01019	15.477525	−72.972891	54633	10.151 ± 0.041	9.454 ± 0.036	IRAC
	15.477640	−72.972943	54728	10.421 ± 0.037	9.713 ± 0.029	IRAC
	15.477380	−72.972887	55319	10.212 ± 0.027	9.625 ± 0.020	(*WISE*)
	15.477600	−72.972900	55426	10.402 ± 0.049	9.832 ± 0.037	IRAC
	15.477600	−72.972900	55452	10.470 ± 0.046	9.826 ± 0.044	IRAC
	15.477380	−72.972887	55500	10.060 ± 0.048	9.505 ± 0.054	(*WISE*)
	15.477600	−72.972900	55555	9.868 ± 0.041	9.283 ± 0.041	IRAC
	15.477600	−72.972900	55729	10.439 ± 0.038	9.724 ± 0.044	IRAC
	15.477393	−72.972892	56783	10.230 ± 0.022	9.737 ± 0.027	(*WISE*)
	15.477401	−72.972893	56964	9.709 ± 0.019	9.260 ± 0.017	(*WISE*)
MSX SMC 232	16.513685	−72.375579	54633	10.027 ± 0.030	9.179 ± 0.021	IRAC
	16.513823	−72.375621	54728	9.605 ± 0.023	8.745 ± 0.039	IRAC
	16.514006	−72.375635	55320	9.487 ± 0.031	8.784 ± 0.026	(*WISE*)
	16.513600	−72.375600	55452	10.162 ± 0.046	9.421 ± 0.035	IRAC
	16.514100	−72.375600	55452	10.162 ± 0.046	9.421 ± 0.035	IRAC
	16.514006	−72.375635	55502	10.049 ± 0.045	9.350 ± 0.043	(*WISE*)
	16.513600	−72.375600	55555	10.035 ± 0.033	9.362 ± 0.042	IRAC
	16.514100	−72.375600	55555	10.035 ± 0.033	9.362 ± 0.042	IRAC
	16.513600	−72.375600	55729	9.757 ± 0.060	9.037 ± 0.058	IRAC
	16.514100	−72.375600	55729	9.757 ± 0.060	9.037 ± 0.058	IRAC
	16.513861	−72.375605	56784	9.585 ± 0.022	8.817 ± 0.019	(*WISE*)
	16.513934	−72.375623	56966	9.715 ± 0.016	8.926 ± 0.012	(*WISE*)
NGC 419 LE 16	17.004559	−72.888207	53498	9.954 ± 0.027	9.669 ± 0.019	IRAC
	17.004698	−72.888129	54633	9.795 ± 0.037	9.741 ± 0.028	IRAC
	17.004934	−72.888163	54728	9.880 ± 0.039	9.851 ± 0.036	IRAC
	17.004685	−72.888177	55319	9.958 ± 0.020	9.828 ± 0.028	(*WISE*)
	17.004685	−72.888177	55501	9.858 ± 0.026	9.754 ± 0.032	(*WISE*)
	17.004771	−72.888193	56783	10.071 ± 0.017	9.998 ± 0.023	(*WISE*)
	17.004703	−72.888178	56965	10.130 ± 0.016	9.998 ± 0.019	(*WISE*)
NGC 419 IR 1	17.053956	−72.878843	54633	9.167 ± 0.049	8.591 ± 0.049	IRAC
	17.054201	−72.878877	54728	9.244 ± 0.041	8.639 ± 0.031	IRAC
	17.054027	−72.878901	55319	8.920 ± 0.094	8.288 ± 0.042	(*WISE*)
	17.054027	−72.878901	55501	8.869 ± 0.080	8.245 ± 0.050	(*WISE*)
	17.054076	−72.878903	56784	8.838 ± 0.021	8.274 ± 0.021	(*WISE*)
	17.054102	−72.878907	56965	9.074 ± 0.036	8.582 ± 0.024	(*WISE*)
NGC 419 MIR 1	17.072691	−72.885985	53498	11.403 ± 0.062	9.831 ± 0.025	IRAC
	17.072821	−72.885868	54633	10.204 ± 0.054	8.725 ± 0.038	IRAC
	17.073123	−72.885924	54728	10.584 ± 0.058	9.068 ± 0.026	IRAC
	17.073011	−72.885667	56784	···	···	(*WISE*)
	17.073217	−72.885696	56965	···	···	(*WISE*)
NGC 419 LE 35	17.072653	−72.883757	53498	10.241 ± 0.064	10.388 ± 0.037	IRAC
	17.072782	−72.883649	54633	10.198 ± 0.064	10.439 ± 0.076	IRAC
	17.073132	−72.883696	54728	10.126 ± 0.055	10.357 ± 0.047	IRAC
NGC 419 LE 27	17.085956	−72.881154	53498	10.323 ± 0.029	10.429 ± 0.021	IRAC
	17.086048	−72.881063	54633	10.324 ± 0.051	10.399 ± 0.038	IRAC
	17.086322	−72.881099	54728	10.279 ± 0.039	10.394 ± 0.042	IRAC
NGC 419 LE 18	17.103782	−72.882538	53498	10.243 ± 0.020	10.379 ± 0.016	IRAC
	17.103874	−72.882443	54633	10.186 ± 0.050	10.355 ± 0.029	IRAC
	17.104129	−72.882477	54728	10.273 ± 0.035	10.462 ± 0.037	IRAC
	17.103831	−72.882511	56784	10.236 ± 0.030	10.336 ± 0.025	(*WISE*)
	17.103810	−72.882491	56965	10.261 ± 0.018	10.352 ± 0.027	(*WISE*)
IRAS 04628−6937	67.125721	−69.513980	53572	9.342 ± 0.060	8.289 ± 0.066	IRAC
	67.125808	−69.513977	53673	8.350 ± 0.032	7.473 ± 0.042	IRAC
	67.125783	−69.513979	55338	9.721 ± 0.049	8.625 ± 0.031	(*WISE*)
	67.125783	−69.513979	55519	9.062 ± 0.054	8.025 ± 0.038	(*WISE*)
	67.125784	−69.513964	56803	9.143 ± 0.026	8.141 ± 0.025	(*WISE*)
	67.125854	−69.513972	56981	8.512 ± 0.014	7.574 ± 0.016	(*WISE*)

TABLE 10 — *Continued*

Target	RA (J2000)	Decl. (J2000)	MJD	[3.6]	[4.5]	Data source[a]
IRAS F04331−6932	68.239043	−69.442546	53572	10.156 ± 0.037	8.690 ± 0.046	IRAC
	68.239114	−69.442532	53673	10.721 ± 0.070	9.132 ± 0.026	IRAC
	68.239180	−69.442546	55338	9.587 ± 0.020	8.198 ± 0.032	(*WISE*)
	68.239180	−69.442546	55519	9.669 ± 0.033	8.284 ± 0.069	(*WISE*)
	68.239078	−69.442537	56803	9.605 ± 0.050	8.217 ± 0.033	(*WISE*)
	68.239203	−69.442551	56981	10.291 ± 0.023	8.831 ± 0.013	(*WISE*)
IRAS F04340−7016	68.431933	−70.164027	53572	9.127 ± 0.042	8.412 ± 0.046	IRAC
	68.432006	−70.164013	53673	9.497 ± 0.056	8.743 ± 0.039	IRAC
	68.432140	−70.163999	55333	8.869 ± 0.022	8.187 ± 0.031	(*WISE*)
	68.432140	−70.163999	55513	9.599 ± 0.038	8.927 ± 0.045	(*WISE*)
	68.432008	−70.164011	56797	9.109 ± 0.023	8.494 ± 0.026	(*WISE*)
	68.432020	−70.164011	56976	9.468 ± 0.014	8.810 ± 0.013	(*WISE*)
IRAS F04353−6702	68.850356	−66.947025	55357	10.496 ± 0.029	9.237 ± 0.022	(*WISE*)
	68.850356	−66.947025	55534	9.785 ± 0.034	8.605 ± 0.037	(*WISE*)
	68.850379	−66.947006	56819	9.335 ± 0.020	8.201 ± 0.023	(*WISE*)
	68.850447	−66.947031	56999	9.968 ± 0.023	8.760 ± 0.020	(*WISE*)
IRAS F04375−7247	69.185468	−72.700289	55317	8.668 ± 0.024	7.652 ± 0.029	(*WISE*)
	69.185468	−72.700289	55498	9.399 ± 0.057	8.351 ± 0.045	(*WISE*)
	69.185303	−72.700306	56781	8.739 ± 0.014	7.689 ± 0.020	(*WISE*)
	69.185557	−72.700287	56962	9.597 ± 0.079	8.476 ± 0.068	(*WISE*)
IRAS 04374−6831	69.344595	−68.417613	53572	9.187 ± 0.048	8.184 ± 0.036	IRAC
	69.344724	−68.417588	53673	9.661 ± 0.031	8.582 ± 0.049	IRAC
	69.344795	−68.417607	55345	8.788 ± 0.023	7.769 ± 0.023	(*WISE*)
	69.344795	−68.417607	55525	9.241 ± 0.043	8.185 ± 0.045	(*WISE*)
	69.344721	−68.417588	56810	9.212 ± 0.020	8.245 ± 0.024	(*WISE*)
	69.344778	−68.417605	56988	9.531 ± 0.026	8.547 ± 0.018	(*WISE*)
IRAS F04433−7018	70.738755	−70.207176	53572	9.083 ± 0.049	8.306 ± 0.044	IRAC
	70.738820	−70.207138	53673	8.983 ± 0.030	8.258 ± 0.028	IRAC
	70.738701	−70.207174	55332	9.679 ± 0.028	8.913 ± 0.028	(*WISE*)
	70.738701	−70.207174	55511	8.967 ± 0.032	8.248 ± 0.039	(*WISE*)
	70.738790	−70.207162	56795	9.576 ± 0.018	8.803 ± 0.023	(*WISE*)
	70.738851	−70.207164	56975	8.741 ± 0.014	8.005 ± 0.017	(*WISE*)
2MASS J044627	71.612937	−68.796405	53572	···	8.966 ± 0.030	IRAC
	71.613022	−68.796382	53673	9.854 ± 0.036	9.329 ± 0.030	IRAC
	71.613161	−68.796396	55342	9.074 ± 0.023	8.526 ± 0.023	(*WISE*)
	71.613161	−68.796396	55522	9.661 ± 0.036	9.122 ± 0.053	(*WISE*)
	71.613086	−68.796398	56806	9.751 ± 0.016	9.209 ± 0.017	(*WISE*)
	71.613076	−68.796400	56984	9.296 ± 0.024	8.786 ± 0.021	(*WISE*)
IRAS 04473−6829	71.816960	−68.407151	53572	7.846 ± 0.036	7.111 ± 0.031	IRAC
	71.817080	−68.407135	53673	7.581 ± 0.031	6.873 ± 0.025	IRAC
	71.817029	−68.407145	55345	8.513 ± 0.030	7.611 ± 0.027	(*WISE*)
	71.817029	−68.407145	55525	7.860 ± 0.026	7.042 ± 0.038	(*WISE*)
	71.817072	−68.407138	56809	7.730 ± 0.022	6.946 ± 0.030	(*WISE*)
	71.817130	−68.407139	56987	8.351 ± 0.030	7.525 ± 0.026	(*WISE*)
IRAS 04496−6958	72.326876	−69.887385	53572	7.525 ± 0.033	6.889 ± 0.031	IRAC
	72.326988	−69.887368	53673	7.730 ± 0.058	7.098 ± 0.031	IRAC
	72.326961	−69.887369	55333	7.836 ± 0.022	7.192 ± 0.036	(*WISE*)
	72.326961	−69.887369	55513	7.284 ± 0.059	6.635 ± 0.039	(*WISE*)
	72.327054	−69.887368	56796	7.689 ± 0.021	7.072 ± 0.025	(*WISE*)
	72.327029	−69.887365	56976	7.664 ± 0.028	7.024 ± 0.021	(*WISE*)
MSX LMC 1128	72.668782	−68.971963	53572	9.404 ± 0.047	8.993 ± 0.042	IRAC
	72.668898	−68.971929	53673	9.325 ± 0.050	8.888 ± 0.048	IRAC
	72.668872	−68.971918	55339	9.077 ± 0.031	8.689 ± 0.031	(*WISE*)
	72.668872	−68.971918	55520	8.918 ± 0.041	8.491 ± 0.049	(*WISE*)
	72.668960	−68.971938	56804	9.323 ± 0.019	9.004 ± 0.017	(*WISE*)
	72.668926	−68.971940	56982	9.067 ± 0.019	8.763 ± 0.016	(*WISE*)
MSX LMC 1308	72.795545	−69.337418	53572	8.008 ± 0.032	7.443 ± 0.038	IRAC
	72.795640	−69.337399	53673	8.299 ± 0.034	7.560 ± 0.028	IRAC
	72.795684	−69.337385	55337	9.066 ± 0.024	8.408 ± 0.027	(*WISE*)
	72.795684	−69.337385	55516	8.941 ± 0.028	8.336 ± 0.044	(*WISE*)
	72.795650	−69.337382	56800	8.425 ± 0.016	7.695 ± 0.025	(*WISE*)
	72.795702	−69.337389	56979	9.137 ± 0.026	8.378 ± 0.021	(*WISE*)
MSX LMC 1205	72.814382	−68.694563	53572	8.310 ± 0.048	7.513 ± 0.034	IRAC
	72.814541	−68.694441	53673	8.800 ± 0.059	7.977 ± 0.033	IRAC
	72.814611	−68.694531	55342	8.600 ± 0.031	7.771 ± 0.034	(*WISE*)
	72.814611	−68.694531	55522	9.194 ± 0.034	8.319 ± 0.036	(*WISE*)
	72.814526	−68.694548	56806	8.896 ± 0.051	8.070 ± 0.034	(*WISE*)
	72.814577	−68.694548	56984	8.314 ± 0.028	7.525 ± 0.017	(*WISE*)
IRAS 04518−6852	72.918977	−68.793010	53572	12.539 ± 0.044	10.301 ± 0.034	IRAC
	72.919144	−68.792885	53673	12.677 ± 0.038	10.471 ± 0.039	IRAC
	72.919177	−68.792953	55341	11.602 ± 0.046	9.578 ± 0.037	(*WISE*)
	72.919177	−68.792953	55521	11.110 ± 0.039	9.098 ± 0.039	(*WISE*)
	72.919146	−68.792959	56805	12.356 ± 0.044	10.161 ± 0.023	(*WISE*)
	72.919339	−68.792971	56983	11.282 ± 0.023	9.156 ± 0.020	(*WISE*)
MSX LMC 1213	73.083913	−68.725063	53572	9.947 ± 0.052	8.856 ± 0.040	IRAC
	73.084104	−68.724946	53673	10.122 ± 0.046	9.040 ± 0.024	IRAC

TABLE 10 — *Continued*

Target	RA (J2000)	Decl. (J2000)	MJD	[3.6]	[4.5]	Data source[a]
	73.084144	−68.725020	55341	9.104 ± 0.020	8.124 ± 0.033	(*WISE*)
	73.084144	−68.725020	55522	10.005 ± 0.043	8.925 ± 0.040	(*WISE*)
	73.084010	−68.725039	56806	9.292 ± 0.036	8.306 ± 0.052	(*WISE*)
	73.084110	−68.725032	56984	10.033 ± 0.016	8.950 ± 0.020	(*WISE*)
KDM 764	73.135508	−67.049741	53572	9.208 ± 0.051	9.406 ± 0.027	IRAC
	73.135672	−67.049832	53673	9.233 ± 0.046	9.332 ± 0.022	IRAC
	73.135420	−67.049876	56820	9.327 ± 0.025	9.372 ± 0.030	(*WISE*)
	73.135338	−67.049866	56999	9.305 ± 0.025	9.349 ± 0.017	(*WISE*)
2MASS J045328	73.369568	−66.059579	53572	9.439 ± 0.056	9.256 ± 0.021	IRAC
	73.369664	−66.059554	53673	9.359 ± 0.052	9.257 ± 0.034	IRAC
	73.369656	−66.059545	55366	9.714 ± 0.024	9.403 ± 0.031	(*WISE*)
	73.369656	−66.059545	55544	9.778 ± 0.035	9.478 ± 0.042	(*WISE*)
	73.369629	−66.059534	56642	9.902 ± 0.018	9.609 ± 0.025	(*WISE*)
	73.369659	−66.059536	56829	9.855 ± 0.026	9.548 ± 0.033	(*WISE*)
	73.369669	−66.059512	57004	9.748 ± 0.018	9.487 ± 0.012	(*WISE*)
IRAS 04535−6616	73.434301	−66.196146	53572	···	9.741 ± 0.027	IRAC
	73.434432	−66.196135	53673	11.510 ± 0.029	9.675 ± 0.031	IRAC
	73.434471	−66.196132	55365	10.103 ± 0.025	8.371 ± 0.037	(*WISE*)
	73.434471	−66.196132	55543	9.941 ± 0.056	8.273 ± 0.038	(*WISE*)
	73.434502	−66.196127	56642	11.285 ± 0.030	9.488 ± 0.016	(*WISE*)
	73.434374	−66.196101	56828	10.247 ± 0.025	8.558 ± 0.034	(*WISE*)
	73.434546	−66.196100	57004	9.696 ± 0.014	8.095 ± 0.034	(*WISE*)
IRAS 04539−6821	73.443157	−68.270301	53572	8.925 ± 0.054	7.840 ± 0.037	IRAC
	73.443314	−68.270146	53673	9.299 ± 0.042	8.079 ± 0.034	IRAC
	73.443209	−68.270272	55345	9.723 ± 0.041	8.435 ± 0.037	(*WISE*)
	73.443209	−68.270272	55525	8.926 ± 0.034	7.766 ± 0.050	(*WISE*)
	73.443247	−68.270273	56810	8.927 ± 0.023	7.738 ± 0.020	(*WISE*)
	73.443355	−68.270281	56988	9.284 ± 0.031	8.041 ± 0.024	(*WISE*)
IRAS F04537−6509	73.506661	−65.081126	55374	8.566 ± 0.023	7.866 ± 0.028	(*WISE*)
	73.506661	−65.081126	55552	8.675 ± 0.034	8.010 ± 0.042	(*WISE*)
	73.506687	−65.081123	56650	9.244 ± 0.025	8.477 ± 0.031	(*WISE*)
	73.506631	−65.081107	56838	9.164 ± 0.025	8.375 ± 0.023	(*WISE*)
MSX LMC 1209	73.828530	−68.775221	53572	9.317 ± 0.052	8.334 ± 0.038	IRAC
	73.828713	−68.775130	53673	8.864 ± 0.039	8.019 ± 0.038	IRAC
	73.828652	−68.775177	55341	9.059 ± 0.036	8.112 ± 0.030	(*WISE*)
	73.828652	−68.775177	55521	8.862 ± 0.044	7.956 ± 0.038	(*WISE*)
	73.828678	−68.775201	56805	9.363 ± 0.021	8.431 ± 0.051	(*WISE*)
	73.828744	−68.775207	56983	9.788 ± 0.021	8.802 ± 0.014	(*WISE*)
IRAS 04557−6753	73.912269	−67.819644	53572	8.624 ± 0.048	7.600 ± 0.044	IRAC
	73.912372	−67.819638	53673	8.505 ± 0.045	7.471 ± 0.040	IRAC
	73.912529	−67.819599	55349	8.902 ± 0.038	7.781 ± 0.038	(*WISE*)
	73.912529	−67.819599	55529	9.712 ± 0.039	8.550 ± 0.052	(*WISE*)
	73.912364	−67.819596	56813	8.943 ± 0.015	7.803 ± 0.016	(*WISE*)
	73.912464	−67.819606	56992	9.795 ± 0.028	8.557 ± 0.018	(*WISE*)
IRAS 04567−6857	74.133806	−68.880857	53572	7.916 ± 0.036	7.024 ± 0.029	IRAC
	74.133936	−68.880807	53673	···	7.576 ± 0.027	IRAC
	74.133889	−68.880828	55339	8.316 ± 0.032	7.378 ± 0.036	(*WISE*)
	74.133889	−68.880828	55520	7.822 ± 0.042	6.959 ± 0.045	(*WISE*)
	74.133963	−68.880841	56804	7.565 ± 0.026	6.778 ± 0.029	(*WISE*)
	74.134042	−68.880846	56982	8.463 ± 0.025	7.622 ± 0.026	(*WISE*)
IRAS 04589−6825	74.691745	−68.343771	53572	10.794 ± 0.033	8.878 ± 0.039	IRAC
	74.691753	−68.343746	53673	10.955 ± 0.034	9.038 ± 0.028	IRAC
	74.691776	−68.343849	55344	11.368 ± 0.038	9.222 ± 0.038	(*WISE*)
	74.691776	−68.343849	55524	12.453 ± 0.055	10.180 ± 0.048	(*WISE*)
	74.691612	−68.343839	56808	11.001 ± 0.025	8.952 ± 0.031	(*WISE*)
	74.691844	−68.343869	56986	12.067 ± 0.045	9.832 ± 0.022	(*WISE*)
KDM 1238	74.729140	−69.188535	53572	10.047 ± 0.044	10.033 ± 0.027	IRAC
	74.729328	−69.188540	53673	9.992 ± 0.035	10.114 ± 0.030	IRAC
	74.729327	−69.188538	56800	10.108 ± 0.039	10.221 ± 0.048	(*WISE*)
	74.729280	−69.188535	56979	10.214 ± 0.021	10.322 ± 0.019	(*WISE*)
IRAS F05013−7213	75.134362	−72.150652	53572	9.695 ± 0.047	8.673 ± 0.045	IRAC
	75.134461	−72.150641	53673	9.026 ± 0.054	8.089 ± 0.030	IRAC
	75.134415	−72.150638	55313	9.133 ± 0.019	8.113 ± 0.028	(*WISE*)
	75.134415	−72.150638	55494	9.389 ± 0.039	8.352 ± 0.041	(*WISE*)
	75.134360	−72.150655	56778	10.090 ± 0.013	9.027 ± 0.017	(*WISE*)
	75.134458	−72.150649	56956	9.165 ± 0.026	8.176 ± 0.038	(*WISE*)
IRAS 05010−6739	75.253577	−67.589919	53572	8.859 ± 0.040	8.020 ± 0.039	IRAC
	75.253627	−67.589874	53673	8.923 ± 0.035	8.110 ± 0.040	IRAC
	75.253779	−67.589898	55349	7.756 ± 0.030	7.059 ± 0.031	(*WISE*)
	75.253779	−67.589898	55530	8.522 ± 0.040	7.779 ± 0.048	(*WISE*)
	75.253676	−67.589894	56815	8.785 ± 0.042	7.929 ± 0.026	(*WISE*)
	75.253732	−67.589893	56994	8.486 ± 0.017	7.633 ± 0.019	(*WISE*)
IRAS 05009−6616	75.268275	−66.211235	53572	8.611 ± 0.055	7.512 ± 0.030	IRAC
	75.268372	−66.211221	53673	8.917 ± 0.054	7.798 ± 0.032	IRAC
	75.268216	−66.211190	55366	9.159 ± 0.035	8.019 ± 0.046	(*WISE*)
	75.268216	−66.211190	55544	8.333 ± 0.048	7.320 ± 0.038	(*WISE*)

TABLE 10 — *Continued*

Target	RA (J2000)	Decl. (J2000)	MJD	[3.6]	[4.5]	Data source[a]
	75.268386	−66.211222	56643	9.428 ± 0.046	8.289 ± 0.036	(*WISE*)
	75.268253	−66.211204	56828	8.488 ± 0.108	7.443 ± 0.089	(*WISE*)
	75.268399	−66.211185	57004	8.615 ± 0.014	7.603 ± 0.019	(*WISE*)
IRAS 05026−6809	75.631080	−68.093346	53572	16.092 ± 0.081	12.828 ± 0.040	IRAC
	75.631266	−68.093302	53673	16.062 ± 0.051	12.727 ± 0.030	IRAC
	75.631203	−68.093313	55344	···	12.575 ± 0.153	(*WISE*)
	75.631203	−68.093314	55526	···	12.692 ± 0.150	(*WISE*)
	75.631042	−68.093313	56810	···	12.913 ± 0.071	(*WISE*)
	75.631441	−68.093346	56989	···	12.832 ± 0.076	(*WISE*)
KDM 1656	75.819144	−65.829227	53572	9.057 ± 0.044	9.096 ± 0.019	IRAC
	75.819211	−65.829171	53673	9.062 ± 0.049	9.072 ± 0.027	IRAC
	75.819213	−65.829190	55369	8.933 ± 0.026	8.821 ± 0.029	(*WISE*)
	75.819213	−65.829190	55548	8.964 ± 0.040	8.828 ± 0.036	(*WISE*)
	75.819179	−65.829188	56646	9.029 ± 0.038	8.951 ± 0.051	(*WISE*)
	75.819179	−65.829202	56833	8.971 ± 0.071	8.865 ± 0.051	(*WISE*)
W60 B14	75.903785	−68.560719	53572	8.978 ± 0.029	9.095 ± 0.023	IRAC
	75.903952	−68.560713	53673	8.935 ± 0.052	9.046 ± 0.026	IRAC
	75.903936	−68.560713	55341	9.009 ± 0.026	9.066 ± 0.030	(*WISE*)
	75.903900	−68.560700	55450	8.848 ± 0.070	···	IRAC
	75.903936	−68.560713	55521	8.845 ± 0.032	8.903 ± 0.047	(*WISE*)
	75.903900	−68.560700	55679	8.883 ± 0.059	9.048 ± 0.033	IRAC
	75.903928	−68.560716	56803	9.071 ± 0.089	9.084 ± 0.075	(*WISE*)
	75.903920	−68.560715	56983	8.923 ± 0.018	8.975 ± 0.014	(*WISE*)
LMC-BM 12-14	75.972360	−70.463226	53572	9.174 ± 0.043	9.309 ± 0.033	IRAC
	75.972667	−70.463235	53673	9.264 ± 0.071	9.291 ± 0.026	IRAC
	75.972522	−70.463221	55324	9.270 ± 0.044	9.337 ± 0.051	(*WISE*)
	75.972522	−70.463221	55503	9.220 ± 0.091	9.333 ± 0.080	(*WISE*)
	75.972552	−70.463234	56787	9.340 ± 0.024	9.424 ± 0.029	(*WISE*)
	75.972498	−70.463229	56968	9.324 ± 0.015	9.398 ± 0.017	(*WISE*)
IRAS 05042−6827	76.023221	−68.394546	53572	16.443 ± 0.105	···	IRAC
	76.023379	−68.394501	53673	16.575 ± 0.088	13.128 ± 0.048	IRAC
	76.023374	−68.394500	55342	···	12.932 ± 0.070	(*WISE*)
	76.023374	−68.394500	55523	···	13.011 ± 0.097	(*WISE*)
	76.023300	−68.394500	55679	···	13.453 ± 0.089	IRAC
	76.023173	−68.394510	56806	···	13.080 ± 0.099	(*WISE*)
	76.023591	−68.394520	56984	···	13.036 ± 0.085	(*WISE*)
NGC 1818 WBT 64	76.032146	−66.418315	53572	10.346 ± 0.038	10.135 ± 0.034	IRAC
	76.032250	−66.418296	53673	10.315 ± 0.039	10.162 ± 0.028	IRAC
	76.032277	−66.418315	55364	10.346 ± 0.033	10.238 ± 0.029	(*WISE*)
	76.032277	−66.418315	55542	10.254 ± 0.036	10.167 ± 0.044	(*WISE*)
	76.032327	−66.418312	56642	10.329 ± 0.061	10.240 ± 0.078	(*WISE*)
	76.032290	−66.418307	56826	10.505 ± 0.078	10.361 ± 0.094	(*WISE*)
	76.032312	−66.418298	57003	10.447 ± 0.040	10.273 ± 0.022	(*WISE*)
NGC 1835 LE 1	76.263282	−69.407382	53572	10.090 ± 0.059	10.166 ± 0.044	IRAC
	76.263527	−69.407365	53673	10.157 ± 0.052	10.250 ± 0.046	IRAC
	76.263682	−69.407274	55332	9.806 ± 0.050	9.928 ± 0.034	(*WISE*)
	76.263400	−69.407400	55426	10.070 ± 0.061	10.187 ± 0.059	IRAC
	76.263400	−69.407400	55450	10.132 ± 0.067	10.202 ± 0.063	IRAC
	76.263682	−69.407274	55512	9.789 ± 0.042	9.903 ± 0.045	(*WISE*)
	76.263400	−69.407400	55556	10.088 ± 0.073	10.162 ± 0.047	IRAC
	76.263400	−69.407400	55679	10.141 ± 0.044	10.237 ± 0.057	IRAC
	76.263888	−69.407263	56795	9.852 ± 0.045	10.016 ± 0.051	(*WISE*)
	76.263596	−69.407290	56975	9.825 ± 0.051	9.961 ± 0.028	(*WISE*)
IRAS 05053−6901	76.269900	−68.963446	53572	12.124 ± 0.062	9.988 ± 0.028	IRAC
	76.270348	−68.963427	53673	11.775 ± 0.034	9.687 ± 0.036	IRAC
	76.270244	−68.963411	55336	12.164 ± 0.065	9.770 ± 0.065	(*WISE*)
	76.270300	−68.963400	55426	12.237 ± 0.042	···	IRAC
	76.270300	−68.963400	55450	12.185 ± 0.061	···	IRAC
	76.270244	−68.963411	55516	12.132 ± 0.072	9.723 ± 0.105	(*WISE*)
	76.270300	−68.963400	55556	11.738 ± 0.050	9.614 ± 0.024	IRAC
	76.270300	−68.963400	55679	10.669 ± 0.030	8.673 ± 0.051	IRAC
	76.270028	−68.963417	56798	10.142 ± 0.072	8.226 ± 0.075	(*WISE*)
	76.270229	−68.963419	56979	10.595 ± 0.026	8.585 ± 0.026	(*WISE*)
LMC-BM 13-2	76.481826	−67.369471	53572	10.196 ± 0.025	9.850 ± 0.022	IRAC
	76.481999	−67.369457	53673	10.142 ± 0.042	9.794 ± 0.028	IRAC
	76.481919	−67.369462	55351	9.920 ± 0.030	9.651 ± 0.026	(*WISE*)
	76.481919	−67.369462	55532	9.870 ± 0.050	9.628 ± 0.038	(*WISE*)
	76.481914	−67.369457	56817	9.820 ± 0.053	9.583 ± 0.065	(*WISE*)
	76.481961	−67.369452	56996	9.835 ± 0.025	9.584 ± 0.017	(*WISE*)
2MASS J050607	76.531282	−71.696777	53572	9.623 ± 0.033	9.269 ± 0.032	IRAC
	76.531424	−71.696757	53673	10.095 ± 0.035	9.729 ± 0.029	IRAC
	76.531480	−71.696756	55314	9.730 ± 0.037	9.359 ± 0.028	(*WISE*)
	76.531480	−71.696756	55495	10.030 ± 0.033	9.603 ± 0.031	(*WISE*)
	76.531443	−71.696774	56778	10.201 ± 0.053	9.779 ± 0.034	(*WISE*)
	76.531447	−71.696774	56957	9.715 ± 0.024	9.265 ± 0.019	(*WISE*)
KDM 1961	76.552425	−64.927116	53572	10.953 ± 0.026	10.938 ± 0.026	IRAC

TABLE 10 — *Continued*

Target	RA (J2000)	Decl. (J2000)	MJD	[3.6]	[4.5]	Data source[a]
	76.552497	−64.927099	53673	10.890 ± 0.043	10.858 ± 0.041	IRAC
	76.552510	−64.927106	55378	10.906 ± 0.023	11.066 ± 0.033	(*WISE*)
	76.552510	−64.927106	55557	10.949 ± 0.059	11.106 ± 0.056	(*WISE*)
	76.552507	−64.927101	56655	10.954 ± 0.049	11.133 ± 0.072	(*WISE*)
	76.552487	−64.927102	56844	10.930 ± 0.023	11.113 ± 0.032	(*WISE*)
KDM 1966	76.579058	−64.936191	53572	10.901 ± 0.027	10.977 ± 0.025	IRAC
	76.579130	−64.936182	53673	10.829 ± 0.037	10.959 ± 0.036	IRAC
	76.579075	−64.936202	56655	10.918 ± 0.065	11.067 ± 0.067	(*WISE*)
	76.579089	−64.936197	56844	10.844 ± 0.018	10.957 ± 0.028	(*WISE*)
2MASS J050620	76.583779	−64.916324	53572	9.279 ± 0.047	9.375 ± 0.021	IRAC
	76.583903	−64.916291	53673	9.375 ± 0.048	9.456 ± 0.032	IRAC
	76.583548	−64.916296	55378	9.353 ± 0.037	9.399 ± 0.037	(*WISE*)
	76.583547	−64.916296	55557	9.402 ± 0.054	9.441 ± 0.042	(*WISE*)
	76.583550	−64.916276	56655	9.347 ± 0.046	9.440 ± 0.053	(*WISE*)
	76.583604	−64.916300	56844	9.425 ± 0.028	9.455 ± 0.028	(*WISE*)
2MASS J050629	76.623243	−68.926363	53572	10.214 ± 0.043	10.394 ± 0.028	IRAC
	76.623475	−68.926377	53673	10.266 ± 0.031	10.427 ± 0.036	IRAC
	76.623400	−68.926400	55426	10.229 ± 0.030	10.426 ± 0.031	IRAC
	76.623400	−68.926400	55450	10.286 ± 0.043	10.362 ± 0.043	IRAC
	76.623400	−68.926400	55556	10.319 ± 0.030	10.491 ± 0.029	IRAC
	76.623400	−68.926400	55679	10.229 ± 0.042	10.424 ± 0.029	IRAC
	76.623450	−68.926323	56798	10.472 ± 0.091	10.593 ± 0.097	(*WISE*)
	76.623393	−68.926325	56979	10.521 ± 0.022	10.619 ± 0.033	(*WISE*)
IRAS 05070−7020	76.646199	−70.280657	53572	10.551 ± 0.028	9.299 ± 0.028	IRAC
	76.646611	−70.280688	53673	9.582 ± 0.031	8.405 ± 0.036	IRAC
	76.646333	−70.280641	55323	9.863 ± 0.045	8.585 ± 0.039	(*WISE*)
	76.646333	−70.280641	55504	9.628 ± 0.036	8.396 ± 0.035	(*WISE*)
	76.646325	−70.280637	56787	10.615 ± 0.073	9.373 ± 0.064	(*WISE*)
	76.646442	−70.280637	56968	10.234 ± 0.016	8.997 ± 0.018	(*WISE*)
SHV 0507252	76.789403	−68.980385	53673	8.551 ± 0.039	8.385 ± 0.046	IRAC
	76.789255	−68.980338	55336	8.827 ± 0.056	8.350 ± 0.024	(*WISE*)
	76.789300	−68.980400	55426	8.877 ± 0.048	8.344 ± 0.040	IRAC
	76.789300	−68.980400	55450	8.741 ± 0.046	8.519 ± 0.044	IRAC
	76.789255	−68.980338	55515	8.677 ± 0.056	8.222 ± 0.049	(*WISE*)
	76.789300	−68.980400	55556	8.762 ± 0.041	8.320 ± 0.046	IRAC
	76.789300	−68.980400	55679	8.959 ± 0.043	8.484 ± 0.048	IRAC
	76.789196	−68.980361	56797	9.029 ± 0.069	8.587 ± 0.078	(*WISE*)
	76.789276	−68.980355	56978	8.754 ± 0.017	8.346 ± 0.027	(*WISE*)
SAGE MC J050752	76.970481	−68.212988	53572	10.129 ± 0.037	9.509 ± 0.031	IRAC
	76.970578	−68.212929	53673	9.738 ± 0.031	9.063 ± 0.029	IRAC
	76.970542	−68.212958	55342	10.141 ± 0.024	9.442 ± 0.033	(*WISE*)
	76.970542	−68.212958	55524	9.844 ± 0.033	9.182 ± 0.052	(*WISE*)
	76.970595	−68.212951	56808	10.347 ± 0.021	9.724 ± 0.019	(*WISE*)
	76.970620	−68.212958	56986	9.835 ± 0.025	9.231 ± 0.024	(*WISE*)
MSX LMC 92	77.106172	−68.900004	53572	8.446 ± 0.044	7.815 ± 0.029	IRAC
	77.106473	−68.900004	53673	8.884 ± 0.040	8.227 ± 0.042	IRAC
	77.106317	−68.899964	55337	9.198 ± 0.033	8.330 ± 0.027	(*WISE*)
	77.106300	−68.900000	55426	9.105 ± 0.044	8.228 ± 0.043	IRAC
	77.106300	−68.900000	55450	9.028 ± 0.058	8.171 ± 0.042	IRAC
	77.106317	−68.899964	55516	8.612 ± 0.043	7.805 ± 0.045	(*WISE*)
	77.106300	−68.900000	55556	8.437 ± 0.035	7.651 ± 0.040	IRAC
	77.106300	−68.900000	55679	8.704 ± 0.049	7.872 ± 0.031	IRAC
	77.106356	−68.899968	56798	8.934 ± 0.063	8.117 ± 0.073	(*WISE*)
	77.106432	−68.899972	56979	8.956 ± 0.022	8.133 ± 0.020	(*WISE*)
2MASS J050826	77.109727	−68.520866	53572	9.444 ± 0.048	8.965 ± 0.050	IRAC
	77.109856	−68.520866	53673	9.290 ± 0.041	8.805 ± 0.044	IRAC
	77.109799	−68.520866	55340	9.147 ± 0.024	8.569 ± 0.034	(*WISE*)
	77.109800	−68.520900	55426	8.874 ± 0.046	8.326 ± 0.040	IRAC
	77.109800	−68.520900	55450	8.904 ± 0.049	8.315 ± 0.056	IRAC
	77.109799	−68.520866	55520	9.047 ± 0.039	8.559 ± 0.053	(*WISE*)
	77.109800	−68.520900	55556	9.108 ± 0.053	8.701 ± 0.059	IRAC
	77.109800	−68.520900	55679	9.099 ± 0.048	8.643 ± 0.035	IRAC
	77.109832	−68.520864	56802	9.461 ± 0.043	9.014 ± 0.040	(*WISE*)
	77.109834	−68.520873	56982	9.228 ± 0.014	8.764 ± 0.020	(*WISE*)
KDM 2187	77.151620	−69.721044	53572	10.739 ± 0.047	10.749 ± 0.032	IRAC
	77.151796	−69.721016	53673	10.835 ± 0.039	10.930 ± 0.036	IRAC
	77.151851	−69.721016	55327	11.009 ± 0.029	10.988 ± 0.030	(*WISE*)
	77.151700	−69.721000	55426	10.833 ± 0.081	10.828 ± 0.172	IRAC
	77.151700	−69.721000	55450	10.843 ± 0.076	10.834 ± 0.045	IRAC
	77.151851	−69.721016	55507	10.884 ± 0.030	10.918 ± 0.038	(*WISE*)
	77.151700	−69.721000	55556	10.652 ± 0.039	10.780 ± 0.045	IRAC
	77.151700	−69.721000	55679	10.695 ± 0.050	10.717 ± 0.054	IRAC
	77.151870	−69.721027	56790	10.802 ± 0.084	10.825 ± 0.092	(*WISE*)
	77.151822	−69.721025	56972	10.839 ± 0.019	10.839 ± 0.027	(*WISE*)
IRAS 05103−6959	77.499900	−69.936004	53572	7.808 ± 0.042	7.118 ± 0.037	IRAC
	77.500029	−69.935982	53673	8.179 ± 0.036	7.470 ± 0.035	IRAC

TABLE 10 — *Continued*

Target	RA (J2000)	Decl. (J2000)	MJD	[3.6]	[4.5]	Data source[a]
	77.500102	−69.935960	55324	7.959 ± 0.036	7.208 ± 0.026	(*WISE*)
	77.500000	−69.936000	55426	8.260 ± 0.107	···	IRAC
	77.500000	−69.936000	55450	8.082 ± 0.079	7.330 ± 0.059	IRAC
	77.500102	−69.935960	55505	8.339 ± 0.037	7.574 ± 0.052	(*WISE*)
	77.500000	−69.936000	55556	8.719 ± 0.078	7.893 ± 0.039	IRAC
	77.500000	−69.936000	55679	9.131 ± 0.067	8.453 ± 0.049	IRAC
	77.499925	−69.936000	56788	9.017 ± 0.089	8.204 ± 0.077	(*WISE*)
	77.500097	−69.935973	56969	9.009 ± 0.042	8.197 ± 0.023	(*WISE*)
IRAS 05107−6953	77.581581	−69.830977	53572	9.177 ± 0.046	8.342 ± 0.034	IRAC
	77.581774	−69.830960	53673	8.926 ± 0.048	8.088 ± 0.047	IRAC
	77.581754	−69.830970	55324	8.826 ± 0.051	8.007 ± 0.034	(*WISE*)
	77.581700	−69.831000	55426	9.082 ± 0.073	8.340 ± 0.050	IRAC
	77.581700	−69.831000	55450	8.971 ± 0.052	8.207 ± 0.061	IRAC
	77.581754	−69.830970	55506	8.674 ± 0.029	7.888 ± 0.062	(*WISE*)
	77.581700	−69.831000	55556	8.735 ± 0.067	7.872 ± 0.058	IRAC
	77.581700	−69.831000	55679	7.988 ± 0.047	7.344 ± 0.065	IRAC
	77.581670	−69.830992	56789	8.530 ± 0.089	7.745 ± 0.071	(*WISE*)
	77.581793	−69.830959	56970	7.910 ± 0.021	7.148 ± 0.021	(*WISE*)
2MASS J051028	77.618039	−68.742082	53572	9.863 ± 0.033	8.889 ± 0.069	IRAC
	77.618161	−68.742046	53673	10.012 ± 0.029	9.067 ± 0.037	IRAC
	77.618343	−68.742022	55337	9.068 ± 0.040	8.249 ± 0.040	(*WISE*)
	77.618100	−68.742100	55426	9.692 ± 0.037	8.755 ± 0.039	IRAC
	77.618100	−68.742100	55450	9.842 ± 0.043	8.854 ± 0.033	IRAC
	77.618343	−68.742022	55516	9.867 ± 0.040	8.992 ± 0.044	(*WISE*)
	77.618100	−68.742100	55556	9.865 ± 0.026	8.978 ± 0.040	IRAC
	77.618100	−68.742100	55679	9.067 ± 0.054	8.262 ± 0.054	IRAC
	77.618176	−68.742047	56799	9.306 ± 0.032	8.521 ± 0.044	(*WISE*)
	77.618242	−68.742046	56980	9.760 ± 0.020	8.926 ± 0.023	(*WISE*)
IRAS 05112−6755	77.793467	−67.869624	53572	8.107 ± 0.038	7.047 ± 0.038	IRAC
	77.793570	−67.869613	53673	8.118 ± 0.043	7.016 ± 0.033	IRAC
	77.793692	−67.869588	55345	8.301 ± 0.034	7.120 ± 0.032	(*WISE*)
	77.793692	−67.869588	55527	9.186 ± 0.036	7.948 ± 0.038	(*WISE*)
	77.793604	−67.869588	56811	7.986 ± 0.022	6.855 ± 0.021	(*WISE*)
	77.793691	−67.869593	56990	8.271 ± 0.027	7.129 ± 0.026	(*WISE*)
IRAS 05113−6739	77.807723	−67.604532	53572	8.694 ± 0.044	7.656 ± 0.040	IRAC
	77.807854	−67.604502	53673	8.479 ± 0.048	7.410 ± 0.031	IRAC
	77.807837	−67.604507	55348	9.423 ± 0.026	8.313 ± 0.027	(*WISE*)
	77.807837	−67.604507	55529	9.222 ± 0.029	8.148 ± 0.049	(*WISE*)
	77.807794	−67.604502	56814	9.225 ± 0.027	8.068 ± 0.021	(*WISE*)
	77.807912	−67.604513	56992	8.412 ± 0.016	7.344 ± 0.020	(*WISE*)
MSX LMC 219	77.831248	−68.707730	53572	8.847 ± 0.035	7.733 ± 0.040	IRAC
	77.831401	−68.707713	53673	8.661 ± 0.039	7.592 ± 0.027	IRAC
	77.831415	−68.707675	55337	9.427 ± 0.028	8.317 ± 0.021	(*WISE*)
	77.831300	−68.707700	55426	9.852 ± 0.069	8.600 ± 0.035	IRAC
	77.831300	−68.707700	55450	9.749 ± 0.032	8.635 ± 0.045	IRAC
	77.831415	−68.707675	55517	9.631 ± 0.040	8.495 ± 0.033	(*WISE*)
	77.831300	−68.707700	55556	9.646 ± 0.044	8.459 ± 0.065	IRAC
	77.831300	−68.707700	55679	8.738 ± 0.060	7.766 ± 0.061	IRAC
	77.831354	−68.707688	56799	9.600 ± 0.037	8.433 ± 0.035	(*WISE*)
	77.831464	−68.707697	56980	9.563 ± 0.020	8.385 ± 0.018	(*WISE*)
TRM 72	77.911136	−66.852652	53572	9.142 ± 0.047	8.067 ± 0.046	IRAC
	77.911038	−66.852743	53673	9.703 ± 0.021	8.559 ± 0.046	IRAC
	77.911015	−66.852742	55358	8.986 ± 0.021	8.201 ± 0.041	(*WISE*)
	77.911015	−66.852742	55537	8.489 ± 0.040	7.743 ± 0.046	(*WISE*)
	77.911138	−66.852752	56640	8.334 ± 0.020	7.581 ± 0.037	(*WISE*)
	77.911044	−66.852760	56822	8.115 ± 0.051	7.366 ± 0.037	(*WISE*)
	77.911101	−66.852761	57001	8.862 ± 0.016	8.056 ± 0.017	(*WISE*)
IRAS 05125−7035	78.003071	−70.540066	53572	9.984 ± 0.047	8.217 ± 0.038	IRAC
	78.003337	−70.540069	53673	10.390 ± 0.028	8.587 ± 0.039	IRAC
	78.003214	−70.540045	55318	10.606 ± 0.030	8.632 ± 0.047	(*WISE*)
	78.003214	−70.540045	55499	9.789 ± 0.047	8.007 ± 0.051	(*WISE*)
	78.003174	−70.540039	56783	9.843 ± 0.018	8.050 ± 0.023	(*WISE*)
	78.003368	−70.540024	56963	9.997 ± 0.020	8.170 ± 0.024	(*WISE*)
MSX LMC 220	78.133458	−69.261293	53572	8.290 ± 0.033	7.440 ± 0.034	IRAC
	78.133622	−69.261226	53673	7.756 ± 0.039	6.932 ± 0.044	IRAC
	78.133644	−69.261236	55330	8.268 ± 0.026	7.378 ± 0.030	(*WISE*)
	78.133600	−69.261200	55426	8.529 ± 0.067	7.617 ± 0.054	IRAC
	78.133600	−69.261200	55450	8.340 ± 0.064	7.484 ± 0.058	IRAC
	78.133644	−69.261236	55511	7.710 ± 0.038	6.880 ± 0.046	(*WISE*)
	78.133600	−69.261200	55556	7.763 ± 0.048	6.892 ± 0.058	IRAC
	78.133600	−69.261200	55679	7.835 ± 0.046	6.985 ± 0.041	IRAC
	78.133607	−69.261228	56793	7.752 ± 0.052	6.883 ± 0.031	(*WISE*)
	78.133703	−69.261226	56974	7.998 ± 0.036	7.121 ± 0.021	(*WISE*)
IRAS 05132−6941	78.212469	−69.630677	53572	9.379 ± 0.043	8.271 ± 0.043	IRAC
	78.212660	−69.630657	53673	8.611 ± 0.046	7.591 ± 0.035	IRAC
	78.212595	−69.630758	55325	8.126 ± 0.185	8.075 ± 0.149	(*WISE*)

TABLE 10 — *Continued*

Target	RA (J2000)	Decl.	MJD	[3.6]	[4.5]	Data source[a]
	78.212500	−69.630700	55426	9.698 ± 0.040	···	IRAC
	78.212500	−69.630700	55450	9.735 ± 0.029	8.637 ± 0.055	IRAC
	78.212593	−69.630759	55507	8.461 ± 0.187	7.789 ± 0.168	(*WISE*)
	78.212500	−69.630700	55556	···	8.338 ± 0.042	IRAC
	78.212500	−69.630700	55679	8.650 ± 0.046	7.593 ± 0.055	IRAC
	78.212559	−69.630653	56789	9.570 ± 0.058	8.465 ± 0.045	(*WISE*)
	78.212709	−69.630643	56971	9.247 ± 0.035	8.141 ± 0.029	(*WISE*)
IRAS 05133−6937	78.257237	−69.564191	53572	15.943 ± 0.086	13.807 ± 0.056	IRAC
	78.257427	−69.564163	53673	15.749 ± 0.067	13.612 ± 0.053	IRAC
	78.257471	−69.564110	55326	···	14.299 ± 0.170	(*WISE*)
	78.257300	−69.564200	55426	15.800 ± 0.155	13.687 ± 0.104	IRAC
	78.257300	−69.564200	55450	15.889 ± 0.099	13.724 ± 0.097	IRAC
	78.257471	−69.564111	55507	···	13.974 ± 0.150	(*WISE*)
	78.257300	−69.564200	55556	15.908 ± 0.075	13.718 ± 0.052	IRAC
	78.257300	−69.564200	55679	15.923 ± 0.163	13.767 ± 0.077	IRAC
	78.257160	−69.564172	56790	···	14.055 ± 0.121	(*WISE*)
	78.257592	−69.564192	56971	···	14.014 ± 0.178	(*WISE*)
OGLE J051306	78.276668	−69.162866	53572	9.135 ± 0.050	8.468 ± 0.050	IRAC
	78.276792	−69.162827	53673	9.530 ± 0.047	8.818 ± 0.046	IRAC
	78.276908	−69.162818	55332	9.429 ± 0.039	8.703 ± 0.029	(*WISE*)
	78.276700	−69.162800	55426	9.556 ± 0.083	8.783 ± 0.053	IRAC
	78.276700	−69.162800	55450	9.568 ± 0.062	8.882 ± 0.054	IRAC
	78.276908	−69.162817	55512	10.081 ± 0.046	9.307 ± 0.043	(*WISE*)
	78.276700	−69.162800	55556	10.237 ± 0.040	9.485 ± 0.040	IRAC
	78.276700	−69.162800	55679	9.525 ± 0.062	···	IRAC
	78.276741	−69.162831	56794	9.542 ± 0.034	8.781 ± 0.033	(*WISE*)
	78.276825	−69.162831	56975	10.323 ± 0.023	9.451 ± 0.036	(*WISE*)
MSX LMC 218	78.318182	−68.736149	53572	7.837 ± 0.047	7.150 ± 0.039	IRAC
	78.318365	−68.736138	53673	7.753 ± 0.054	7.047 ± 0.027	IRAC
	78.318265	−68.736120	55337	8.700 ± 0.026	7.915 ± 0.028	(*WISE*)
	78.318300	−68.736100	55426	8.640 ± 0.056	7.857 ± 0.046	IRAC
	78.318300	−68.736100	55450	8.591 ± 0.053	7.805 ± 0.043	IRAC
	78.318265	−68.736120	55516	7.917 ± 0.047	7.206 ± 0.053	(*WISE*)
	78.318300	−68.736100	55556	7.637 ± 0.049	7.009 ± 0.051	IRAC
	78.318300	−68.736100	55679	7.767 ± 0.096	6.957 ± 0.041	IRAC
	78.318348	−68.736114	56798	8.572 ± 0.028	7.807 ± 0.026	(*WISE*)
	78.318432	−68.736116	56979	7.622 ± 0.023	6.943 ± 0.020	(*WISE*)
MSX LMC 349	79.362134	−68.916271	53572	10.389 ± 0.035	9.115 ± 0.023	IRAC
	79.362335	−68.916257	53673	9.346 ± 0.045	8.162 ± 0.035	IRAC
	79.362275	−68.916253	55333	9.775 ± 0.169	8.555 ± 0.098	(*WISE*)
	79.362300	−68.916300	55426	9.461 ± 0.059	8.226 ± 0.063	IRAC
	79.362300	−68.916300	55450	9.373 ± 0.076	8.148 ± 0.050	IRAC
	79.362275	−68.916253	55512	9.039 ± 0.127	7.892 ± 0.093	(*WISE*)
	79.362300	−68.916300	55556	9.189 ± 0.053	8.057 ± 0.044	IRAC
	79.362300	−68.916300	55679	9.709 ± 0.044	8.500 ± 0.042	IRAC
	79.362229	−68.916258	56794	9.447 ± 0.033	8.271 ± 0.038	(*WISE*)
	79.362374	−68.916253	56975	10.362 ± 0.024	9.074 ± 0.021	(*WISE*)
SAGE MC J051803	79.513477	−68.830763	53572	9.380 ± 0.044	9.076 ± 0.033	IRAC
	79.513707	−68.830738	53673	9.638 ± 0.029	9.316 ± 0.027	IRAC
	79.513718	−68.830720	55334	9.748 ± 0.033	9.459 ± 0.028	(*WISE*)
	79.513600	−68.830800	55426	9.991 ± 0.034	9.820 ± 0.039	IRAC
	79.513600	−68.830800	55450	10.064 ± 0.043	9.797 ± 0.036	IRAC
	79.513719	−68.830720	55513	10.101 ± 0.039	9.734 ± 0.051	(*WISE*)
	79.513600	−68.830800	55556	10.027 ± 0.044	9.589 ± 0.031	IRAC
	79.513600	−68.830800	55679	9.827 ± 0.046	9.414 ± 0.031	IRAC
	79.513685	−68.830725	56795	9.526 ± 0.031	9.220 ± 0.030	(*WISE*)
	79.513684	−68.830729	56976	9.690 ± 0.019	9.339 ± 0.017	(*WISE*)
IRAS 05187−7033	79.548701	−70.507502	53572	15.073 ± 0.051	12.146 ± 0.038	IRAC
	79.548868	−70.507499	53673	15.250 ± 0.073	12.313 ± 0.039	IRAC
	79.548832	−70.507448	55314	13.702 ± 0.150	11.347 ± 0.091	(*WISE*)
	79.548832	−70.507448	55497	13.808 ± 0.126	11.432 ± 0.119	(*WISE*)
	79.548605	−70.507500	56780	14.715 ± 0.148	12.035 ± 0.056	(*WISE*)
	79.549037	−70.507448	56960	14.560 ± 0.181	12.027 ± 0.065	(*WISE*)
IRAS 05191−6936	79.701380	−69.559688	53572	14.996 ± 0.075	12.308 ± 0.044	IRAC
	79.701531	−69.559632	53673	15.109 ± 0.052	12.377 ± 0.030	IRAC
	79.701500	−69.559600	55426	15.243 ± 0.092	12.680 ± 0.035	IRAC
	79.701500	−69.559600	55450	15.137 ± 0.084	12.750 ± 0.041	IRAC
	79.701500	−69.559600	55556	15.291 ± 0.089	12.788 ± 0.037	IRAC
	79.701500	−69.559600	55679	15.382 ± 0.122	13.075 ± 0.049	IRAC
IRAS 05190−6758	79.734336	−67.751260	53572	8.677 ± 0.048	7.316 ± 0.038	IRAC
	79.734384	−67.751229	55346	8.810 ± 0.041	7.390 ± 0.038	(*WISE*)
	79.734384	−67.751229	55528	8.579 ± 0.034	7.209 ± 0.035	(*WISE*)
	79.734334	−67.751230	56810	9.696 ± 0.103	8.178 ± 0.103	(*WISE*)
	79.734477	−67.751230	56990	10.143 ± 0.072	8.542 ± 0.076	(*WISE*)
2MASS J051908	79.785144	−69.387318	53572	9.570 ± 0.052	9.655 ± 0.028	IRAC
	79.785381	−69.387301	53673	9.497 ± 0.050	9.671 ± 0.021	IRAC

TABLE 10 — *Continued*

Target	RA (J2000)	Decl. (J2000)	MJD	[3.6]	[4.5]	Data source[a]
	79.785300	−69.387300	55426	9.539 ± 0.037	9.689 ± 0.030	IRAC
	79.785300	−69.387300	55450	9.512 ± 0.041	9.708 ± 0.027	IRAC
	79.785300	−69.387300	55556	9.441 ± 0.037	9.705 ± 0.028	IRAC
	79.785300	−69.387300	55679	9.481 ± 0.043	9.639 ± 0.032	IRAC
	79.785431	−69.387262	56789	9.760 ± 0.029	9.834 ± 0.029	(*WISE*)
	79.785356	−69.387264	56970	9.762 ± 0.020	9.825 ± 0.014	(*WISE*)
TRM 78	80.080679	−66.596655	53572	8.988 ± 0.063	···	IRAC
	80.080805	−66.596632	53673	8.463 ± 0.058	7.795 ± 0.037	IRAC
	80.080902	−66.596633	55363	8.366 ± 0.033	7.658 ± 0.039	(*WISE*)
	80.080902	−66.596633	55544	9.215 ± 0.043	8.445 ± 0.055	(*WISE*)
	80.080746	−66.596617	56644	9.090 ± 0.058	8.509 ± 0.073	(*WISE*)
	80.080779	−66.596619	56825	8.628 ± 0.041	8.043 ± 0.049	(*WISE*)
	80.080820	−66.596622	57002	8.265 ± 0.018	7.668 ± 0.015	(*WISE*)
MSX LMC 341	80.251491	−69.348721	53572	9.843 ± 0.030	8.645 ± 0.036	IRAC
	80.251766	−69.348688	53673	9.066 ± 0.027	7.977 ± 0.029	IRAC
	80.251600	−69.348700	55426	9.026 ± 0.041	7.940 ± 0.034	IRAC
	80.251600	−69.348700	55450	9.066 ± 0.045	7.916 ± 0.045	IRAC
	80.251600	−69.348700	55556	9.440 ± 0.043	8.280 ± 0.045	IRAC
	80.251600	−69.348700	55679	10.308 ± 0.032	8.968 ± 0.039	IRAC
OGLE J052242	80.674780	−69.257265	53572	9.461 ± 0.046	8.724 ± 0.037	IRAC
	80.674937	−69.257210	53673	10.012 ± 0.038	9.198 ± 0.027	IRAC
	80.674863	−69.257231	55324	9.567 ± 0.044	8.856 ± 0.037	(*WISE*)
	80.674700	−69.257300	55426	9.809 ± 0.063	9.049 ± 0.032	IRAC
	80.674700	−69.257300	55450	9.703 ± 0.046	8.982 ± 0.049	IRAC
	80.674863	−69.257231	55506	9.186 ± 0.057	8.500 ± 0.061	(*WISE*)
	80.674700	−69.257300	55556	8.906 ± 0.047	8.258 ± 0.040	IRAC
	80.674700	−69.257300	55679	8.965 ± 0.073	8.455 ± 0.060	IRAC
	80.674873	−69.257235	56788	9.298 ± 0.050	8.577 ± 0.047	(*WISE*)
	80.674933	−69.257226	56969	9.158 ± 0.025	8.446 ± 0.031	(*WISE*)
BE 74	80.683310	−69.641071	53572	8.702 ± 0.038	8.086 ± 0.043	IRAC
	80.683310	−69.641146	53673	8.805 ± 0.046	8.161 ± 0.031	IRAC
	80.683329	−69.641126	55320	8.699 ± 0.025	8.113 ± 0.029	(*WISE*)
	80.683300	−69.641100	55426	8.727 ± 0.065	8.185 ± 0.056	IRAC
	80.683300	−69.641100	55450	8.840 ± 0.050	8.146 ± 0.065	IRAC
	80.683329	−69.641126	55501	8.720 ± 0.030	8.148 ± 0.056	(*WISE*)
	80.683300	−69.641100	55556	8.869 ± 0.067	8.119 ± 0.049	IRAC
	80.683300	−69.641100	55679	8.683 ± 0.053	8.096 ± 0.041	IRAC
	80.683275	−69.641141	56785	8.898 ± 0.023	8.267 ± 0.030	(*WISE*)
MSX LMC 494	80.787604	−69.296376	53572	9.168 ± 0.062	8.512 ± 0.041	IRAC
	80.787777	−69.296360	53673	9.354 ± 0.062	8.600 ± 0.049	IRAC
	80.787833	−69.296347	55324	9.050 ± 0.039	8.395 ± 0.040	(*WISE*)
	80.787700	−69.296400	55426	9.858 ± 0.099	8.962 ± 0.053	IRAC
	80.787700	−69.296400	55450	9.725 ± 0.045	9.030 ± 0.038	IRAC
	80.787833	−69.296347	55505	9.472 ± 0.054	8.808 ± 0.048	(*WISE*)
	80.787700	−69.296400	55556	9.289 ± 0.043	8.494 ± 0.050	IRAC
	80.787700	−69.296400	55679	8.916 ± 0.060	8.202 ± 0.066	IRAC
	80.787697	−69.296379	56788	9.638 ± 0.028	8.972 ± 0.023	(*WISE*)
	80.787783	−69.296352	56969	8.833 ± 0.015	8.202 ± 0.013	(*WISE*)
IRAS F05236−6655	80.909576	−66.890282	53572	8.759 ± 0.053	7.887 ± 0.038	IRAC
	80.909697	−66.890313	53673	8.862 ± 0.032	7.980 ± 0.049	IRAC
	80.909828	−66.890291	55358	9.176 ± 0.053	8.144 ± 0.052	(*WISE*)
	80.909828	−66.890291	55541	10.104 ± 0.051	8.962 ± 0.046	(*WISE*)
	80.909760	−66.890294	56643	10.119 ± 0.061	8.965 ± 0.046	(*WISE*)
	80.909640	−66.890272	56821	9.107 ± 0.059	8.082 ± 0.053	(*WISE*)
	80.909744	−66.890284	57001	9.250 ± 0.059	8.196 ± 0.049	(*WISE*)
2MASS J052405	81.022114	−68.300718	53572	9.465 ± 0.050	9.044 ± 0.021	IRAC
	81.022309	−68.300699	53673	9.694 ± 0.027	9.224 ± 0.032	IRAC
	81.022142	−68.300677	55336	9.837 ± 0.021	9.352 ± 0.029	(*WISE*)
	81.022142	−68.300677	55518	9.193 ± 0.041	8.703 ± 0.048	(*WISE*)
	81.022128	−68.300670	56799	9.421 ± 0.058	8.917 ± 0.050	(*WISE*)
	81.022208	−68.300674	56982	9.962 ± 0.049	9.437 ± 0.063	(*WISE*)
MSX LMC 441	81.160977	−70.399213	53572	9.871 ± 0.041	8.698 ± 0.040	IRAC
	81.161101	−70.399182	53673	9.159 ± 0.038	8.009 ± 0.039	IRAC
	81.161112	−70.399181	55312	9.459 ± 0.045	8.259 ± 0.027	(*WISE*)
	81.161000	−70.399200	55450	9.996 ± 0.039	8.765 ± 0.054	IRAC
	81.161112	−70.399181	55494	9.962 ± 0.043	8.716 ± 0.038	(*WISE*)
	81.161000	−70.399200	55556	10.071 ± 0.038	8.789 ± 0.049	IRAC
	81.160997	−70.399186	56777	10.025 ± 0.022	8.755 ± 0.024	(*WISE*)
	81.161131	−70.399170	56957	9.358 ± 0.048	8.171 ± 0.045	(*WISE*)
IRAS F05254−7149	81.181872	−71.790699	53572	9.616 ± 0.043	8.509 ± 0.040	IRAC
	81.182014	−71.790666	53673	9.850 ± 0.027	8.739 ± 0.046	IRAC
	81.182009	−71.790652	55304	9.007 ± 0.021	7.907 ± 0.027	(*WISE*)
	81.182009	−71.790652	55484	8.971 ± 0.032	7.883 ± 0.045	(*WISE*)
	81.181914	−71.790657	56771	8.901 ± 0.025	7.759 ± 0.025	(*WISE*)
	81.182004	−71.790638	56947	9.431 ± 0.025	8.251 ± 0.022	(*WISE*)
OGLE J052445	81.189011	−69.268171	53572	9.026 ± 0.080	8.518 ± 0.042	IRAC

TABLE 10 — *Continued*

Target	RA (J2000)	Decl. (J2000)	MJD	[3.6]	[4.5]	Data source[a]
	81.189200	−69.268157	53673	9.087 ± 0.043	8.612 ± 0.040	IRAC
	81.189243	−69.268156	55323	9.227 ± 0.040	8.767 ± 0.036	(*WISE*)
	81.189100	−69.268200	55426	9.607 ± 0.039	9.121 ± 0.031	IRAC
	81.189100	−69.268200	55450	9.509 ± 0.068	9.076 ± 0.037	IRAC
	81.189243	−69.268156	55505	9.437 ± 0.047	8.953 ± 0.041	(*WISE*)
	81.189100	−69.268200	55556	8.969 ± 0.037	8.604 ± 0.056	IRAC
	81.189100	−69.268200	55679	8.932 ± 0.067	8.579 ± 0.062	IRAC
	81.189174	−69.268177	56786	9.109 ± 0.086	8.645 ± 0.079	(*WISE*)
	81.189211	−69.268165	56968	9.665 ± 0.059	9.146 ± 0.061	(*WISE*)
MSX LMC 443	81.273798	−70.169621	53572	9.144 ± 0.055	8.082 ± 0.042	IRAC
	81.273700	−70.169632	53673	8.848 ± 0.045	7.944 ± 0.040	IRAC
	81.273966	−70.169687	55314	9.030 ± 0.045	8.090 ± 0.040	(*WISE*)
	81.273800	−70.169600	55426	9.902 ± 0.076	8.775 ± 0.057	IRAC
	81.273800	−70.169600	55450	10.016 ± 0.049	8.834 ± 0.054	IRAC
	81.273966	−70.169687	55495	9.796 ± 0.077	8.864 ± 0.062	(*WISE*)
	81.273800	−70.169600	55556	10.132 ± 0.041	9.068 ± 0.041	IRAC
	81.273800	−70.169600	55679	9.393 ± 0.065	8.320 ± 0.057	IRAC
	81.273761	−70.169687	56779	8.927 ± 0.047	8.006 ± 0.024	(*WISE*)
	81.273933	−70.169672	56958	9.368 ± 0.045	8.403 ± 0.028	(*WISE*)
LI-LMC 1028	81.331197	−71.067429	53572	8.679 ± 0.044	7.882 ± 0.041	IRAC
	81.331403	−71.067413	53673	8.374 ± 0.062	7.613 ± 0.034	IRAC
	81.331336	−71.067402	55308	9.041 ± 0.021	8.109 ± 0.025	(*WISE*)
	81.331336	−71.067402	55488	8.718 ± 0.067	7.833 ± 0.054	(*WISE*)
	81.331334	−71.067407	56773	8.127 ± 0.025	7.294 ± 0.021	(*WISE*)
	81.331402	−71.067390	56951	8.907 ± 0.031	7.967 ± 0.024	(*WISE*)
IRAS 05260−7010	81.419672	−70.140788	53572	15.820 ± 0.085	13.095 ± 0.042	IRAC
	81.419394	−70.140904	53673	16.070 ± 0.099	13.205 ± 0.043	IRAC
	81.419500	−70.140800	55450	15.978 ± 0.193	13.323 ± 0.058	IRAC
	81.419500	−70.140800	55556	16.344 ± 0.188	13.472 ± 0.046	IRAC
	81.419500	−70.140800	55679	16.548 ± 0.213	13.479 ± 0.077	IRAC
MSX LMC 474	81.465936	−68.776205	53572	9.124 ± 0.045	8.046 ± 0.029	IRAC
	81.466066	−68.776180	53673	9.055 ± 0.045	7.970 ± 0.045	IRAC
	81.466083	−68.776173	55328	8.839 ± 0.038	7.972 ± 0.039	(*WISE*)
	81.466000	−68.776200	55450	8.944 ± 0.076	8.156 ± 0.055	IRAC
	81.466083	−68.776174	55511	8.801 ± 0.043	7.893 ± 0.042	(*WISE*)
	81.466000	−68.776200	55556	8.680 ± 0.055	7.823 ± 0.044	IRAC
	81.466000	−68.776200	55679	8.074 ± 0.050	7.272 ± 0.054	IRAC
	81.466038	−68.776180	56791	8.784 ± 0.052	7.789 ± 0.037	(*WISE*)
	81.466122	−68.776168	56975	8.017 ± 0.056	7.095 ± 0.056	(*WISE*)
WBP 17	81.582818	−69.693621	53572	10.132 ± 0.034	10.137 ± 0.032	IRAC
	81.582827	−69.693710	53673	10.350 ± 0.031	10.321 ± 0.031	IRAC
	81.582853	−69.693705	55318	10.418 ± 0.029	10.459 ± 0.031	(*WISE*)
	81.582800	−69.693700	55426	10.174 ± 0.055	10.236 ± 0.043	IRAC
	81.582800	−69.693700	55450	10.140 ± 0.040	10.221 ± 0.046	IRAC
	81.582854	−69.693705	55499	10.311 ± 0.033	10.346 ± 0.044	(*WISE*)
	81.582800	−69.693700	55556	10.176 ± 0.055	10.264 ± 0.049	IRAC
	81.582800	−69.693700	55679	10.298 ± 0.059	10.348 ± 0.049	IRAC
	81.582863	−69.693691	56782	10.336 ± 0.042	10.304 ± 0.025	(*WISE*)
MSX LMC 774	81.596160	−69.188968	53572	9.739 ± 0.034	8.631 ± 0.045	IRAC
	81.596278	−69.188951	53673	9.106 ± 0.048	8.011 ± 0.044	IRAC
	81.596441	−69.188930	55322	9.085 ± 0.041	7.995 ± 0.049	(*WISE*)
	81.596300	−69.189000	55426	9.785 ± 0.044	8.547 ± 0.064	IRAC
	81.596300	−69.189000	55450	9.759 ± 0.060	8.529 ± 0.074	IRAC
	81.596441	−69.188930	55505	9.702 ± 0.046	8.575 ± 0.043	(*WISE*)
	81.596300	−69.189000	55556	9.738 ± 0.036	8.580 ± 0.056	IRAC
	81.596300	−69.189000	55679	8.943 ± 0.062	7.913 ± 0.045	IRAC
	81.596290	−69.188959	56786	9.616 ± 0.095	8.480 ± 0.072	(*WISE*)
	81.596394	−69.188942	56968	9.507 ± 0.054	8.379 ± 0.058	(*WISE*)
MSX LMC 634	81.648566	−69.139691	53572	8.802 ± 0.030	8.104 ± 0.049	IRAC
	81.648745	−69.139679	53673	9.181 ± 0.045	8.434 ± 0.042	IRAC
	81.648752	−69.139686	55323	9.105 ± 0.029	8.357 ± 0.028	(*WISE*)
	81.648600	−69.139700	55426	9.109 ± 0.183	7.990 ± 0.063	IRAC
	81.648600	−69.139700	55450	8.664 ± 0.050	7.955 ± 0.053	IRAC
	81.648751	−69.139687	55506	8.647 ± 0.034	7.928 ± 0.039	(*WISE*)
	81.648600	−69.139700	55556	8.851 ± 0.071	8.107 ± 0.049	IRAC
	81.648600	−69.139700	55679	9.474 ± 0.062	8.691 ± 0.061	IRAC
	81.648762	−69.139688	56786	9.398 ± 0.093	8.545 ± 0.082	(*WISE*)
	81.648830	−69.139674	56969	8.940 ± 0.062	8.149 ± 0.063	(*WISE*)
WBP 29	81.670490	−69.386535	53572	10.573 ± 0.036	10.370 ± 0.035	IRAC
	81.670624	−69.386504	53673	10.270 ± 0.032	10.162 ± 0.024	IRAC
	81.670676	−69.386490	55320	10.572 ± 0.027	10.619 ± 0.030	(*WISE*)
	81.670600	−69.386500	55426	10.448 ± 0.058	10.452 ± 0.046	IRAC
	81.670600	−69.386500	55450	10.455 ± 0.043	10.438 ± 0.037	IRAC
	81.670676	−69.386490	55502	10.776 ± 0.044	10.727 ± 0.042	(*WISE*)
	81.670600	−69.386500	55556	10.529 ± 0.034	10.015 ± 0.038	IRAC
	81.670600	−69.386500	55679	10.437 ± 0.054	10.551 ± 0.043	IRAC

TABLE 10 — *Continued*

Target	RA (J2000)	Decl. (J2000)	MJD	[3.6]	[4.5]	Data source[a]
	81.670612	−69.386498	56784	10.645 ± 0.107	10.637 ± 0.083	(*WISE*)
	81.670592	−69.386492	56965	10.725 ± 0.066	10.702 ± 0.064	(*WISE*)
MSX LMC 601	81.711617	−69.526924	53572	8.919 ± 0.047	8.154 ± 0.043	IRAC
	81.711848	−69.526882	53673	8.434 ± 0.063	7.628 ± 0.040	IRAC
	81.711900	−69.526876	55319	8.275 ± 0.031	7.576 ± 0.036	(*WISE*)
	81.711800	−69.526900	55426	8.403 ± 0.063	7.704 ± 0.038	IRAC
	81.711800	−69.526900	55450	8.398 ± 0.074	7.807 ± 0.054	IRAC
	81.711901	−69.526876	55501	8.677 ± 0.045	8.020 ± 0.047	(*WISE*)
	81.711800	−69.526900	55556	8.945 ± 0.059	8.256 ± 0.054	IRAC
	81.711800	−69.526900	55679	8.811 ± 0.053	8.031 ± 0.041	IRAC
	81.711747	−69.526888	56782	9.053 ± 0.083	8.135 ± 0.086	(*WISE*)
	81.711860	−69.526881	56963	8.442 ± 0.044	7.587 ± 0.048	(*WISE*)
WBP 42	81.769693	−69.637830	53572	9.305 ± 0.041	9.148 ± 0.018	IRAC
	81.769749	−69.637874	53673	9.248 ± 0.044	9.003 ± 0.037	IRAC
	81.769781	−69.637854	55318	9.526 ± 0.026	9.130 ± 0.026	(*WISE*)
	81.769700	−69.637800	55426	9.363 ± 0.071	8.887 ± 0.050	IRAC
	81.769700	−69.637800	55450	···	8.935 ± 0.059	IRAC
	81.769780	−69.637854	55499	9.437 ± 0.038	9.105 ± 0.050	(*WISE*)
	81.769700	−69.637800	55556	9.577 ± 0.059	9.245 ± 0.032	IRAC
	81.769700	−69.637800	55679	9.393 ± 0.062	9.043 ± 0.057	IRAC
	81.769754	−69.637842	56782	9.598 ± 0.059	9.382 ± 0.064	(*WISE*)
IRAS 05278−6942	81.850424	−69.662477	53572	8.270 ± 0.037	7.015 ± 0.023	IRAC
	81.850464	−69.662482	53673	8.656 ± 0.035	7.367 ± 0.030	IRAC
	81.850540	−69.662489	55317	8.256 ± 0.188	6.986 ± 0.068	(*WISE*)
	81.850500	−69.662500	55426	8.218 ± 0.069	6.954 ± 0.064	IRAC
	81.850500	−69.662500	55450	8.207 ± 0.061	6.891 ± 0.040	IRAC
	81.850539	−69.662489	55499	8.043 ± 0.114	6.756 ± 0.067	(*WISE*)
	81.850500	−69.662500	55556	8.167 ± 0.048	6.987 ± 0.054	IRAC
	81.850500	−69.662500	55679	8.812 ± 0.062	7.335 ± 0.043	IRAC
	81.850402	−69.662492	56781	9.189 ± 0.069	7.828 ± 0.059	(*WISE*)
SHV 0528350	82.024635	−70.131466	53572	8.877 ± 0.038	8.854 ± 0.044	IRAC
	82.024652	−70.131554	53673	9.002 ± 0.036	8.832 ± 0.043	IRAC
	82.024671	−70.131558	55313	9.234 ± 0.029	9.023 ± 0.032	(*WISE*)
	82.024600	−70.131500	55426	9.247 ± 0.044	9.122 ± 0.050	IRAC
	82.024600	−70.131500	55450	9.204 ± 0.039	9.135 ± 0.035	IRAC
	82.024671	−70.131558	55494	9.388 ± 0.047	9.186 ± 0.053	(*WISE*)
	82.024600	−70.131500	55556	9.265 ± 0.042	9.149 ± 0.028	IRAC
	82.024600	−70.131500	55679	9.230 ± 0.080	8.992 ± 0.055	IRAC
	82.024618	−70.131551	56777	9.136 ± 0.019	9.028 ± 0.022	(*WISE*)
	82.024590	−70.131561	56956	9.164 ± 0.017	9.007 ± 0.018	(*WISE*)
MSX LMC 754	82.047741	−70.566324	53572	9.128 ± 0.036	8.574 ± 0.039	IRAC
	82.047883	−70.566302	53673	8.674 ± 0.039	8.070 ± 0.043	IRAC
	82.047920	−70.566332	55309	9.276 ± 0.045	8.744 ± 0.033	(*WISE*)
	82.047700	−70.566300	55450	···	8.286 ± 0.068	IRAC
	82.047920	−70.566332	55490	8.604 ± 0.039	8.078 ± 0.047	(*WISE*)
	82.048016	−70.566310	56774	9.305 ± 0.029	8.659 ± 0.022	(*WISE*)
	82.048006	−70.566298	56952	8.807 ± 0.029	8.182 ± 0.015	(*WISE*)
KDM 4257	82.107552	−69.779760	53572	9.897 ± 0.030	9.923 ± 0.035	IRAC
	82.107584	−69.779841	53673	9.879 ± 0.025	9.931 ± 0.028	IRAC
	82.107603	−69.779836	55315	9.812 ± 0.033	9.901 ± 0.031	(*WISE*)
	82.107600	−69.779800	55426	9.796 ± 0.037	9.792 ± 0.039	IRAC
	82.107600	−69.779800	55450	9.837 ± 0.039	9.780 ± 0.035	IRAC
	82.107603	−69.779836	55497	9.793 ± 0.038	9.860 ± 0.036	(*WISE*)
	82.107600	−69.779800	55556	9.915 ± 0.095	9.798 ± 0.033	IRAC
	82.107600	−69.779800	55679	9.888 ± 0.047	9.871 ± 0.028	IRAC
	82.107544	−69.779822	56779	9.864 ± 0.063	9.920 ± 0.039	(*WISE*)
NGC 1978 IR 1	82.167405	−66.231732	53673	8.654 ± 0.046	8.028 ± 0.024	IRAC
	82.167370	−66.231692	55371	9.058 ± 0.031	8.485 ± 0.036	(*WISE*)
	82.167370	−66.231692	55551	8.569 ± 0.040	8.013 ± 0.038	(*WISE*)
	82.167417	−66.231719	56650	9.230 ± 0.026	8.662 ± 0.028	(*WISE*)
	82.167367	−66.231698	56833	8.584 ± 0.049	8.025 ± 0.060	(*WISE*)
NGC 1978 IR 4	82.185345	−66.234440	53572	8.958 ± 0.034	9.145 ± 0.021	IRAC
	82.185442	−66.234446	53673	9.008 ± 0.036	9.156 ± 0.024	IRAC
	82.185007	−66.234434	56650	8.584 ± 0.046	8.663 ± 0.046	(*WISE*)
	82.185081	−66.234474	56833	8.630 ± 0.057	8.687 ± 0.056	(*WISE*)
IRAS 05295−7121	82.194138	−71.320185	53572	9.375 ± 0.044	8.280 ± 0.041	IRAC
	82.194259	−71.320143	53673	8.631 ± 0.043	7.639 ± 0.034	IRAC
	82.194262	−71.320150	55304	9.420 ± 0.023	8.299 ± 0.032	(*WISE*)
	82.194262	−71.320150	55484	9.310 ± 0.034	8.204 ± 0.038	(*WISE*)
	82.194235	−71.320159	56772	9.466 ± 0.015	8.337 ± 0.025	(*WISE*)
	82.194303	−71.320140	56947	8.466 ± 0.017	7.434 ± 0.037	(*WISE*)
NGC 1978 MIR 1	82.196369	−66.237226	53572	10.447 ± 0.034	9.308 ± 0.022	IRAC
	82.196493	−66.237232	53673	9.504 ± 0.037	8.489 ± 0.029	IRAC
	82.196240	−66.237206	56650	9.375 ± 0.070	8.610 ± 0.073	(*WISE*)
	82.196155	−66.237205	56833	9.565 ± 0.077	8.761 ± 0.052	(*WISE*)
MSX LMC 679	82.202373	−69.800255	53572	9.996 ± 0.037	8.966 ± 0.036	IRAC

TABLE 10 — *Continued*

Target	RA (J2000)	Decl. (J2000)	MJD	[3.6]	[4.5]	Data source[a]
	82.202510	−69.800346	53673	10.354 ± 0.032	9.232 ± 0.030	IRAC
	82.202515	−69.800335	55314	9.326 ± 0.027	8.251 ± 0.029	(*WISE*)
	82.202500	−69.800300	55426	9.379 ± 0.047	8.292 ± 0.058	IRAC
	82.202500	−69.800300	55450	9.507 ± 0.056	8.451 ± 0.054	IRAC
	82.202515	−69.800335	55497	9.684 ± 0.047	8.603 ± 0.051	(*WISE*)
	82.202500	−69.800300	55556	10.079 ± 0.035	9.053 ± 0.029	IRAC
	82.202500	−69.800300	55679	10.367 ± 0.031	9.223 ± 0.022	IRAC
	82.202390	−69.800352	56779	9.321 ± 0.066	8.279 ± 0.085	(*WISE*)
GRRV 38	82.281548	−66.970866	53572	8.539 ± 0.070	8.235 ± 0.031	IRAC
	82.281669	−66.970832	53673	8.862 ± 0.037	8.618 ± 0.041	IRAC
	82.281587	−66.970845	55355	8.703 ± 0.037	8.345 ± 0.042	(*WISE*)
	82.281587	−66.970845	55539	8.341 ± 0.032	8.019 ± 0.039	(*WISE*)
	82.281683	−66.970857	56642	8.567 ± 0.020	8.173 ± 0.017	(*WISE*)
	82.281656	−66.970850	56819	9.076 ± 0.025	8.597 ± 0.034	(*WISE*)
	82.281670	−66.970852	56999	8.727 ± 0.028	8.282 ± 0.025	(*WISE*)
IRAS 05305−7251	82.407775	−72.831388	53572	13.993 ± 0.068	11.301 ± 0.039	IRAC
	82.407944	−72.831341	53673	13.437 ± 0.052	10.844 ± 0.034	IRAC
	82.407960	−72.831324	55296	13.036 ± 0.082	10.315 ± 0.045	(*WISE*)
	82.407960	−72.831324	55477	12.771 ± 0.070	10.067 ± 0.042	(*WISE*)
	82.408089	−72.831319	56940	13.340 ± 0.117	10.592 ± 0.061	(*WISE*)
IRAS 05300−6651	82.516118	−66.823416	53572	9.341 ± 0.068	8.209 ± 0.032	IRAC
	82.516280	−66.823385	53673	8.695 ± 0.048	7.631 ± 0.065	IRAC
	82.516337	−66.823391	55359	8.999 ± 0.056	7.837 ± 0.056	(*WISE*)
	82.516337	−66.823391	55541	9.711 ± 0.042	8.512 ± 0.041	(*WISE*)
	82.516286	−66.823414	56644	8.629 ± 0.019	7.508 ± 0.027	(*WISE*)
	82.516203	−66.823391	56822	9.351 ± 0.047	8.160 ± 0.035	(*WISE*)
	82.516295	−66.823403	57000	9.727 ± 0.017	8.490 ± 0.019	(*WISE*)
IRAS 05306−7032	82.525756	−70.511463	53572	10.992 ± 0.028	9.204 ± 0.022	IRAC
	82.526005	−70.511410	53673	11.148 ± 0.035	9.418 ± 0.028	IRAC
	82.525955	−70.511374	55308	10.892 ± 0.028	9.097 ± 0.034	(*WISE*)
	82.525900	−70.511400	55426	11.573 ± 0.043	9.737 ± 0.036	IRAC
	82.525955	−70.511374	55489	11.700 ± 0.054	9.790 ± 0.052	(*WISE*)
	82.525900	−70.511400	55556	···	9.894 ± 0.045	IRAC
	82.525900	−70.511400	55679	11.328 ± 0.061	9.549 ± 0.041	IRAC
	82.525783	−70.511408	56774	10.842 ± 0.024	9.098 ± 0.026	(*WISE*)
	82.525955	−70.511378	56951	11.233 ± 0.037	9.434 ± 0.017	(*WISE*)
2MASS J053044	82.687405	−68.358088	53572	9.097 ± 0.070	8.694 ± 0.046	IRAC
	82.687691	−68.358065	53673	8.933 ± 0.041	8.569 ± 0.038	IRAC
	82.687443	−68.358087	55330	8.944 ± 0.022	8.432 ± 0.030	(*WISE*)
	82.687443	−68.358087	55514	8.500 ± 0.038	8.005 ± 0.046	(*WISE*)
	82.687454	−68.358074	56793	8.694 ± 0.038	8.134 ± 0.037	(*WISE*)
	82.687483	−68.358071	56977	9.150 ± 0.023	8.580 ± 0.022	(*WISE*)
MSX LMC 841	82.804604	−66.161474	53572	9.132 ± 0.055	8.420 ± 0.036	IRAC
	82.804659	−66.161435	53673	8.924 ± 0.033	8.288 ± 0.039	IRAC
	82.804622	−66.161436	55374	8.716 ± 0.042	7.965 ± 0.031	(*WISE*)
	82.804622	−66.161436	55554	8.768 ± 0.048	8.025 ± 0.055	(*WISE*)
	82.804669	−66.161450	56652	8.849 ± 0.039	8.131 ± 0.037	(*WISE*)
	82.804595	−66.161431	56836	9.401 ± 0.033	8.553 ± 0.037	(*WISE*)
MSX LMC 768	82.920273	−69.655527	53572	8.328 ± 0.033	7.418 ± 0.040	IRAC
	82.920384	−69.655499	53673	8.846 ± 0.045	7.922 ± 0.042	IRAC
	82.920443	−69.655476	55314	8.213 ± 0.030	7.282 ± 0.033	(*WISE*)
	82.920300	−69.655500	55426	8.186 ± 0.066	7.244 ± 0.034	IRAC
	82.920300	−69.655500	55450	8.216 ± 0.058	7.332 ± 0.034	IRAC
	82.920443	−69.655476	55497	8.397 ± 0.036	7.461 ± 0.049	(*WISE*)
	82.920300	−69.655500	55556	8.778 ± 0.041	7.861 ± 0.040	IRAC
	82.920300	−69.655500	55679	9.167 ± 0.043	8.286 ± 0.040	IRAC
	82.920344	−69.655518	56778	8.133 ± 0.072	7.377 ± 0.084	(*WISE*)
	82.920424	−69.655481	56959	8.670 ± 0.052	7.873 ± 0.052	(*WISE*)
KDM 4665	82.995478	−72.743344	53572	10.637 ± 0.035	10.688 ± 0.038	IRAC
	82.995600	−72.743330	53673	10.571 ± 0.034	10.632 ± 0.033	IRAC
	82.995614	−72.743318	55295	10.808 ± 0.036	10.889 ± 0.024	(*WISE*)
	82.995614	−72.743318	55475	10.784 ± 0.042	10.895 ± 0.043	(*WISE*)
	82.995566	−72.743325	56939	10.712 ± 0.021	10.806 ± 0.023	(*WISE*)
MSX LMC 782	83.013607	−69.291790	53572	9.294 ± 0.051	8.426 ± 0.037	IRAC
	83.013733	−69.291774	53673	8.730 ± 0.039	7.982 ± 0.036	IRAC
	83.013753	−69.291747	55316	9.312 ± 0.036	8.495 ± 0.039	(*WISE*)
	83.013600	−69.291800	55426	9.738 ± 0.044	8.799 ± 0.058	IRAC
	83.013600	−69.291800	55450	9.502 ± 0.073	8.774 ± 0.068	IRAC
	83.013753	−69.291747	55501	9.125 ± 0.052	8.312 ± 0.060	(*WISE*)
	83.013600	−69.291800	55556	8.745 ± 0.058	···	IRAC
	83.013600	−69.291800	55679	8.676 ± 0.067	7.865 ± 0.046	IRAC
	83.013710	−69.291765	56779	9.441 ± 0.093	8.602 ± 0.094	(*WISE*)
	83.013821	−69.291743	56963	8.875 ± 0.059	8.049 ± 0.054	(*WISE*)
KDM 4718	83.110398	−73.168593	53572	9.862 ± 0.034	10.046 ± 0.033	IRAC
	83.110542	−73.168571	53673	9.866 ± 0.038	10.010 ± 0.030	IRAC
	83.110518	−73.168576	55293	9.929 ± 0.034	10.015 ± 0.030	(*WISE*)

TABLE 10 — *Continued*

Target	RA (J2000)	Decl. (J2000)	MJD	[3.6]	[4.5]	Data source[a]
	83.110518	−73.168576	55473	9.918 ± 0.052	9.990 ± 0.037	(*WISE*)
	83.110483	−73.168585	56938	9.847 ± 0.012	9.943 ± 0.024	(*WISE*)
KDM 4774	83.229086	−67.613144	53572	9.818 ± 0.038	9.843 ± 0.031	IRAC
	83.229188	−67.613099	53673	9.808 ± 0.021	9.761 ± 0.014	IRAC
	83.229180	−67.613098	55342	9.865 ± 0.026	9.935 ± 0.048	(*WISE*)
	83.229180	−67.613098	55526	9.765 ± 0.043	9.839 ± 0.044	(*WISE*)
	83.229181	−67.613092	56805	9.896 ± 0.024	9.981 ± 0.038	(*WISE*)
	83.229189	−67.613090	56988	9.919 ± 0.029	9.988 ± 0.020	(*WISE*)
MSX LMC 783	83.231012	−69.340771	53572	9.346 ± 0.043	8.601 ± 0.044	IRAC
	83.231176	−69.340715	53673	9.360 ± 0.048	8.517 ± 0.040	IRAC
	83.231187	−69.340717	55315	8.918 ± 0.050	8.113 ± 0.044	(*WISE*)
	83.231100	−69.340700	55426	8.795 ± 0.085	7.948 ± 0.064	IRAC
	83.231100	−69.340700	55450	8.717 ± 0.041	7.994 ± 0.057	IRAC
	83.231187	−69.340717	55500	8.912 ± 0.041	8.137 ± 0.057	(*WISE*)
	83.231100	−69.340700	55556	9.226 ± 0.068	···	IRAC
	83.231100	−69.340700	55679	···	8.887 ± 0.073	IRAC
	83.231131	−69.340741	56778	9.304 ± 0.082	8.558 ± 0.089	(*WISE*)
	83.231214	−69.340728	56962	8.569 ± 0.053	7.885 ± 0.055	(*WISE*)
LMC-BM 32-9	83.234049	−68.213557	53572	7.710 ± 0.041	7.076 ± 0.026	IRAC
	83.234191	−68.213585	53673	7.843 ± 0.053	7.215 ± 0.032	IRAC
	83.234070	−68.213533	55331	7.789 ± 0.025	7.115 ± 0.034	(*WISE*)
	83.234070	−68.213533	55515	7.662 ± 0.033	7.019 ± 0.034	(*WISE*)
	83.234061	−68.213535	56793	7.617 ± 0.026	7.074 ± 0.026	(*WISE*)
	83.234099	−68.213523	56978	7.834 ± 0.029	7.238 ± 0.025	(*WISE*)
MSX LMC 736	83.278319	−70.509485	53572	9.811 ± 0.037	8.436 ± 0.045	IRAC
	83.278469	−70.509414	55306	10.541 ± 0.050	9.225 ± 0.034	(*WISE*)
	83.278469	−70.509414	55486	9.499 ± 0.046	8.183 ± 0.038	(*WISE*)
	83.278459	−70.509417	56773	9.876 ± 0.026	8.568 ± 0.018	(*WISE*)
2MASS J053318	83.327403	−66.011191	53572	9.560 ± 0.043	8.995 ± 0.045	IRAC
	83.327451	−66.011166	53673	9.625 ± 0.034	9.013 ± 0.030	IRAC
	83.327360	−66.011145	55205	9.577 ± 0.018	8.957 ± 0.038	(*WISE*)
	83.327360	−66.011145	55376	10.237 ± 0.041	9.643 ± 0.032	(*WISE*)
	83.327360	−66.011145	55558	9.757 ± 0.041	9.174 ± 0.046	(*WISE*)
	83.327445	−66.011162	56655	9.777 ± 0.026	9.169 ± 0.033	(*WISE*)
	83.327447	−66.011155	56840	9.538 ± 0.041	8.928 ± 0.045	(*WISE*)
IRAS 05348−7024	83.566489	−70.381310	53572	8.809 ± 0.056	7.511 ± 0.041	IRAC
	83.566655	−70.381285	53673	9.436 ± 0.049	8.171 ± 0.043	IRAC
	83.566588	−70.381278	55306	9.309 ± 0.043	8.060 ± 0.025	(*WISE*)
	83.566600	−70.381300	55426	9.575 ± 0.039	8.248 ± 0.066	IRAC
	83.566600	−70.381300	55450	9.423 ± 0.069	8.184 ± 0.055	IRAC
	83.566588	−70.381278	55486	9.117 ± 0.060	7.879 ± 0.025	(*WISE*)
	83.566600	−70.381300	55556	9.132 ± 0.067	7.968 ± 0.065	IRAC
	83.566600	−70.381300	55679	8.229 ± 0.061	7.082 ± 0.045	IRAC
	83.566514	−70.381301	56773	8.293 ± 0.037	7.153 ± 0.028	(*WISE*)
	83.566618	−70.381268	56949	9.419 ± 0.026	8.148 ± 0.019	(*WISE*)
2MASS J053441	83.672447	−69.441863	53572	9.065 ± 0.052	8.331 ± 0.047	IRAC
	83.672573	−69.441851	53673	8.945 ± 0.049	8.252 ± 0.030	IRAC
	83.672584	−69.441873	55312	8.848 ± 0.021	8.149 ± 0.034	(*WISE*)
	83.672500	−69.441900	55426	8.532 ± 0.060	7.970 ± 0.032	IRAC
	83.672500	−69.441900	55450	8.632 ± 0.043	7.962 ± 0.034	IRAC
	83.672584	−69.441873	55497	8.678 ± 0.043	8.039 ± 0.046	(*WISE*)
	83.672500	−69.441900	55556	8.826 ± 0.038	8.254 ± 0.067	IRAC
	83.672500	−69.441900	55679	9.050 ± 0.058	8.401 ± 0.063	IRAC
	83.672541	−69.441887	56776	8.773 ± 0.058	8.148 ± 0.082	(*WISE*)
	83.672660	−69.441867	56959	8.420 ± 0.050	7.832 ± 0.042	(*WISE*)
MSX LMC 743	83.723741	−70.490229	53572	9.271 ± 0.048	8.143 ± 0.041	IRAC
	83.724048	−70.490199	53673	8.992 ± 0.042	7.926 ± 0.038	IRAC
	83.723866	−70.490175	55305	8.843 ± 0.032	7.861 ± 0.028	(*WISE*)
	83.724000	−70.490200	55426	9.398 ± 0.063	8.332 ± 0.047	IRAC
	83.724000	−70.490200	55450	9.611 ± 0.066	8.391 ± 0.054	IRAC
	83.723866	−70.490175	55485	9.446 ± 0.064	8.461 ± 0.038	(*WISE*)
	83.724000	−70.490200	55556	9.972 ± 0.042	8.826 ± 0.050	IRAC
	83.724000	−70.490200	55679	9.757 ± 0.062	8.694 ± 0.059	IRAC
	83.723498	−70.490208	56772	9.572 ± 0.039	8.570 ± 0.044	(*WISE*)
	83.723793	−70.490192	56948	8.937 ± 0.021	7.951 ± 0.021	(*WISE*)
MSX LMC 787	83.734013	−69.154652	53572	9.267 ± 0.041	8.281 ± 0.044	IRAC
	83.734154	−69.154629	53673	8.682 ± 0.044	7.778 ± 0.030	IRAC
	83.734100	−69.154600	55426	···	8.766 ± 0.058	IRAC
	83.734200	−69.154629	56779	9.878 ± 0.047	8.710 ± 0.050	(*WISE*)
	83.734276	−69.154624	56962	8.837 ± 0.043	7.775 ± 0.031	(*WISE*)
MSX LMC 950	83.764623	−69.879260	53572	9.584 ± 0.035	8.669 ± 0.050	IRAC
	83.765132	−69.879360	53673	8.853 ± 0.041	8.003 ± 0.040	IRAC
	83.764776	−69.879294	55309	9.014 ± 0.086	8.115 ± 0.056	(*WISE*)
	83.764900	−69.879300	55426	8.512 ± 0.063	7.563 ± 0.038	IRAC
	83.764900	−69.879300	55450	8.426 ± 0.066	7.611 ± 0.053	IRAC
	83.764776	−69.879294	55492	8.379 ± 0.047	7.539 ± 0.041	(*WISE*)

TABLE 10 — *Continued*

Target	RA (J2000)	Decl. (J2000)	MJD	[3.6]	[4.5]	Data source[a]
	83.764900	−69.879300	55556	8.564 ± 0.055	7.823 ± 0.059	IRAC
	83.764900	−69.879300	55679	9.445 ± 0.051	8.451 ± 0.044	IRAC
	83.764760	−69.879303	56774	9.323 ± 0.060	8.398 ± 0.069	(*WISE*)
	83.764846	−69.879278	56954	9.114 ± 0.040	8.199 ± 0.044	(*WISE*)
MSX LMC 749	83.861742	−69.874393	53572	9.073 ± 0.045	8.210 ± 0.041	IRAC
	83.862308	−69.874479	53673	8.813 ± 0.037	8.020 ± 0.044	IRAC
	83.861933	−69.874412	55309	9.243 ± 0.027	8.398 ± 0.028	(*WISE*)
	83.862200	−69.874500	55426	8.696 ± 0.055	7.898 ± 0.053	IRAC
	83.862200	−69.874500	55450	8.668 ± 0.069	7.828 ± 0.063	IRAC
	83.861934	−69.874412	55491	8.560 ± 0.036	7.806 ± 0.049	(*WISE*)
	83.862200	−69.874500	55556	8.824 ± 0.075	8.036 ± 0.043	IRAC
	83.862200	−69.874500	55679	9.383 ± 0.054	8.589 ± 0.058	IRAC
	83.861909	−69.874425	56774	9.159 ± 0.036	8.357 ± 0.059	(*WISE*)
	83.862023	−69.874403	56954	8.827 ± 0.032	8.069 ± 0.034	(*WISE*)
IRAS F05355−6521	83.915436	−65.332379	53572	8.846 ± 0.042	8.208 ± 0.044	IRAC
	83.915515	−65.332346	53673	9.233 ± 0.047	8.545 ± 0.042	IRAC
	83.915583	−65.332348	55211	9.149 ± 0.038	8.456 ± 0.028	(*WISE*)
	83.915583	−65.332348	55392	8.855 ± 0.048	8.164 ± 0.045	(*WISE*)
	83.915583	−65.332348	55572	8.418 ± 0.034	7.793 ± 0.043	(*WISE*)
	83.915617	−65.332361	56670	8.667 ± 0.037	8.016 ± 0.037	(*WISE*)
	83.915587	−65.332347	56856	9.371 ± 0.025	8.648 ± 0.026	(*WISE*)
IRAS 05360−6648	84.005097	−66.777599	53572	9.426 ± 0.041	8.201 ± 0.034	IRAC
	84.005118	−66.777663	53673	10.066 ± 0.032	8.761 ± 0.033	IRAC
	84.005004	−66.777662	55359	10.266 ± 0.039	8.952 ± 0.039	(*WISE*)
	84.005004	−66.777662	55542	9.253 ± 0.057	8.087 ± 0.060	(*WISE*)
	84.005154	−66.777671	56645	9.062 ± 0.016	7.895 ± 0.023	(*WISE*)
	84.005056	−66.777646	56822	10.031 ± 0.062	8.738 ± 0.048	(*WISE*)
	84.005151	−66.777667	57000	10.287 ± 0.032	8.955 ± 0.025	(*WISE*)
IRAS F05373−7243	84.100521	−72.692410	53572	9.652 ± 0.029	8.463 ± 0.048	IRAC
	84.100596	−72.692385	53673	10.178 ± 0.031	8.836 ± 0.039	IRAC
	84.100643	−72.692363	55292	8.964 ± 0.033	7.829 ± 0.027	(*WISE*)
	84.100643	−72.692363	55473	9.517 ± 0.023	8.360 ± 0.043	(*WISE*)
	84.100607	−72.692380	56937	9.688 ± 0.013	8.632 ± 0.013	(*WISE*)
MSX LMC 967	84.152977	−69.789482	53572	9.122 ± 0.048	8.356 ± 0.042	IRAC
	84.153461	−69.789596	53673	8.928 ± 0.052	8.158 ± 0.043	IRAC
	84.153203	−69.789554	55309	8.538 ± 0.039	7.794 ± 0.040	(*WISE*)
	84.153400	−69.789600	55426	8.439 ± 0.071	7.662 ± 0.056	IRAC
	84.153400	−69.789600	55450	8.373 ± 0.048	7.659 ± 0.038	IRAC
	84.153203	−69.789554	55491	8.602 ± 0.046	7.843 ± 0.048	(*WISE*)
	84.153400	−69.789600	55556	9.056 ± 0.072	8.244 ± 0.066	IRAC
	84.153400	−69.789600	55679	9.087 ± 0.053	8.345 ± 0.064	IRAC
	84.153129	−69.789587	56774	8.937 ± 0.045	8.169 ± 0.047	(*WISE*)
	84.153229	−69.789556	56954	8.272 ± 0.040	7.558 ± 0.046	(*WISE*)
OGLE J053930	84.874840	−69.965463	53572	9.551 ± 0.044	8.979 ± 0.051	IRAC
	84.875320	−69.965579	53673	9.165 ± 0.048	8.584 ± 0.037	IRAC
	84.875100	−69.965500	55426	9.038 ± 0.051	8.560 ± 0.051	IRAC
	84.875100	−69.965500	55450	8.969 ± 0.055	8.548 ± 0.050	IRAC
	84.875100	−69.965500	55556	9.541 ± 0.045	8.981 ± 0.062	IRAC
	84.875100	−69.965500	55679	9.188 ± 0.056	8.623 ± 0.066	IRAC
	84.875009	−69.965534	56772	9.454 ± 0.057	8.913 ± 0.029	(*WISE*)
	84.875069	−69.965515	56950	8.871 ± 0.041	8.313 ± 0.029	(*WISE*)
MSX LMC 971	84.965855	−70.021379	53572	10.485 ± 0.033	9.123 ± 0.031	IRAC
	84.966360	−70.021457	53673	10.083 ± 0.041	8.730 ± 0.047	IRAC
	84.966059	−70.021376	55303	9.414 ± 0.040	8.132 ± 0.050	(*WISE*)
	84.965900	−70.021400	55426	10.211 ± 0.061	8.809 ± 0.057	IRAC
	84.965900	−70.021400	55450	10.348 ± 0.047	8.921 ± 0.046	IRAC
	84.966059	−70.021376	55486	10.304 ± 0.041	8.909 ± 0.039	(*WISE*)
	84.965900	−70.021400	55556	10.398 ± 0.048	9.088 ± 0.029	IRAC
	84.965900	−70.021400	55679	9.632 ± 0.070	8.276 ± 0.037	IRAC
	84.965950	−70.021438	56772	10.126 ± 0.020	8.797 ± 0.021	(*WISE*)
	84.966047	−70.021405	56949	9.770 ± 0.048	8.485 ± 0.042	(*WISE*)
MSX LMC 1400	85.085716	−66.245665	53572	9.207 ± 0.051	8.118 ± 0.039	IRAC
	85.085861	−66.245646	53673	8.843 ± 0.033	7.766 ± 0.026	IRAC
	85.085786	−66.245603	55204	9.149 ± 0.026	8.065 ± 0.030	(*WISE*)
	85.085786	−66.245603	55373	9.695 ± 0.040	8.587 ± 0.032	(*WISE*)
	85.085786	−66.245603	55556	9.072 ± 0.065	8.004 ± 0.059	(*WISE*)
	85.085884	−66.245614	56653	9.789 ± 0.044	8.668 ± 0.029	(*WISE*)
	85.085808	−66.245593	56839	9.353 ± 0.075	8.252 ± 0.077	(*WISE*)
IRAS 05410−6954	85.150205	−69.880441	53572	8.624 ± 0.075	7.604 ± 0.038	IRAC
	85.150698	−69.880552	53673	7.729 ± 0.049	6.805 ± 0.033	IRAC
	85.150397	−69.880471	55302	8.179 ± 0.049	7.254 ± 0.047	(*WISE*)
	85.150200	−69.880400	55426	9.055 ± 0.065	8.058 ± 0.065	IRAC
	85.150200	−69.880400	55450	9.059 ± 0.058	8.037 ± 0.035	IRAC
	85.150397	−69.880471	55486	8.867 ± 0.056	7.906 ± 0.038	(*WISE*)
	85.150200	−69.880400	55556	8.762 ± 0.045	7.752 ± 0.066	IRAC
	85.150200	−69.880400	55679	8.297 ± 0.048	7.349 ± 0.034	IRAC

TABLE 10 — *Continued*

Target	RA (J2000)	Decl.	MJD	[3.6]	[4.5]	Data source[a]
	85.150308	−69.880522	56772	8.641 ± 0.029	7.670 ± 0.029	(*WISE*)
	85.150370	−69.880491	56949	8.789 ± 0.032	7.804 ± 0.027	(*WISE*)
MSX LMC 974	85.242355	−69.886752	53572	8.895 ± 0.045	8.119 ± 0.042	IRAC
	85.242809	−69.886879	53673	8.693 ± 0.053	7.933 ± 0.034	IRAC
	85.242500	−69.886800	55426	8.682 ± 0.057	7.843 ± 0.048	IRAC
	85.242500	−69.886800	55450	8.719 ± 0.053	7.999 ± 0.062	IRAC
	85.242500	−69.886800	55556	9.381 ± 0.121	8.402 ± 0.064	IRAC
	85.242500	−69.886800	55679	9.002 ± 0.047	8.190 ± 0.066	IRAC
	85.242461	−69.886848	56772	8.778 ± 0.021	8.132 ± 0.019	(*WISE*)
	85.242509	−69.886835	56949	8.233 ± 0.032	7.588 ± 0.030	(*WISE*)
IRAS 05416−6906	85.336337	−69.078760	53572	12.698 ± 0.073	10.323 ± 0.024	IRAC
	85.336454	−69.078810	53673	12.297 ± 0.048	10.024 ± 0.029	IRAC
	85.336430	−69.078793	55310	12.537 ± 0.065	10.014 ± 0.036	(*WISE*)
	85.336430	−69.078793	55492	11.590 ± 0.100	9.231 ± 0.086	(*WISE*)
	85.336360	−69.078824	56775	11.181 ± 0.047	8.936 ± 0.035	(*WISE*)
	85.336575	−69.078771	56956	12.482 ± 0.069	9.961 ± 0.034	(*WISE*)
KDM 5841	85.869841	−69.712127	53572	10.289 ± 0.038	10.406 ± 0.034	IRAC
	85.870458	−69.712149	53673	10.331 ± 0.044	10.396 ± 0.025	IRAC
	85.870004	−69.712163	55299	10.432 ± 0.031	10.466 ± 0.040	(*WISE*)
	85.870200	−69.712100	55426	10.366 ± 0.053	10.406 ± 0.043	IRAC
	85.870004	−69.712163	55484	10.459 ± 0.040	10.502 ± 0.037	(*WISE*)
	85.870073	−69.712158	56771	10.489 ± 0.016	10.550 ± 0.022	(*WISE*)
	85.870024	−69.712171	56948	10.549 ± 0.029	10.599 ± 0.034	(*WISE*)
MSX LMC 1384	85.900130	−70.176310	53572	···	8.227 ± 0.045	IRAC
	85.900131	−70.176421	53673	8.735 ± 0.044	7.825 ± 0.038	IRAC
	85.900271	−70.176395	55295	8.583 ± 0.020	7.735 ± 0.029	(*WISE*)
	85.900100	−70.176400	55426	···	7.787 ± 0.046	IRAC
	85.900100	−70.176400	55450	···	8.014 ± 0.049	IRAC
	85.900271	−70.176395	55480	8.879 ± 0.050	8.002 ± 0.042	(*WISE*)
	85.900276	−70.176398	56944	8.649 ± 0.041	7.792 ± 0.041	(*WISE*)
IRAS 05446−6945	86.056859	−69.738366	53572	9.530 ± 0.032	8.073 ± 0.033	IRAC
	86.057429	−69.738455	53673	9.179 ± 0.051	7.865 ± 0.045	IRAC
	86.057098	−69.738382	55297	9.503 ± 0.052	8.092 ± 0.049	(*WISE*)
	86.057400	−69.738400	55426	···	8.809 ± 0.067	IRAC
	86.057098	−69.738382	55483	10.266 ± 0.038	8.780 ± 0.045	(*WISE*)
	86.057123	−69.738400	56946	10.090 ± 0.023	8.618 ± 0.026	(*WISE*)
2MASS J054437	86.157732	−67.616046	53572	9.286 ± 0.037	8.636 ± 0.032	IRAC
	86.157813	−67.616038	53673	9.516 ± 0.035	8.924 ± 0.031	IRAC
	86.157827	−67.616000	55329	9.420 ± 0.065	8.712 ± 0.040	(*WISE*)
	86.157827	−67.616000	55513	10.067 ± 0.053	9.335 ± 0.040	(*WISE*)
	86.157718	−67.616013	56792	9.537 ± 0.056	8.915 ± 0.059	(*WISE*)
	86.157779	−67.616012	56975	9.996 ± 0.033	9.311 ± 0.032	(*WISE*)
2MASS J054546	86.442988	−67.544316	53572	11.469 ± 0.036	10.625 ± 0.028	IRAC
	86.443089	−67.544277	53673	11.466 ± 0.026	10.626 ± 0.024	IRAC
	86.443047	−67.544276	55328	11.222 ± 0.036	10.461 ± 0.030	(*WISE*)
	86.443047	−67.544276	55512	11.305 ± 0.032	10.562 ± 0.037	(*WISE*)
	86.442973	−67.544279	56792	11.213 ± 0.035	10.536 ± 0.032	(*WISE*)
	86.443033	−67.544274	56975	11.207 ± 0.027	10.538 ± 0.028	(*WISE*)
NGC 2121 LE 6	87.069860	−71.477607	53572	9.182 ± 0.043	8.992 ± 0.046	IRAC
	87.070061	−71.477590	53673	9.152 ± 0.052	8.911 ± 0.038	IRAC
	87.069975	−71.477599	55285	9.004 ± 0.024	8.590 ± 0.029	(*WISE*)
	87.069975	−71.477599	55468	9.428 ± 0.038	8.923 ± 0.032	(*WISE*)
	87.069974	−71.477596	56749	9.265 ± 0.014	8.939 ± 0.012	(*WISE*)
	87.069978	−71.477595	56931	8.935 ± 0.023	8.635 ± 0.014	(*WISE*)
MSX LMC 1492	87.286799	−71.535263	53572	7.920 ± 0.048	7.430 ± 0.042	IRAC
	87.286992	−71.535235	53673	7.864 ± 0.043	7.341 ± 0.036	IRAC
	87.286867	−71.535295	55284	7.937 ± 0.029	7.427 ± 0.029	(*WISE*)
	87.286867	−71.535295	55467	7.492 ± 0.049	7.009 ± 0.044	(*WISE*)
	87.286904	−71.535260	56749	8.289 ± 0.016	7.685 ± 0.020	(*WISE*)
	87.286942	−71.535246	56930	8.257 ± 0.020	7.659 ± 0.017	(*WISE*)
IRAS 05506−7053	87.485663	−70.886643	53572	9.972 ± 0.030	8.370 ± 0.039	IRAC
	87.485629	−70.886596	53673	8.571 ± 0.057	7.168 ± 0.036	IRAC
	87.485629	−70.886601	55285	9.547 ± 0.044	7.960 ± 0.036	(*WISE*)
	87.485629	−70.886601	55469	10.122 ± 0.049	8.475 ± 0.031	(*WISE*)
	87.485614	−70.886620	56749	8.884 ± 0.057	7.529 ± 0.043	(*WISE*)
	87.485656	−70.886587	56931	8.233 ± 0.014	6.943 ± 0.022	(*WISE*)
LI-LMC 1758	87.528027	−71.767474	53572	9.235 ± 0.032	8.464 ± 0.040	IRAC
	87.528107	−71.767471	55283	8.764 ± 0.032	7.936 ± 0.031	(*WISE*)
	87.528107	−71.767471	55466	9.208 ± 0.042	8.341 ± 0.021	(*WISE*)
	87.528100	−71.767464	56747	9.112 ± 0.018	8.222 ± 0.019	(*WISE*)
	87.528153	−71.767453	56929	8.348 ± 0.030	7.527 ± 0.016	(*WISE*)
IRAS 05509−6956	87.608738	−69.934268	53572	14.761 ± 0.056	11.702 ± 0.035	IRAC
	87.608811	−69.934229	53673	15.024 ± 0.062	11.920 ± 0.039	IRAC
	87.608788	−69.934213	55288	13.969 ± 0.131	10.527 ± 0.032	(*WISE*)
	87.608788	−69.934213	55474	14.389 ± 0.146	10.895 ± 0.042	(*WISE*)
	87.608734	−69.934272	56747	15.048 ± 0.157	11.538 ± 0.058	(*WISE*)

TABLE 10 — *Continued*

Target	RA (J2000)	Decl. (J2000)	MJD	[3.6]	[4.5]	Data source[a]
	87.609027	−69.934156	56936	15.547 ± 0.187	12.068 ± 0.052	(*WISE*)
KDM 6486	87.652801	−68.481207	53572	11.058 ± 0.044	11.083 ± 0.036	IRAC
	87.652960	−68.481226	53673	11.095 ± 0.035	11.097 ± 0.035	IRAC
	87.652875	−68.481180	55298	11.133 ± 0.033	11.222 ± 0.029	(*WISE*)
	87.652875	−68.481180	55484	11.049 ± 0.042	11.125 ± 0.048	(*WISE*)
	87.652856	−68.481164	56765	11.000 ± 0.022	11.019 ± 0.027	(*WISE*)
	87.652875	−68.481161	56947	11.033 ± 0.021	11.041 ± 0.028	(*WISE*)
IRAS 05516−7124	87.707877	−71.393235	53572	9.235 ± 0.050	8.032 ± 0.031	IRAC
	87.707995	−71.393269	55283	10.286 ± 0.030	8.957 ± 0.033	(*WISE*)
	87.707995	−71.393269	55466	9.293 ± 0.035	8.085 ± 0.029	(*WISE*)
	87.708033	−71.393243	56747	9.380 ± 0.026	8.183 ± 0.015	(*WISE*)
	87.708122	−71.393209	56929	9.278 ± 0.025	8.091 ± 0.020	(*WISE*)
PMP 337	88.212600	−69.477682	53572	10.134 ± 0.041	10.251 ± 0.030	IRAC
	88.212782	−69.477660	53673	10.259 ± 0.058	10.297 ± 0.030	IRAC
	88.212772	−69.477663	55287	10.333 ± 0.027	10.408 ± 0.032	(*WISE*)
	88.212772	−69.477663	55473	10.276 ± 0.042	10.381 ± 0.033	(*WISE*)
	88.212781	−69.477664	56747	10.247 ± 0.024	10.353 ± 0.047	(*WISE*)
	88.212753	−69.477673	56935	10.263 ± 0.018	10.371 ± 0.020	(*WISE*)
IRAS 05568−6753	89.161560	−67.892743	53572	11.709 ± 0.032	9.463 ± 0.028	IRAC
	89.161464	−67.892741	53673	12.012 ± 0.032	9.787 ± 0.030	IRAC
	89.161446	−67.892773	55287	10.758 ± 0.063	8.459 ± 0.061	(*WISE*)
	89.161446	−67.892773	55475	10.064 ± 0.035	7.924 ± 0.038	(*WISE*)
	89.161431	−67.892791	56745	10.136 ± 0.022	8.003 ± 0.023	(*WISE*)
	89.161538	−67.892723	56936	10.731 ± 0.051	8.486 ± 0.034	(*WISE*)
IRAS 06025−6712	90.629357	−67.213049	53572	8.002 ± 0.034	6.813 ± 0.029	IRAC
	90.629443	−67.213032	53673	···	6.639 ± 0.034	IRAC
	90.629424	−67.213006	55257	9.169 ± 0.048	7.848 ± 0.046	(*WISE*)
	90.629424	−67.213006	55439	8.919 ± 0.099	7.612 ± 0.086	(*WISE*)
	90.629424	−67.213006	55591	8.166 ± 0.017	6.949 ± 0.009	(*WISE*)
	90.629411	−67.213020	56719	7.756 ± 0.032	6.539 ± 0.048	(*WISE*)
	90.629385	−67.212979	56898	8.001 ± 0.079	6.812 ± 0.077	(*WISE*)
IRAS 06028−6722	90.687952	−67.378674	53572	8.570 ± 0.042	7.306 ± 0.032	IRAC
	90.688046	−67.378640	53673	9.206 ± 0.071	7.733 ± 0.030	IRAC
	90.688041	−67.378636	55258	8.478 ± 0.082	7.138 ± 0.068	(*WISE*)
	90.688040	−67.378636	55440	9.490 ± 0.091	8.014 ± 0.073	(*WISE*)
	90.688047	−67.378688	56721	8.449 ± 0.039	7.117 ± 0.030	(*WISE*)
	90.688037	−67.378642	56901	8.430 ± 0.053	7.096 ± 0.040	(*WISE*)
IRAS F06108−7045	92.544512	−70.767579	55263	9.336 ± 0.044	8.222 ± 0.034	(*WISE*)
	92.544512	−70.767579	55447	9.292 ± 0.031	8.198 ± 0.025	(*WISE*)
	92.544497	−70.767592	56727	9.866 ± 0.059	8.706 ± 0.068	(*WISE*)
	92.544509	−70.767549	56909	9.090 ± 0.047	8.027 ± 0.050	(*WISE*)

NOTE. — Table 10 is published in its entirety in the electronic edition of the Astrophysical Journal. A portion is shown here for guidance regarding its form and content.

[a] *WISE* data are corrected as described in Appendix A.